Production and Evaluation of a TiO$_2$ based ^{68}Ge/^{68}Ga Generator

By

Sizwe Buwa

A thesis submitted in fulfillment of the requirements for the degree of Magister Scientiae in the Department of Chemistry, University of the Western Cape

Supervisor: Dr. Clive Naidoo

Head: Radionuclide Production

iThemba LABS

Co-supervisor: Prof. Leslie Petrik

Dept. of Chemistry

University of the Western Cape

May 2014

DECLARATION

I, Sizwe Buwa, declare that the contents of this thesis represent my own unaided work, and that the thesis has not previously been submitted for academic examination towards any qualification. Furthermore, it represents my own opinions and not necessarily those of the University of the Western Cape.

Signed   **Date**

UNIVERSITY *of the*

WESTERN CAPE

ABSTRACT

^{68}Ge/^{68}Ga generators rely on metal oxide, inorganic and organic sorbents in order to prepare radionuclides useful for clinical applications. The requirements for ^{68}Ge/^{68}Ga generators are that the ^{68}Ga obtained from the ^{68}Ge loaded column should be optimally suited for the routine synthesis of ^{68}Ga-labelled radiopharmaceuticals, that the separation of the ^{68}Ga daughter from the ^{68}Ge parent should happen easily, with a high yield of separation, a low specific volume of ^{68}Ga and should not contain trace elements owing to the solubility of the metal oxide sorbent. Beginning with a metal oxide preparation and continuing through recent developments, several approaches for processing generator derived ^{68}Ga have altered the production of ^{68}Ge/^{68}Ga generators. Still, the effects of sorbent modification on the properties of ^{68}Ge/^{68}Ga radionuclide generator systems are not necessarily optimally designed for direct application in a medical context. The objective of this research was to analyze and document characteristics of Titanium Oxide (TiO$_2$) sorbents relevant to processing of a ^{68}Ge/^{68}Ga generator that is able to produce ^{68}Ga eluates that are adequate for clinical requirements.

Interest was shown in TiO$_2$ based ^{68}Ge/^{68}Ga generators by a number of overseas companies for tumour imaging using ^{68}Ga-labelled 1,4,7,10-tetraazacyclododecane-1,4,7,10-tetraacetic acid (DOTA)-conjugated peptides. While a method involving production of the ^{68}Ga radionuclide using TiO$_2$ metal oxide had been published, problems with the production persisted. A method, using TiO$_2$ metal oxide for ion exchange chromatography, was devised in this study to produce the ^{68}Ga radionuclide, with the aim of being adopted for production purposes. The study focuses on the development of a dedicated procedure for the achievement of sufficient ^{68}Ga yield along with low ^{68}Ge breakthrough and low metallic impurities. Literature from 1970 to 2011 was reviewed to assess the radiochemical aspects of the ^{68}Ga production and processing thereof. Various commercially available TiO$_2$ metal oxides were characterized by subjecting the materials to x-ray diffraction (XRD), x-ray fluorescence (XRF) and scanning electron microscopy (SEM) for quantitative and qualitative analysis.

By means of the characterization techniques used, particle size, mineralogical phase and amorphous nature seemed to be influenced by the pretreatment temperature applied to the commercial TiO_2 powders. Increased surface area and anatase nature of the TiO_2 powders (Sigma-Aldrich) suggested that the particle size of this source of TiO_2 was smaller and that no heat was necessary for the ^{68}Ge loading.

In order to identify conditions necessary for the loading of ^{68}Ge onto a Soci & acute Technique Medium Ionization (STMI). xH_2O TiO_2 based micro column, various parameters were investigated. Eluent analysis from 0.01-0.1 M HCl was used to establish the acid concentration necessary for the ^{68}Ge uptake, based on the maximum amount of ^{68}Ge activity loaded. In two of the different experimental conditions applied, 100% ^{68}Ge loading was achieved. Other TiO_2 metal oxides in anatase and rutile form (Sigma-Aldrich and Alfa-Aesar) were then investigated for the loading of ^{68}Ge. However, both commercially TiO_2 forms provided disappointing results as ^{68}Ge could not be loaded successfully. Evonik Industries entered the market for the production of Aerolyst® and Aeroxide® P-25 TiO_2 metal oxides, due to photochemical properties that TiO_2 possessed. Once 100% ^{68}Ge loading was achieved using both Aerolyst® and Aeroxide® TiO_2 sorbents, thereafter a successful separation of the ^{68}Ga radionuclide from the TiO_2 materials could be performed by means of cation-exchange chromatography. Both systems provided an elution yield of not less than 40% of ^{68}Ga, when 5 ml of 0.1 M HCl as the required eluent was applied. The systems remained stable for a period of up to 12 months and showed satisfactory stable elution during this time. The generated ^{68}Ga radionuclide was eluted with 5 ml, 0.1 M HCl for up to 300 elutions. The breakthrough of ^{68}Ge from the systems ranged from less than 0.05% up to 0.05% within the 12 months of operation. Of utmost interest, more than 90 % of the ^{68}Ga activity available at a specific time could be eluted within the first 5 ml of 0.1 M HCl, and up to 85% of the activity could be obtained in 3 ml of the eluate when the fractions were collected.

The behaviour of the generators corresponded well to the technical characteristics required by the regulators in the market of the $^{68}Ge/^{68}Ga$ generators. Recent developments in ^{68}Ga regeneration have heightened the need for maximization of the yield of the desired radionuclide and minimization of the yield of the radioactive contaminants. In the past, far too little attention has been paid to the strict regulatory and quality requirements. This study has been able to show the separation technique, generator system design and provided ^{68}Ga

elution yield and radiochemical purity (i.e. low breakthrough of the long-lived parent radionuclide). This study was also able to demonstrate that in order for TiO_2 metal oxide to function as an effective sorbent for the production of the ^{68}Ga radionuclide, particle size and mineralogical phase were the key parameters.
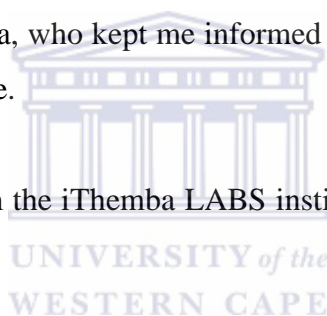
ACKNOWLEDGEMENTS

TABLE OF CONTENTS

GLOSSARY

^{68}Ga - gallium-68 isotope.

^{68}Ge - germanium-68 isotope.

Alpha particle (α) – A positively charged nuclear particle identical with the nucleus of a helium atom that consists of two protons and two neutrons and is ejected at high speed in certain radioactive transformations, it is characterised by being not very penetrating and is stopped by paper/skin.

Beta particle (β) - A high-speed electron or positron emitted by a nucleus during radioactive decay or nuclear fission, it is characterised by travelling several meters in air and passes through paper/skin.

Computed Tomography (CT) - A scan technique that uses X-rays to make detailed pictures of structures inside the body.

Count – A single detected event or total number of events registered by a detection system

Curie - The curie is a quantity of radioactive material in which 3.7×10^{10} atoms disintegrate per second.

Cyclotron - A commonly used accelerator for the production of nuclear medicine radionuclides.

Daughter radionuclide – A radionuclide produced by the decay of a parent radionuclide.

Decay – The disintegration of the nucleus of an unstable atom by spontaneous fission.

DOTA - 1,4,7,10-tetraazacyclododecane-1,4,7,10-tetraacetic acid, $C_{16}H_{28}N_4O_8$. DOTA is used as a complexing agent, especially for lanthanide ions. Its complexes have medical applications as contrast agents and cancer treatments.

DOTA-TATE – DOTA-(Tyr^3)-octreotate, $C_{65}H_{90}N_{14}O_{19}S_2$. A substance which, when bound to various radionuclides, has been tested for the treatment and diagnosis of certain types of cancer, mainly neuro-endocrine tumours.

DOTA-TOC- DOTA-Phe^1-Tyr^3-octreotide, $C_{65}H_{92}N_{14}O_{18}S_2$. A substance which, when bound to various radionuclides, is used in the treatment and diagnosis of certain types of cancer.

Efficiency – The fraction of decay events from a standard sample seen by a detector in the peak corresponding to gamma ray energy of the emission and stored by a detection system.

Electron volt (eV) – The amount of kinetic energy gained by an electron as it passes through a potential difference of 1 volt. It is equivalent to 1.602×10^{-19} joules per second.

Gamma rays (γ) – A photon or high-energy quantum emitted from the nucleus of a radioactive atom. Gamma rays have high energy, a short wave length, are extremely penetrating, and can pass even through several centimetres of lead.

Half-life (T$_{1/2}$) – Time it takes for half of the original amount of nuclei to decay.

HPGe - High Purity Germanium Detector.

Ion – An atom or molecule that has become electrically charged by having lost or gained one or more electrons.

Isotope – One of two or more atoms with the same atomic number but with different atomic weights.

JCPDS – Joint Committee of Powder Diffraction Standards.

Magnetic Resonance Imaging (MRI) – The use of neuro-imaging technology to measure an aspect of brain function, often with a view to understanding the relationship between activity in certain brain areas and specific mental functions.

Multi Channel Analyzer (MCA) – An instrument which collects, stores and analyses time-correlated or energy correlated events.

NODAPA-OH – 1,4,7-triazacyclononane-1,4-diacetic acid-7-p-hydroxyphenylacetic acid. Bifunctional chelators with potential for molecular imaging.

Parent radionuclide – A radionuclide that produces a daughter radionuclide during decay

PET – Positron Emission Tomography (PET) is a test that uses a special type of camera and a tracer (radioactive chemical) to look at organs in the body. The technique produces a three-dimensional image or picture of functional processes in the body. The system detects pairs of gamma rays emitted indirectly by a positron-emitting radionuclide (tracer), which is introduced into the body on a biologically active molecule.

Positron – An elementary particle, "anti-electron"; with the mass of electron but having a positive charge. It is emitted by some radionuclides and is also created in pair production by the interaction of high-energy gamma rays with matter.

Radiation – The emission or propagation of energy through matter or space by electromagnetic disturbances which display both wave-like and particle-like behaviour.

Radioactivity – The emission of radiation from the spontaneous disintegration (decay) of an unstable radionuclide.

Radionuclide – A radioactive isotope.

Radionuclide generator– Any system incorporating a fixed parent radionuclide from which a daughter product is to be obtained by elution or any other method used in a radiopharmaceutical. In a radionuclide generator, both mother and daughter radionuclides are to be considered active ingredients.

Radiopharmaceutical - A radiopharmaceutical is a radioactive drug used for diagnosis or therapy in tracer quantities with no pharmacological effect.

Scintillator – A type of detector which produces a flash of light as the results of an ionizing event.

Single Photon Emission Tomography (SPECT) – The use of radioactive materials to assess the physiological properties of organ systems (e.g. blood flow, glucose metabolism or protein aggregates).

STMI - Soci & acute Technique Medium Ionization

XRD (X-ray Diffraction) – A penetrating form of electromagnetic radiation emitted during electron transitions in an atom to lower energy state; usually when outer orbital electrons give up some energy to replace missing inner orbital electrons.

UNIVERSITY *of the*
WESTERN CAPE

LIST OF TABLES

LIST OF ABBREVIATIONS

CT	Computed Tomography
GMP	Good Manufacturing Practice
HRTEM	High Resolution Transmission Electron Microscopy
PET	Positron Emission Tomography
SEM	Scanning Electron Microscopy
SSC	Separated Sector Cyclotron
STMI	Soci & acute Technique Medium Ionization
XRD	X-Ray Diffraction
XRF	X-Ray Fluorescence
BET	Brunauer-Emmett-Teller

LIST OF FIGURES

Chapter One

INTRODUCTION

1.1   Background

The co-ordination chemistry of gallium is of considerable interest, mostly due to the potential use of its radionuclides in radiopharmacy. In particular, the coordination chemistry of Ga(III) is defined by the number of coordination 6 and by the octahedral coordination sphere. Gallium is a metal belonging to III B group of the periodic table and under physiological conditions it only exists in the +3 oxidation state. This fact is determinant for its radiochemistry. Ga^{+3} is redox-inert, and its coordination chemistry is dominated by its hard acid character. Such metals are classified as "hard acids" and they prefer to form chemical bonds with ionic and non-polarizable Lewis bases such as nitrogen and oxygen atoms (carboxylate, phosphonate and amino groups). In solution, the hydrated cations of Ga(III) are only stable under acidic conditions, hydrolyzing at higher pH values and leading to insoluble hydroxides ($Ga(OH)_3$).

$$M(H_2O)_6{}^{+3} + H_2O \longrightarrow M(OH)(H_2O)_5{}^{+2} + H_2 0 \tag{1.1}$$

$$M(OH)(H_2O)_5{}^{+2} + H_2 0 \longrightarrow M(OH)_2 + (H_2O)_4{}^{+} + H_3O^{+} \tag{1.2}$$

$$M(OH)_2 + (H_2O)_4{}^{+} \longrightarrow M(OH)_3\,(s) + H_3O^{+} + 3H_2O \tag{1.3}$$
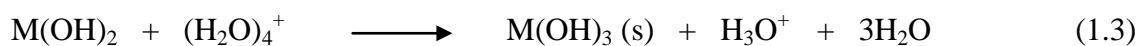
Zhernosekov et al. (2006) explained that in aqueous solutions, gallium is stable only as a trivalent cation. As a result, it cannot be incorporated into the structure of targeting vectors by covalent bonding, but must be complexed by a ligand that is conjugated to the biological vector. The Ga^{3+} ion possesses a d^{10} electron configuration and accepts different coordination numbers (usually 4–6), while not displaying preference for any particular coordination

polyhedron. According to the literature (Zhernosekov et al., 2007), at pH>4, formation of colloidal hydroxide [Ga(OH)$_3$]$_n$ commences. Although this molecule does not generally inhibit complex formation, radiolabeling is nevertheless substantially hampered due to formation of insoluble colloids (particularly at high activities) and their adhesion to the surface of the reaction vessel. At pH values above 8, a water soluble hydroxo complex, [Ga(OH)$_4$], is formed. As ligand exchange with the tetra hydroxo complex is a much slower process than complexation of free Ga^{3+}, complexation is achieved best at pH<4.

Velikyan et al. (2004) developed a list of parameters in which they described the chemical separation specificity requirements. In summary, they argued that ligands for ^{68}Ga-based PET radiopharmaceuticals should ideally combine the following set of properties:

- Stability: Ga^{+3} complexes should be as stable as possible; a kinetic inertness of the complex is more important than high thermodynamic stability.

- Quick complexation under radiochemical conditions: Formation of Ga^{+3} complexes should be fast at low temperatures, low concentration, and minimal excess of the ligand. A desirable ligand will chelate Ga^{3+} in solutions of nanomolar concentration at room temperature within minutes.

- Selectivity: The ligand should ideally be selective for the Ga^{3+} ion. Particularly, complexation of serum metals like Ca^{2+}, Mg^{2+}, and Zn^{2+} ions (the last being produced by decay of ^{68}Ga) should be disfavored in order to avoid transmetallation in vivo or diminishing of radiochemical yield.

- Conjugation ability: The chelating unit has to possess a functional group which allows covalent binding to the targeting vector (biomolecule) without a significant breakdown of complexation performance.

- Long shelf-life: In medical applications, excellent chemical stability is necessary.

- Accessibility: Preparation of the compound in practical amounts should be quick, facile, and inexpensive.

There are three gallium radionuclides (^{66}Ga, ^{67}Ga and ^{68}Ga) with suitable physical characteristics for use in gamma scintigraphy or PET. The isotope ^{67}Ga (t$_{1/2}$ = 78.1h) is produced by a nuclear reaction ^{68}Zn(p,2n)^{67}Ga starting with a ^{68}Zn enriched sample. The ^{67}Ga obtained is then separated either by solvent extraction or by an anion exchange process. ^{68}Ga,

a positron emitter, is obtained from a ^{68}Ge generator and decays by positron emission in 89% yield. The maximum energy of this positron is 1.899 keV, whereas the average energy per disintegration is 740 keV. It follows that the chemical properties of Ge^{+4} and Ga^{+3} are sufficiently different to allow several different methods of efficient separation.

A radionuclide generator is a means of having 'on tap' a short-lived radionuclide. It is technically achieved by the chemical separation of the daughter radionuclide from the parent. This can be accomplished through the use of chromatographic techniques, distillation or phase partitioning. However, chromatographic techniques have been the most widely explored and are the current state-of-the-art technology (Greene and Tucker, 1961; Kopecky et al., 1973; Yano and Anger, 1964; Erhardt and Welch, 1978; Neirinckx and Davis, 1980; Loc'h et al., 1980; Horiguchi et al., 1983; Deutsch, 1993; Naidoo et al., 2002; Qaim, 2003; Aardaneh and Van der Walt, 2006; Röesch and Filosofov, 2010) for the majority of generator systems in use today. Debate continues about the best suitable sorbent material for the preparation of ^{68}Ge/^{68}Ga generators. Among the many sorbents that are reported in the literature (Kozlova et. al., 1970; Zhernosekov et. al., 2007; Bao and Song, 1996; Erhardt and Welsh, 1978; Aardaneh and Van der Walt, 2006; Loc'h et al., 1980; Waters et al., 1983), the following are worth mentioning, silica gel, SiO_2, TiO_2, SnO_2, Al_2O_3, ZnO, ZrO_2, HFO_2 or organic inert polymers and copolymers, in particular styrene-divinylbenzene, polystyrene, styrene-acrylonitrile, styrene-acrylonitrile-methylmethacrylate, polyacrylates, acrylic methacrylic esters, acrylonitrile-unsaturated dicarboxylic acid-styrene and vinylidene chloride-acrylonitrile. In this respect, TiO_2 metal oxide, which despite a considerable amount of discussion in the literature, still has not been treated in much detail. A major concern is the fact that the chemical and radiochemical requirements in relation to its usefulness as a medical generator application have not been fully resolved. Additionally, a shortcoming in the available theory and discussions seemed to be a poor consideration of chemical aspects. Beside the radiopharmacy, the development of production and processing routes using TiO_2 as a sorbent remain unsolved and studies are ongoing to make them available. Inorganic sorbents developed to date have hydrated amorphous structure, which has disadvantageous properties regarding chemical and physical stability. The low physical stability causes the sorbent particles to break easily, blocking the flow of eluent in the sorbent bed of the

chromatographic column. The low chemical stability causes leaching of the metal ions from the sorbent material into the separated eluent product.

The availability of a highly efficient, reliable, long lived ^{68}Ge/^{68}Ga generator system has been the basis of the development of ^{68}Ga radiopharmaceuticals. The equations governing generator systems stem from the formula:

$$A_2 = \frac{\lambda_2}{\lambda_2 - \lambda_1} A_1^0 [\exp(-\lambda_1 t) - \exp(\lambda_2 t)] \tag{1.4}$$

where A_1^0 is the parent activity at time t = 0, t is the time since the last elution of the generator, A_2 is the activity of the daughter product (A~ = 0), and λ_1 and λ_2 are the decay constants of parent and daughter radionuclides, respectively. For the special case of secular equilibrium, defined by $\lambda_2 >>> \lambda_1$, the following is obtained:

$$A_2 = A_1^0 [\exp(-\lambda_1 t) - \exp(\lambda_2 t)] \tag{1.5}$$

If *t* is much less than the half-life of the parent, $\ln(2)/\lambda_1$, and greater than approximately seven times the daughter half-life, $\ln(2)/\lambda_2$, then

$$A_2 = A_1^0 \tag{1.6}$$

This is the secular equilibrium condition. The growth of the daughter here is given by:

$$A_2 = A_1^0 [1 - \exp(\lambda_2 t)] \tag{1.7}$$

For transient equilibrium, defined by $\lambda_2 > \lambda_1$ but λ_2 not very much greater than λ_1, the following is obtained:

$$A_2 = \lambda_2 A_1^0 / (\lambda_2 - \lambda_1) \tag{1.8}$$

1.2   Rationale

Positron emission tomography (PET) is an imaging modality which provides quantitative images of biological processes in vivo at molecular level. It provides clinically important information for tumour diagnosis and staging as well as for neurological applications. Most of the PET radiopharmaceuticals are labelled with radionuclides (^{18}F, ^{11}C, ^{15}O, ^{13}N) which are produced by medical cyclotrons, thus limiting the availability of these short-lived tracers.

Generator-produced radionuclides such as ^{68}Ga represent an important and interesting alternative to cyclotron-produced radionuclides because of some important advantages. [68]Ga decays 89% by positron emission, with E_{max} of 1.92 MeV, and 11% via electron capture. Its physical half-life of 67.71 min is compatible with the pharmacokinetics of most radiopharmaceuticals of low molecular weight.

The review article by Decristoforo and colleagues published in 2005 (Decristoforo et al., 2005) gives an account of the feasibility and availability of [68]Ga –labelled peptides. In their study it is reported that [68]Ga^{3+} is stable and forms complexes with the cyclic ligand DOTA with high affinity. 1,4,7,10-tetra-azacyclododecane-1,4,7,10-tetra-acetic acid (DOTA) (Figure. 1.3) is an octa-coordinating ligand based on the tetra-azacyclododecane (cyclen) macrocyclic framework in which each nitrogen atom bears an acetic substituent. DOTA forms thermodynamically stable and kinetically inert complexes with a large number of metal ions and is widely used to design metalloradiopharmaceuticals (Mäcke et al., 2005).
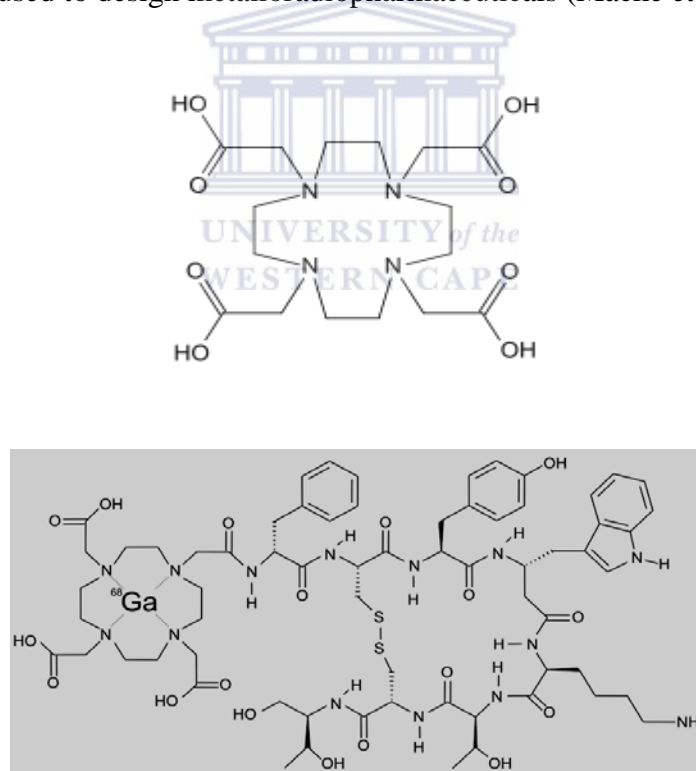
Figure 1.1: Structure of DOTA (top); DOTA-octreotide (bottom)

An example of DOTA-conjugated somatostatin analogue DOTA-octreotide (DOTATOC) is shown in Figure: 1.1. According to the literature (Reubi et al., 2000; Antunes et al., 2007; Mäcke et al., 2005), DOTA-TOC (DOTA-D-Phe1-Tyr3- octreotide) labeled with ^{68}Ga have

5

shown high binding affinity for human somatostatin receptors and possess excellent tumour imaging capabilities. A major reason for the current interest in ^{68}Ga was the development of a group of ^{68}Ga-labelled radiopharmaceuticals that attracted considerable clinical interest (Antunes et al., 2007). These are the somatostatin analogues conjugated with DOTA (1,4,7,10-tetraazacyclododecane-N,N′,N″,N‴-tetraacetic acid) that were initially developed by researchers (Zhernosekov et al., 2007; Breeman et al., 2005; Meyer et al., 2004; Bauwens et al., 2010) for targeted radionuclide therapy of somatostatin receptor-expressing tumours. It was shown that the DOTA chelator, that was originally attached to these stabilized octreotide analogues to bind trivalent radiometals such as ^{90}Y, ^{111}In and ^{177}Lu can also strongly bind ^{68}Ga, resulting in complexes with high stability both in vitro and in vivo. These ^{68}Ga-labelled complexes also unexpectedly showed a higher binding affinity and a different receptor binding profile than those of their ^{111}In, ^{90}Y and ^{177}Lu counterparts with consequently higher accumulation of the radiolabelled peptides in somatostatin receptor-positive tissue (Antunes et al., 2007; Breeman et al., 2003; Hofmann et al., 2001; Henze et al., 2001).

After publication (Hofmann et al., 2001; Henze et al., 2001) of the first clinical examples of PET images with ^{68}Ga-labelled somatostatin, ^{68}Ge/^{68}Ga generators have became widely commercially available, which has resulted in a rapid spread of these peptide-based radiopharmaceuticals and clinical implementation for PET imaging particularly in Europe. Today detection of somatostatin receptor-expressing tumours using ^{68}Ga-labelled somatostatin analogues is clinically well established, but there are factors influencing the feasibility and availability of this method.

1.3   Problem Statement

Drivers for chemical regulations such as radioprotection, higher reproducibility and robustness, better Good Manufacturing Practise (GMP) compliance and better control of sterility have been begging for optimization and further developments of ^{68}Ge/^{68}Ga generators. The development of a valuable ^{68}Ge/^{68}Ga generator, capable of providing a ^{68}Ga eluate suitable for biomedical applications, requires different specific technical solutions. These solutions would include a sorbent for immobilizing the parent nuclide ^{68}Ge, a suitable eluent to be used for elution of the daughter nuclide ^{68}Ga, and radiation robustness of component parts and materials used for the setup of the generator. Presently, commercial

^{68}Ge/^{68}Ga generators using tin dioxide, titanium oxide or silica gel sorbent for ^{68}Ge immobilization are available. However, the high HCl concentration of the eluent and the unavoidably high metallic ion contamination makes utilization of these generators for labeling radiopharmaceuticals impossible. Moreover, the critical level of ^{68}Ge breakthrough and acidity of the ^{68}Ga eluate produced from the above generator systems also present a disadvantage, in that the decay of ^{68}Ge itself does not provide any detectable emissions. The amount of ^{68}Ge can be determined only after sufficient decay (preferably more than 24 h) of ^{68}Ga generated by the decay of the residual ^{68}Ge. The use of high concentrations of hydrochloric acid, particularly, in automated systems, is a challenge as it places severe constraints on the eluent that is to be used and as a result, excess acid has to be removed to ensure appropriate labelling conditions. In addition, the limit of ^{68}Ge in patient preparations has been a matter of continual discussion over recent years. Concerns about the presence of ^{68}Ge is a quality consideration, but also GMP aspects as well as the regulatory framework involved, still remain a hurdle for development of ^{68}Ge/^{68}Ga generator systems. In view of the above described drawbacks, the development of alternate sorbents with high sorption capacity and selectivity for ^{68}Ge along with appreciable radiation resistance and chemical stability in acidic medium, was of considerable importance and deserved serious consideration. Use of such sorbents would not only facilitate the elution of ^{68}Ga with high radioactive concentration and avoid the need of an additional concentration step, but also render ^{68}Ga of acceptable radionuclidic and chemical purity.

1.4   Aims and Objectives

The sorbent used in a ^{68}Ga/^{68}Ga generator should be highly resistant to the high radiation dose delivered from the positron and gamma radiation emitted from the ^{68}Ge/^{68}Ga generators for the entire life of the generator (generally 12 months), which is long due to the long half-life of the parent ^{68}Ge. Components for generator setup should be nonmetallic to avoid metallic ion contamination of ^{68}Ga eluate and also be highly resistant to high radiation dose. The chromatographic column of the generator should be made from either quartz or plastic material. Suprapur water and chemicals should be used for preparation and elution of the generator. To be successfully applied for formulating ^{68}Ga-labeled targeted radiopharmaceuticals currently used in clinical PET imaging, the ^{68}Ga eluate should be evaluated based on three important parameters: ^{68}Ga solution eluted from the ^{68}Ge/^{68}Ga

7

generators should of very high radionuclidic purity with absolute low levels of breakthrough of the ^{68}Ge parent nuclide contamination (generally <10^{-3}% is specified) and, chemical impurities, particularly metal ion content in the ^{68}Ga solution, should be kept as low as possible to eliminate any concurrent coordination chemistry reactions which may reduce the ^{68}Ga labeling yield. High quality ^{68}Ga is of great importance for the successful labeling of ^{68}Ga with nanomole quantities of biomedical tracers used in routine molecular imaging. Additional parameters are that the ^{68}Ga eluate should be free from either complexing agents or organic solvents which may be harmful to both bio-molecules and complexation of Ga^{+3} ions.

1.5 Research Questions

The renaissance of ^{68}Ga radiopharmacy has led to great advances in developments and applications of ^{68}Ge/^{68}Ga generators in the last 50 years. Different production strategies are now available, which can also be tailored to different needs. Designs have implemented different purification approaches leading to increased chemical and radionuclidic purity (minimizing ^{68}Ge breakthrough) as well as high radioactivity of the final preparation. However, there are still some drawbacks to the direct use of ^{68}Ga eluate for radiolabelling of peptides in clinical PET. The most relevant issues are measurable activities of the long lived parent radionuclide (^{68}Ge – breakthrough), the high eluent volume and the high HCl concentration (0.1-1 M).

The following research questions were formulated for the study as they represent progressive developments towards the optimization of the ^{68}Ge/^{68}Ga generators from both the chemical and regulatory point of view:

- What are the modifications required to the TiO$_2$ metal oxide for quantitative adsorption of ^{68}Ge?
- Will the modification favour low concentration of HCl eluent and avoid large HCl volumes for ^{68}Ga separation from ^{68}Ge?
- Does the cation exchange capacity of the TiO$_2$ provide qualities such as high chemical separation of ^{68}Ga from ^{68}Ge, high radiation resistance and chemical stability for periods of up to 3 year?

- Does the ^{68}Ga solution produced from the $^{68}Ge/^{68}Ga$ generator have a low metallic ion content?

- How durable and stable is the ^{68}Ga generator?

1.6 Research Approach

In the interest of addressing the above mentioned research questions and addressing the negative aspects of current generators as well as developing a protocol similar to that of SnO_2 based systems in the case of the TiO_2 which would be able to function well as $^{68}Ge/^{68}Ga$ generators, the following research approach was adopted and monitored:

- Investigate the various kinds of commercially available TiO_2 powders (Aeroxide® TiO_2, TiO_2 (rutile), TiO_2 (anatase), TiO_2 (Oxtain) and Aerolyst® TiO_2.

- Compare and study the ^{68}Ga elutions from the TiO_2 support in terms of yield, quality and stability using methods adopted from the literature.

- Analyse the ^{68}Ge breakthrough, metal ion content and generator stability which should be monitored for a period of up to 1 year.

The first stage of the study required making use of a micro Curie (µCi) of ^{68}Ge to determine the optimal loading and retention conditions of the various TiO_2 column matrices. According to the literature, phase and particle size are the important parameters that influence physical properties of the TiO_2 material. Extensive review on the pre-treatment of TiO_2 metal oxide was carried out and features such as particle size, temperature and XRD analyses were adopted. The variables most likely to affect the chemical and physical properties of TiO_2 metal oxide during the loading of the ^{68}Ge and separation of the ^{68}Ga from the ^{68}Ge process were identified. These variables (heat and particle size) were optimised by subjecting the metal oxides to elevated temperatures and sieving which was followed by characterisation using an XRD technique adopted from the literature review. The results obtained were then compared to the standard XRD spectrums of TiO_2 oxides (JCPDS no.: 88-1175 and 84-1286).

After the optimal conditions were obtained for the loading of ^{68}Ge on the specified TiO_2 metal oxide, a 15 mCi TiO_2 based $^{68}Ge/^{68}Ga$ generator was manufactured and its performance was evaluated over a period of 12 months.

1.7   Hypothesis

It is hypothesized that a TiO_2 metal oxide based $^{68}Ge/^{68}Ga$ generator produced under the same conditions as the SnO_2 based support would produce a better generator than other existing metal oxides.

1.8   Scope and delimitations of the study

The basis for today's success with ^{68}Ga was laid with the development of generator systems providing the radionuclide in ionic form. These generators are characterized by a strongly acidic hydrochloric acid eluate wherein gallium is in the form of Ga^{3+} that can be utilized for radiolabelling applications. These generators vary in terms of column eluate, elution yields, and strength of hydrochloric acid in the eluent. The other relevant data found in the literature was by Loc'h et al., (1980) who used SnO_2 as the column eluate and performed elution with 1 M HCl, and their generator formed the basis of a commercially available generator developed at iThemba LABS, which could be used for clinical applications. The extensive knowledge developed by the researchers (De Blois, et al., 2011; Breeman et al., 2005; Meyer et al., 2004; Velikyan et al., 2004; Zhernosekov et al., 2010) on $^{68}Ge/^{68}Ga$ generators in South Africa or elsewhere around the world, created a good foundation for this study.

In the choice of the adsorption parameters to be optimised (heat, phase and particle size) during the course of this study, the variables that had previously shown some significant influence on the adsorption of ^{68}Ge were chosen (Röesch and Riss, 2010; Zhernosekov et. al., 2007; De Blois et. al., 2011). Owing to the time consuming nature of pre-treatment optimization and adsorption experiments, once loading was achieved, the battery of experiments that followed were only investigated on the Aerolyst® TiO_2 metal oxide, following the SnO_2 method.

The scope of the investigations was limited to the following:

- To determine the optimum micron size of TiO_2 to be used as column eluate for the $^{68}Ge/^{68}Ga$ generator.

- To determine whether heat treating the TiO_2 would improve $^{68}Ge/^{68}Ga$ generator performance i.e. retention of the ^{68}Ge.

- To determine the optimum HCl concentration for loading the ^{68}Ge onto the TiO$_2$ column.

- To elute the developed ^{68}Ge/^{68}Ga generator column with 0.1M HCl over a 12 month period and evaluate the eluate for the following:

  - ^{68}Ga efficiency

  - ^{68}Ge breakthrough

  - Determination of metal impurities such as Al, Ti, Sn, Fe, Ge, and Zn

However, it is important to note that loading TiO$_2$ metal oxide with approximately 15 mCi ^{68}Ge was not the complete account for a ^{68}Ge/^{68}Ga generator as activity loads usually go up to 100 mCi's. Working with huge amounts of activities would result in accumulation of a high activity dose and this would impact negatively on the researcher. A practical solution was to use a fairly usable ^{68}Ge activity which in turn could be used to interpret the full picture if a high activity ^{68}Ge were to be loaded. The study also omitted parameters such as sterilities and endotoxins test due to the use of hydrochloric acid solutions, as this eluent provides an environment which is highly unfavourable for microorganisms. Also omitted in the study was the process of radiolabelling, again due to the number of requirements for high specific activity labelling, in particular for peptide labelling approaches.

1.9   Thesis structure

This thesis is divided into five chapters (including this one; Chapter 1) and is structured as follows:

Chapter one: This chapter presents the introduction to the study, the motivation and objectives of the study. This chapter also provides an outline of the research framework and contextualizes the study by presenting a brief overview of the background, problem statement and a brief general literature survey of ^{68}Ge/^{68}Ga generator.

Chapter two: This chapter presents the literature review which covers relevant aspects of ^{68}Ge/^{68}Ga generator in general and specifically TiO$_2$ based systems. Secondly, the chapter

also presents an overview of iThemba LAB as the radionuclides production facility with the focus on key radioinuclides, their characteristics, and applications in different fields. Lastly, the chapter also describes the mechanisms attributed to the production of $^{68}Ge/^{68}Ga$ generators.

Chapter three: This chapter gives an account of the materials used, the study design and methodologies, and gives the rationale behind the selection of the procedure for TiO_2 experimental work. Details of the actual methodologies and research instruments used and the relevant analysis techniques are presented in this chapter.

Chapter four: The results and discussion of the TiO_2 based $^{68}Ge/^{68}Ga$ generator are presented in this chapter. The chapter will focus on parameters such as production method, final product, chemical separation and lastly if the ^{68}Ga radionuclide produced complied with certain specifications as per regulatory requirements.

Chapter five: The summary of the main findings of the study is presented in this chapter. The conclusions and recommendations for possible future work are also presented in this chapter.
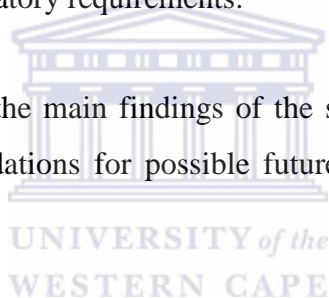
Chapter Two

LITERATURE REVIEW AND INSTRUMENTAL TECHNIQUES

2.1 Background

2.1.1 Overview of Radionuclide Production

Accelerated charged particles from a cyclotron can be used to induce many different nuclear reactions, the heavy residues of which often include useful radionuclides for biomedical imaging, internal radiotherapy and various kinds of tracer studies. This process realizes the ancient alchemist's dream – the ability to transform one element into another. Cyclotron-produced radionuclides are usually proton-rich (Van der Meulen, 2008).

Another way of creating radionuclides is by means of neutron-induced reactions in a nuclear reactor. Although the reactor-produced radionuclides are often comparatively cheaper than cyclotron-produced ones, they usually have a much lower specific activity than those produced using a cyclotron. Nevertheless, accelerator and reactor produced radionuclides are complementary, most neutron-induced reactions leading to radionuclides which are neutron-rich. Even though the two production methods create wholly different classes of radionuclides, both are important in biomedical applications. Cyclotron-produced radionuclides have become increasingly popular in the medical field (especially the PET radionuclides) and in the industrial field, as well as for research purposes (Van der Meulen, 2008).

Radionuclides produced at iThemba LABS are generally used to prepare radiopharmaceuticals for medical diagnostic purposes, such as the possible diagnosis of tumours in the human body. The radiopharmaceutical is either injected into the body or ingested by the patient. The radiopharmaceutical makes it possible for the nuclear medicine

departments in hospitals to identify any tumours, as they scan the body, providing high-quality images of the activity distribution in the patient's system (Van der Meulen, 2008).

To produce a radionuclide and/or radiopharmaceutical (Van der Meulen, 2008; Van der Walt and Vermeulen, 2004), the following are important factors to consider:

- The production method, involving the bombardment as well as the chemical separation of the radionuclide, must be economically viable.

- The final product must have a high specific activity, with little or, preferably, no radionuclidic, radiochemical or chemical impurities.

- The chemical separation must be as simple as possible, making it easy to perform the production within a hot cell with the minimum radiation exposure to the technician.

- The radionuclide and/or radiopharmaceutical must comply with certain specifications as per regulatory requirements.

According to Röesh and Riss (2010) a carrier-free radionuclide is one that is recognized as having a high specific activity, high radionuclidic purity (i.e. free from other radionuclides), high radiochemical purity (i.e. free from any chemical form other than the required chemical form of the radionuclide) and high chemical purity (i.e. a low presence of non-radioactive material). Whereas the chemical and radiochemical purity levels in a final product are determined solely by the efficiency of the chemical procedures, the radionuclidic purity of the product is determined by both chemical and physical means. Two types of radionuclidic impurities can be distinguished, namely, radionuclides present in the product other than that of the desired product, which can be reduced to acceptable levels by chemical means, and radionuclides of the same element as that of the product, i.e. chemically indistinguishable from the desired radionuclide (Van der Meulen, 2008).

Quality control is performed on the final product to determine its adherence to the specifications of international regulatory requirements (generally based on European Pharmacopeia). A high-resolution gamma ray spectrometer is used to determine the radionuclidic purity, while the radiochemical purity is determined using paper, gel or thin layer chromatography. The chemical purity is determined using induced coupled plasma emission spectrometry, electrothermal atomisation spectrometry, flame atomic absorption spectrometry or colorimetric spectrophotometry. The radiochemical separation i.e. the

separation of the radionuclide of interest from its target material and co-produced contaminates is the most critical aspect of the production process to ensure a high quality product is produced (Van der Meulen, 2008).

2.1.2 History of Cyclotron Facilities in South Africa

The first cyclotron built in South Africa in 1956 was located in Pretoria and was managed by the Council for Scientific and Industrial Research (CSIR). This cyclotron was designed to produce both internal and external beams of protons (5.8 – 15.3 MeV), deuterons (11.5 – 17.3 MeV), ^{3}He (18 – 38 MeV) and alpha particles (23 – 34.6 MeV), making it a versatile machine for radionuclide production. The routine radionuclide production programme existed from 1965 until its closure in 1988 (Van der Meulen, 2008).

The radionuclide production programme in Pretoria began by producing radionuclides such as ^{67}Ga, ^{109}Cd and ^{123}I, albeit in relatively low quantities. The radiochemical separations of these radionuclides were performed in normal ("cold") laboratories, using fume cupboards and a few lead bricks for shielding purposes. The methods used to separate the radionuclides from their respective target materials were based on solvent extraction and co-precipitation, which resulted in staff members involved being directly exposed to high levels of radiation (Van der Meulen, 2008).

Operators tended to pick up a severe hand dose, as well as an unacceptable radiation dose to the head area (in terms of today's standards), when performing solvent extraction procedures. Contamination issues were also rife in those early days as a result of the grease on the glass tap at the bottom of the extraction flask dissolving in the organic solvent used in the solution, allowing radioactive solution to seep through the bottom of the flask. The situation was aggravated by the fact that the operator would have to shake the flask, thereby spraying the radioactivity over himself and contaminating the laboratory at the same time. It was as a result of these issues that production procedures were converted to more user-friendly techniques such as ion exchange chromatography and distillation. This paved the way for South African radiochemists to perform productions more efficiently, safely and produce a final product that was more radiochemically pure (Van der Meulen, 2008).

While there was a discussion to build a bigger cyclotron in the Transvaal area (now known as Gauteng), the government decided that a new facility was to be built in the Cape Province (now known as Western Cape). The National Accelerator Centre (name change to iThemba LABS in 2001) was established in Faure, near Somerset West in 1977 under the management of the CSIR. The new 200 MeV Separated Sector Cyclotron (SSC) at Faure produced its first extracted proton beam in 1987. The new facility was mandated to support three main disciplines: 1) sub-atomic nuclear physics research using accelerated ion beams, 2) radiotherapy using both neutrons and protons, and 3) radionuclide production. The Radionuclide Production Department (RPD) produced its first routine radionuclides such as ^{67}Ga, ^{81}Rb/^{81}Kr generators and ^{123}I in 1988. These three radionuclides have been in production at Faure ever since (Van der Meulen, 2008).

Various other radionuclide and radiopharmaceutical products have been added to the list in the years to follow, some of which have been discontinued due to a lack of market interest. Some of the radionuclides which were regularly produced and later discontinued are ^{111}In, ^{201}Tl, ^{81}Rb, ^{64}Cu, ^{88}Y, ^{133}Ba, ^{139}Ce, ^{109}Cd and ^{103}Pd (Van der Meulen, 2008). Today, iThemba LABS produces ^{123}I labeled products, ^{67}Ga-citrate, ^{18}F-FDG, ^{68}Ge/^{68}Ga generators, ^{22}Na and ^{22}Na positron sources and ^{82}Sr (Rb metal target).

Five accelerators are currently operated by iThemba LABS, four of them are at the Faure facility: the SSC, the 8 MeV injector cyclotron (SPC1) providing light ions for the SSC, a second 8 MeV injector cyclotron (SPC2) providing heavy ions and polarized protons for the SSC and the 6 MeV Van der Graaff accelerator with a Nuclear Microprobe used for material science. The SSC is a variable-energy machine capable of accelerating protons to a maximum energy of 200 MeV. A 6 MeV Tandem Accelerator coupled to the Accelerator Mass spectrometer (AMS) is at the iThemba LABS (Gauteng) facility. A layout of the SSC facility and the various disciplines it services is shown in Figure 2.1.
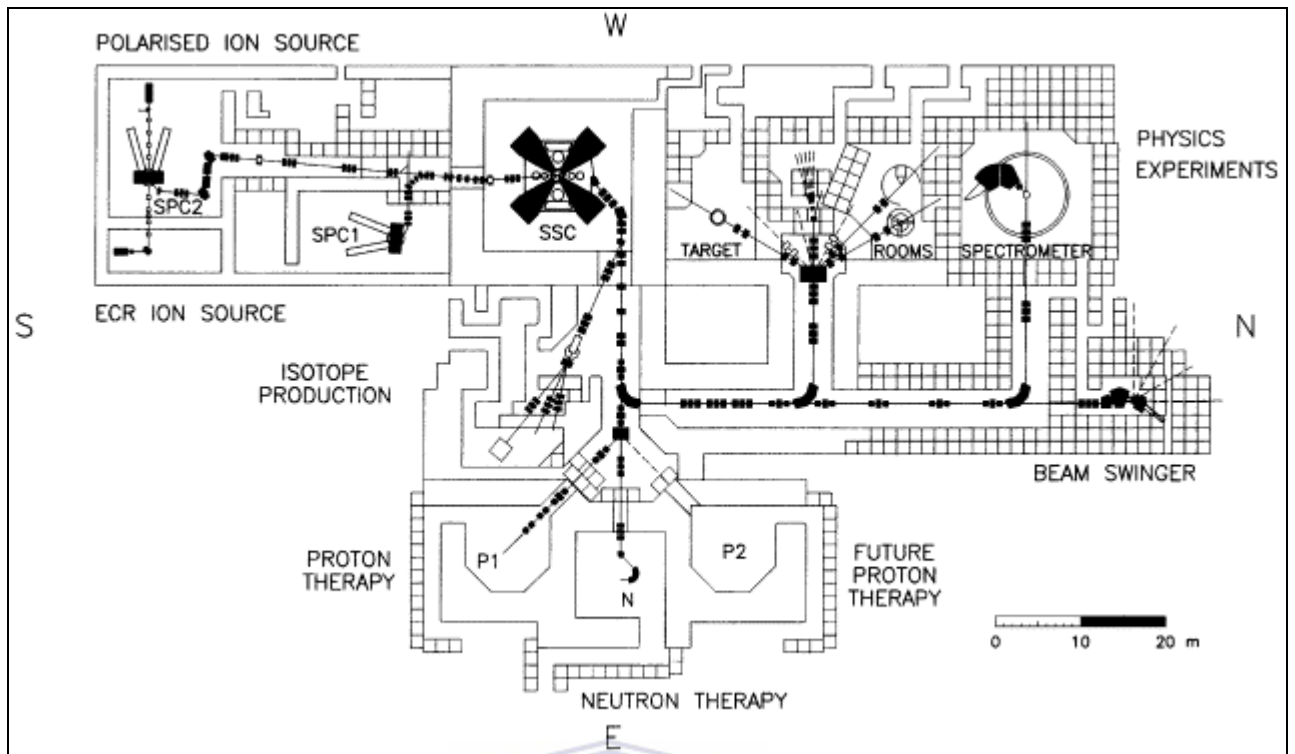
Figure 2.1: The Separated Sector Cyclotron facility layout at iThemba LABS

2.1.3 iThemba LABS Radionuclide Production Facility
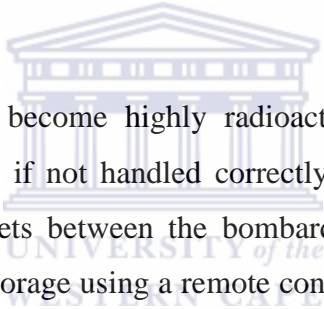
The primary mandate of the Radionuclide Production Department of iThemba LABS is 1) to provide an efficient supply of radionuclides and radiopharmaceuticals to the South African Nuclear Medicine community, 2) to provide radionuclides for the export market to aid cost recovery and, 3) to have an active research and development and training programme that supports the above services (Van der Meulen, 2008).

The building layout of the Radionuclide Production Department was strongly influenced by the safety considerations and regulatory requirements for the production, storage and control of radioactive material. The complex is divided into three areas, namely, the so-called "red", "blue" and "white" areas. The "red" area is a high-risk radiation environment where high levels of activity are handled, while the lower-risk or low-activity materials are handled in the "blue" area. The "white" area is, in principle, a clean area and this is where the staff offices, mechanical workshop, electronic workshop and storage areas are located (Van der Meulen, 2008).

Personnel moving from the "red" area to the "blue" area, or from the "blue" area to the "white" area, have to pass through a monitoring and decontamination station. In this way, the accidental spreading of radioactive contamination can be prevented. As the inhalation of radioactivity is a possible health hazard, negative pressures of 50 Pa (in the "blue" area) and 100 Pa (in the "red" area) with respect to ambient pressure are maintained by the air-conditioning system to ensure that any accidentally released radioactive dust, vapour or gases are contained (i.e. won't spread to an area of lower risk).

Support facilities, such as the target transport system, helium-cooling system, water-cooling system, the hot cells and a radioactive waste management system are housed in the "red" area, which also includes two irradiation vaults. Other facilities required, such as those for chemical separation preparation, quality control, cleanrooms for dispensing and radiopharmaceutical labelling are situated in the "blue" area. The packing and dispatch area is located in the "white" area.

Radionuclide production targets become highly radioactive when irradiated and pose a potential health risk to personnel if not handled correctly. This problem is overcome to a large extent by transporting targets between the bombardment stations, hot-cell complex, target loading station and target storage using a remote controlled rail transport system. Once the bombardment of a batch target has been completed, it is transported from the irradiation vault to one (of two) reception hot cells, where the target material is removed from the target holder. The radiochemical separation of the particular radionuclide is performed in one (of twelve) processing hot cells. Note that a designated hot cell is used for each of the routinely produced radionuclides in order to prevent any cross contamination of the final product. Once the chemical separation has been completed and the radiopharmaceutical prepared, it is transported to the dispensing laboratory, where, under the guidance of the pharmacist, the dispensing of products in aseptic conditions are performed according to the orders received from the client. A sample of the final product will be taken for quality control purposes (e.g. chemical purity, radionuclidic purity, etc.) to ensure that it meets the prescribed specifications as registered with the relevant regulatory authorities (Van der Meulen, 2008).

After the product has been dispensed into patient doses, the vials containing the radiopharmaceutical are sealed and packed into lead pots. The lead pots, in turn, are packed into tins and sealed, before placing them into their respective boxes. The boxes are dispatched to the various hospitals or clinics via road or air transport.

2.1.4 Positron Emission Tomography (PET)

Positron emission tomography (PET) is an imaging method which uses gamma radiotracers to track the biochemical, molecular, and/or physiological processes in humans and animals. A considerable amount of literature (Meyer et al., 2004; Meyer et al., 2005; Keidar et al., 2003) has been published on PET. These studies suggest that Positron Emission Tomography (PET) is based on the detection in coincidence of the two 511 keV photons emitted in completely opposite directions after annihilation of the electron-positron pair. Positrons can be emitted by a radioactive decay of a neutron-deficient nucleus. A proton in the nucleus is converted to a neutron, a positron and a neutrino. In the interaction with matter a positron loses its energy by excitation or ionisation. Finally it collides with an electron and annihilates to produce (in most cases) two photons of 511 keV, which are emitted in opposite directions. PET detectors in return detect the back to back annihilation photons that are produced when a positron interacts with an ordinary electron (Figure 2.2).
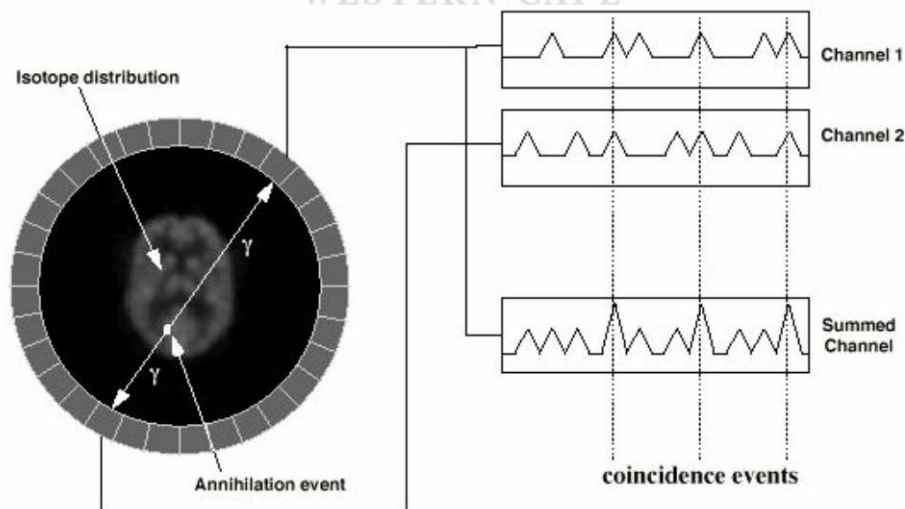
Figure 2.2:   Coincidence detection in a PET camera (from University of Washington Division of Nuclear Medicine)

By means of ^{68}Ga–labelled peptides such as ^{68}Ga-DOTA-d-Phe(1)-Tyr(3)-octreotide (^{68}Ga-DOTATOC) it is possible, for example, to detect and localize neuroendocrine tumours as well as their metastases with the aid of imaging methods such as PET. With the general growth of ^{68}Ga–labelled peptides work in many academic fields, it is hardly surprising that the relationship between somatostatin-expressing tumours and their metastases has attracted considerable attention in recent years (Hofmann et al., 2001). The ^{68}Ga-DOTATOC accumulates at the correspondingly degenerated cells. These areas emit distinctly higher radiation in comparison with the normal tissue. The radiation is localized by means of detectors and processed into a three-dimensional representation by image processing. The cost-effective production, easy availability and versatile linker-based chemistry system has opened up enormous research interest in the development of ^{68}Ga-labelled radiopharmaceuticals. Unlike ^{67}Ga, which is produced by cyclotron, ^{68}Ga is produced by ^{68}Ge/^{68}Ga generators (Kopecky et al., 1973; Kopecky and Mudrova, 1974; Aardaneh and Van Der Walt, 2006; Zhenorsekov et al., 2007). Applications of ^{68}Ga-labelled peptides with macrocyclic chelating agent 1,4,7,10-tetraazacyclododecane-*N-N',N'',N''*-tetraacetic acid (DOTA) have been successfully introduced by Maecke and colleagues (2005). The applications also allowed bifunctional chelators such as NODAPA-OH (Riss et al., 2008), specifically to target tumour imaging by positron emission tomography (PET). Subsequently, several potential ^{68}Ga-labelled somatostatin analogs such as ^{68}Ga-DOTA-NOC and ^{68}Ga-DOTA-TATE were described and clinically utilized by Prasad and Baum (2010). Recent developments in PET have heightened the need for the preparation of ^{68}Ga-labeled radiopharmaceuticals. One of the most significant current discussions in legal and moral philosophy is the unavailability of a suitable sorbent material. It is becoming increasingly difficult to ignore that ^{68}Ge/^{68}Ga generator development, now - more than ever, requires the systematic chemical, radiochemical, technological and radiopharmaceutical characteristics, to guarantee reliable, highly-efficient and medically approved ^{68}Ge/^{68}Ga generator systems.

2.1.5 Single Photon Emission Computed Tomography (SPECT)

Receptors identified with somatostatin analogues labelled with ^{68}Ga, using SPECT and PET respectively, has led to a major breakthrough in the management of neuroendocrine (NE) tumours. Localization and staging of endocrine tumours depends on the conventional anatomical modalities such as computed tomography (CT), ultra sound (US) or magnetic resonance imaging (MRI) and transport mechanisms in the presence of high density of

membrane receptors (Keidar et al., 2003). Functional and metabolic imaging using single photon emission tomography such as ^{68}Ga may detect a tumour prior to its visualization on CT with an impact on the treatment strategy. SPECT studies use radiopharmaceuticals labelled with a single-photon emitter that emits one gamma-ray photon with each radioactive decay event. Again, ^{68}Ga is readily available from a ^{68}Ge/^{68}Ga generator, making it less expensive as a single photon emitter labelling isotope. Like any technology, emission tomography is constantly evolving, with improvements taking place in four broad areas: radiotracers, imaging systems, hardware components and protocols. The goal, as far as radiotracers are concerned, is that the radiotracer be designed to maximise the information its distribution conveys about human bodies (Wernick and Aarsvold, 2004). Recent studies indicated a possible role for ^{68}Ga-chloride to monitor bone healing in experimental osteomyelitis (Makinen et al., 2005) and for pancreatic adenocarcinoma xenografts in rats (Ujula et al., 2009).

2.2 Radionuclide Generator Principle

A radionuclide generator is a self-contained system housing a mother/daughter mixture in equilibrium and designed to produce a daughter radionuclide formed by the decay of a mother radionuclide free from contamination of the mother (Bjørnstad, 2004 and International Atomic Energy Agency, 2005). The mother/daughter nuclear relationships offer the possibility to make radionuclide generators to separate the short lived daughter at suitable time intervals. For practical reasons, most radionuclide generator systems that can be used for industrial radiotracer applications involve secular equilibrium, where the parent radionuclide has a half-life significantly longer than that of the daughter. This scenario permits long shelf life of the generator.
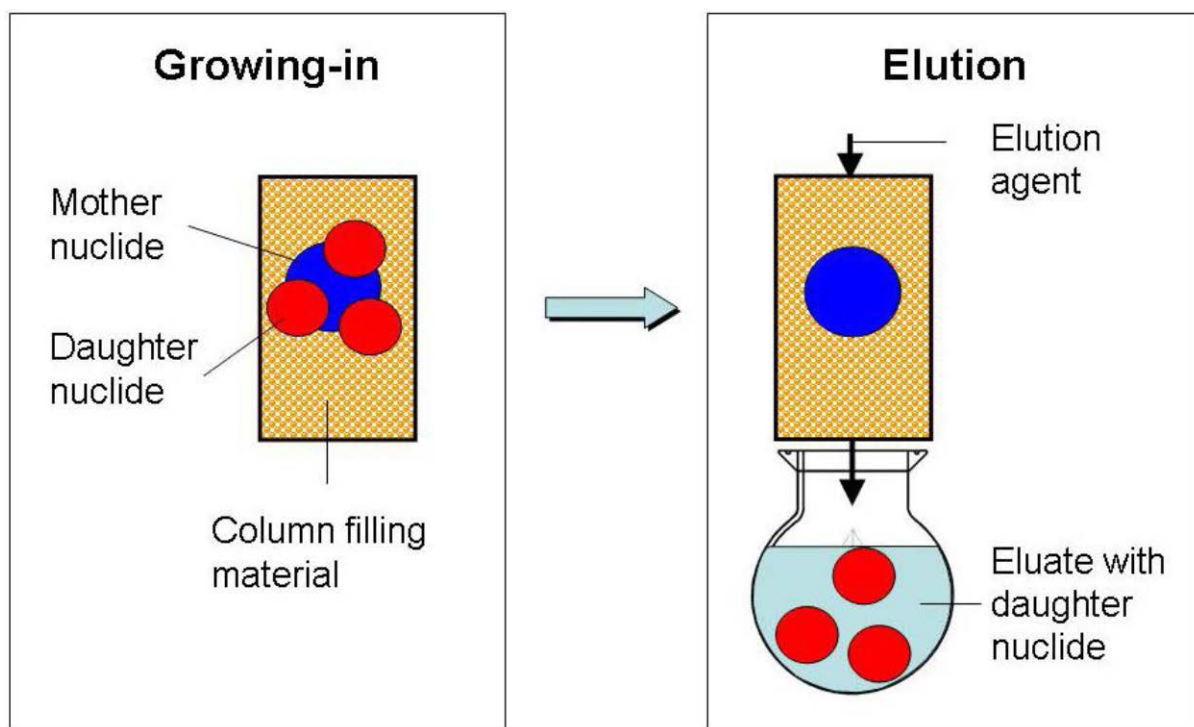
Figure 2.3: Principle of a column based radionuclide generator (International Atomic Energy Agency (IAEA), 2013)

Moreover, it is necessary to ensure that there is a method of removing the daughter and leaving the mother behind to regenerate more daughter activity. Recent evidence (Rösch and Knapp, 2003) suggests that the daughter radionuclide is a different chemical element to the mother, and will therefore exhibit chemical and physical properties different from those of the mother. With this difference in characteristics between mother and daughter radionuclides, the latter can usually be separated by chemical or physical means. It is said (Gleason, 1960) that the daughter is eluted from the generator (a radionuclide generator is also commonly called a 'cow' and the elution process 'milking of the cow'). Once the activity of the daughter is recovered, there is a growth of the daughter activity on the generator until it again reaches equilibrium with the mother. This separation and growth can be continued as long as there are useful amounts of the parent radionuclide available, and the breakthrough of the mother stays within acceptable limits. In Figure 2.3, the principle of the ^{68}Ge/^{68}Ga generators is illustrated.

For the past three decades, a good deal of attention has been paid to how researchers constructed conceptual and procedural understandings of ^{68}Ga generators. As a result, a

number of theories have become increasingly refined to explain how researchers construct and modify their ^{68}Ge/^{68}Ga generator knowledge structures. This was due to the interest in radionuclide ^{68}Ga in nuclear medicine, especially for use in positron emission tomography (PET). ^{68}Ga is best obtained via a ^{68}Ge/^{68}Ga generator system. The parent radionuclide ^{68}Ge has a long half-life of 270.82 days and decays 100 % by electron capture to the short-lived daughter ^{68}Ga ($t_{1/2}$ = 67.63 min) which decays mainly by positron mission (β^+ = 89%, EC = 11%) and therefore is suitable for PET imaging (Zhernosekov et al., 2007).

An ideal generator should possess the following properties (Bjørnstad, 2004 and International Atomic Energy Agency, 2005):

• The chemical and/or physical properties of the daughter must be different from those of the mother to permit efficient separation of daughter from mother.

• The separation of the daughter radionuclide should be easy and efficient using appropriate chemical or physical techniques.

• The daughter radionuclide separation should involve no violent chemical reactions.

• Human intervention in generator operation should be minimal to minimize radiation dose.

• The daughter radionuclide to be used as a tag on tracers for radiotracer investigations should be short lived and gamma emitting.

• In any case, a gamma emitter with a high gamma branching ratio is desirable.

• The elution yield and purity of the daughter radionuclide should be within the acceptable range.

• The physical half-life of the parent should be long enough for extending the shelf life of the generator.

• The generator constituents (i.e. eventual column packing material, liquids involved, tubings and fittings) should be radiation resistant.

• The daughter chemistry should be amenable to the preparation of a wide variety of compounds for radiotracer applications (such as water tracing, oil tracing, particle tracing, etc.).

• Shielding, handling and transportation of the generator, even across national borders, should be straightforward.

• The grand-daughter should be stable (or very long lived) to limit concern about site contamination, environmental persistence and waste disposal issues.

2.3   Production of Germanium Radionuclide

The Germanium-68 (^{68}Ge), as the parent of the positron emitter ^{68}Ga, is commonly produced via the ^{69}Ga (p, 2n) ^{68}Ge nuclear reaction.

$$^{69}_{31}\text{Ga} + ^{1}_{1}\text{p} \longrightarrow ^{68}_{32}\text{Ge} + 2\,^{1}_{0}\text{n}$$

(2.1)
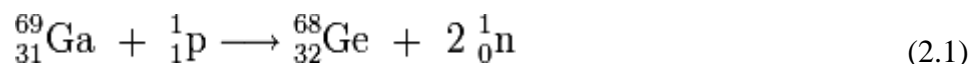
^{68}Ga, which has the physical characteristics desirable for PET, is obtained via the decay of ^{68}Ge, making the production of ^{68}Ge an important factor. ^{68}Ge, having a half-life of 288 days, decays entirely by electron capture to produce ^{68}Ga ($T_{1/2}$ = 68 m), which disintegrates mainly by positron emission (89%) to a stable ^{68}Zn. The daughter (^{68}Ga) is obtained from ^{68}Ge when in secular equilibrium with the mother.

The chemical and mechanical designs of the target are crucial issues, mainly owing to the thermal aspects of high current irradiations, as the power dissipating the targets reaches values of about 300–1000 W or more. It is mandatory to provide sufficient cooling for thermal stability of a given target. Thus the main criteria are adequate thermal properties such as the melting points, boiling point and heat transfer coefficients of the target materials and their cooling systems. Other criteria are corrosion and radiation resistance. For Ga(p,xn) production routes, potentially useful target compounds include Ga_2O_3 with melting point: 1900 °C and Ga_4Ni alloy with melting point: 900°C (Horiguchi et al., 1983). Mixtures of Ga metal as well as Ga_2O_3 and Ga_2O have been used (Naidoo et al., 2002). At iThemba LABS, the Ga metal with melting point of 29.8°C is used as a target material. These Ga targets are encapsulated in corrosion resistant Nb canisters that allow for effective water and helium cooling of the target (Van der Walt & Vermeulen, 2004).

2.4   Background of Properties of ^{68}Ge/^{68}Ga generators

Productions, radiochemical processing and quality evaluation of ^{68}Ge suitable for use in ^{68}Ge/^{68}Ga generator were elaborated by Röesh & Knapp (2003) and Röesh & Filosov (2010). The production of a generator covers various aspects in the production chain that involves the radiochemical separation of the radionuclide, ^{68}Ge, from the target material, the chemical and technical construction of the radionuclide generator using the processed ^{68}Ge and then finally the quality control evaluation of the generator. Processes for the production of the generator

for clinical applications generally should follow Good Manufacturing Practice (GMP) standards (Röesh and Riss, 2010).

2.5   Review of Radionuclide Generators

Various $^{68}Ge/^{68}Ga$ generators have been developed using various absorbent material as a column eluate. Some studies included the use of inorganic matrices such as alumina, $Al(OH)_3$ and $Fe(OH)_3$, (Kopecky et al., 1973, 1974), SnO_2 (Loc´h et al., 1980), ZrO_2 (Pao et al., 1981; Neirinckx and Davies, 1980), TiO_2 (Kozlova et. al., 1970) and CeO_2 (Bao and Song, 1996). One of the first generators with high elution yields of >75% and low ^{68}Ge breakthrough was reported by Loc'h et al., (1980) who used SnO_2 as the column matrix and 1M HCl as the eluting media.

The latest reviews have shown that the Kozlova et al., (1970) paper was the only published work around a TiO_2 based $^{68}Ge/^{68}Ga$ generator. It was reported that sorption of the ^{68}Ge on the modified TiO_2 was done in a 0.001-0.05 M HCl range which only allowed for 95% retention of the ^{68}Ge on the column eluate. Elution of the ^{68}Ga using 0.1 M HCl as the eluting media (5 ml) had an efficiency of 60% at calibration time and decreased to 35% over 2 years or 200 elutions. The ^{68}Ge breakthrough was reported to be $<5 \times 10^{-3}$ over the same period. The metal impurities (Ti, Fe, and Si) in the 5 ml eluate were found to be < 2 ppm in total. The micron size of the modified TiO_2 used as the column eluate was not specified and this was perhaps due to commercial intellectual property rights. The work by Kozlova and colleagues (1970) will serve as a basis for the work that will be investigated in this thesis.

Early generator systems separated ^{68}Ga as an EDTA complex from ^{68}Ge, absorbed on Al_2O_3, Sb_2O_5, ZrO_2, TiO_2, $Fe(OH)_3$ and SnO_2 (Green and Tucker, 1961). The eluents used for the elution of ^{68}Ga were diluted EDTA, HCl and HNO_3 or NaOH. Among these studies, Loc'h et al., (1980) have defined a very promising commercially available generator of ionic ^{68}Ga based on elution from tin dioxide with 1 N HCl, with special regard to the simplicity of the operation. Sadeghi et al., (2009) studied the separation of ^{68}Ga from proton irradiated ^{68}Zn using cation exchange resin (BIO-RAD AG 50W) and used a solvent extraction method to achieve high purity ^{68}Ga. Average yields of ^{68}Ga of 75% during a period of 250 days were reported (Schumacher and Maier-Borst, 1981). The Ge breakthrough was < 1 ppm. The

pyrogallol-formaldehyde resin was found by Schumacher et al., (1981) and Neirinckx et al., (1980) to be resistant to dissociation from radiation. Another generator system was developed using an organic polymer containing N-methylglucamine groups as adsorbent for ^{68}Ge (Nakayama et al., 2003). The ^{68}Ga was eluted from the resin with a solution of low-affinity gallium chelates such as citric or phosphoric acid. The ^{68}Ge leakage was reported to be less than 4×10^{-4}%.

Organic ion exchange resins such as Bio-Rad AG1-X8 as well as synthetic chelate resins (condensation of pyrogallol and formaldehyde) using dilute hydrofluoric acid solutions as an eluent allowed high purity separations due to the significant differences in distribution coefficients of the ^{68}Ga and ^{68}Ge elements (Neirinckx and Davies, 1980; Neirinckx et al., 1980; Schumacher and Maier-Borst, 1981). The breakthrough of ^{68}Ge was $<10^{-4}$ for up to 600 elutions, and the ^{68}Ga yield was >90%. Another generator system was developed using an organic polymer containing N-methyl-glucamine groups as adsorbent for ^{68}Ge (Nakayama et al., 2003). The ^{68}Ga was eluted from the metal oxide with a solution of low-affinity gallium chelates such as citric or phosphoric acid. The ^{68}Ge leakage was reported to be less than 4×10^{-4}%. Unfortunately, organic polymers have relatively low radiation stability compared to their inorganic competitors (Sen et al., 2012)

Recently, a new nanoceria-polyacrylonitrile (PAN) composite sorbent has been synthesized by decomposition of a cerium oxalate precursor to cerium oxide and its subsequent incorporation in PAN matrix for the development of a clinical grade ^{68}Ge/^{68}Ga generator (Chakravarty et al., 2011). The X-ray diffraction (XRD) studies and BET nitrogen adsorption technique revealed that nanocrystalline ceria had an average particle size of approximately 10 nm, surface area of 72 +/- 3 m^2/g and an average pore size of 0.38 +/- 0.01 nm. Investigation of the distribution values [K(d)] for the prepared sorbent in 0.01 N HCl medium revealed the suitability of the sorbent for the quantitative retention of ^{68}Ge and efficient elution of clinical grade ^{68}Ga. ^{68}Ga could be regularly eluted from this kind of generator with >80% elution yield. The eluted ^{68}Ga possessed high radionuclidic purity ($<1 \times 10^{-5}$% of ^{68}Ge impurity), chemical purity (<0.1 ppm of Ce, Fe and Mn ions) and was amenable for the preparation of ^{68}Ga-labeled radiopharmaceuticals. Furthermore, it was reported (Chakravarty et al., 2011)

that the generator gave a consistent performance with respect to the elution yield and purity of ^{68}Ga over an extended period of seven months.

On the other hand, nano-zirconia was also synthesized by Chakravarty et al., (2011) using an in situ reaction of zirconyl chloride with ammonium hydroxide in alkaline medium. The material synthesized was nanocrystalline with average particle size of ~7 nm, pore-size of ~0.4 nm and a high surface area of 340 ± 10 m^2g^{-1}. ^{68}Ga could be regularly eluted from this generator in 0.01N HCl medium with an overall radiochemical yield >80% and with high radionuclidic (<10^{-5}% of ^{68}Ge impurity) and chemical purity (<0.1 ppm of Zr, Fe and Mn ions).
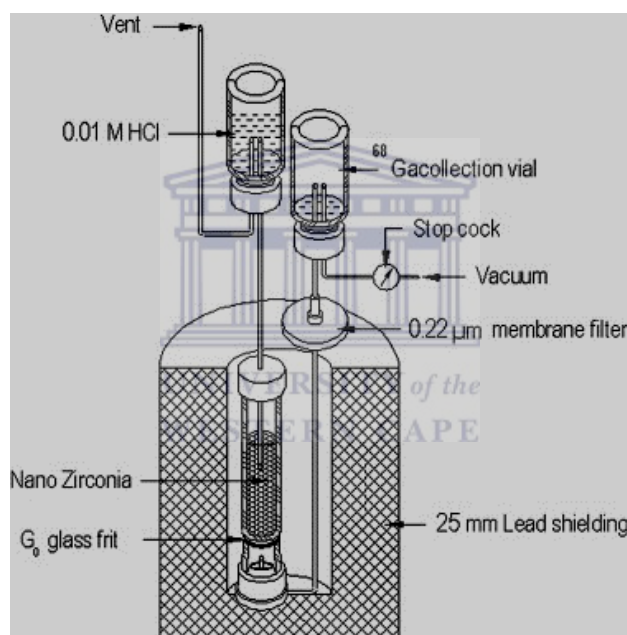
Figure 2.4: A nanozirconia (ZrO$_2$) ^{68}Ge/^{68}Ga generator (Chakravarty et al., 2011)

Again, the compatibility of the product for preparation of ^{68}Ga-labeled DOTA-TATE under the optimized reaction conditions was found to be satisfactory in terms of high labeling yields (>99%). The generator gave a consistent performance with respect to the elution yield and purity of ^{68}Ga over a period of 1 year. However, these generators are not commercially available due to the fact that they are not optimally designed for direct applications in a clinical context.

It is well known that the most widely used radionuclide generator in nuclear medicine is ^{99m}Tc (Figure 2.5). This accounts for more than 80% of the nuclear medicine applications in the world. The parent, ^{99}Mo, has a half-life of about 66 h, can be produced through neutron activation or fission, can be chemically adsorbed onto an Al_2O_3 (alumina) column and decays to ^{99m}Tc (85%) and ^{99}Tc (15%). ^{99m}Tc has a half-life of 6.02 h, decays to ^{99}Tc by isomeric transition and emits a 140 keV γ-ray (98%) with no associated particulate radiations:

$$^{99}\text{Mo} \longrightarrow {}^{99m}\text{Tc} \longrightarrow {}^{99}\text{Tc} + \gamma \qquad (2.2)$$
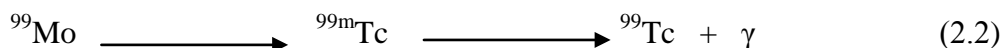
Figure 2.5: ^{99m}Tc Generator from China Institute of Atomic Energy (CIAE)

The ^{99m}Tc is 'milked' from the chromatographic column of alumina by passing a solution of isotonic saline through the column (0.9% NaCl). This saline solution and the solid phase of Al_2O_3 allow for efficient separation of ^{99m}Tc from the ^{99}Mo with only minute amounts of ^{99}Mo breakthrough (less than 0.1%). The eluted ^{99m}Tc can be chemically manipulated so that it binds to a variety of compounds, which will then determine its fate in vivo.

For commercial generator productions, a modified TiO_2 phase has been used by Cyclotron Ltd, Obninsk, Russian Federation, since about 2000 (see Figure 2.6). These generators are eluted with 0.1N HCl and show initial ^{68}Ga elution yields of about 80%, with ^{68}Ge breakthrough of about 1×10^{-3}%. These data deteriorate over time (e.g. after about 1 year) or with increasing number of elutions (e.g. 200), approaching values of about 50% of ^{68}Ga elution and about 10^{-2}% of ^{68}Ge breakthrough.

Figure 2.6: A 10 mCi (370 MBq) commercial TiO_2 generator from Obninsk, Russia by Cyclotron Company Limited

Another possible method for producing ^{68}Ga was engineered by Eckert and Ziegler Company whereby a $^{68}Ge/^{68}Ga$ generator in a form of a stand-alone device was manufactured. The apparatus is a fully-shielded generator and consists of a boro-silicate glass column with TiO_2 matrix. An example of such a generator is shown in Figure 2.7. Other reports (Baum and Röesch, 2012) on the model IGG100 generator system are that the IGG100 requires no disassembly and it is shipped ready-to-use. Next, the $^{68}Ge/^{68}Ga$ generator is eluted with 0.1 M HCl; when new, the $^{68}Ge/^{68}Ga$ generator will meet a minimum elution efficiency of 65%. The breakthrough for this generator typically ranges from $3x10^{-5}$% when new to $5x10^{-3}$% after 200 elutions. The actual ^{68}Ge activity at the assay date is indicated on the label at the side of the generator. The minimum efficiency must be measured from a freshly eluted generator, specifically the measurement elution must occur within 24 hours of a prior elution.

Figure 2.7:   An Eckert and Ziegler Isotope Production ^{68}Ge/^{68}Ga generator, Berlin

In addition, the potential of silica gel as a sorbent for reducing a ^{68}Ge/^{68}Ga radionuclide generator for clinical use was recognized by Caletka and Kotas (2004) as well as Neirinckx and Davies (1980). The silica gel typically has an average particle size of 10-150 μm and an average pore size of 6-50 nm. Recently an improved technology generator using silica gel as a non metallic sorbent for ^{68}Ga generator production has been developed by Sen et al., (2012). Consequently, today, Isotope Technologies Garching Company, ITG Co. is commercializing a silica based ^{68}Ga generator (Figure 2.8).

Figure 2.8: Manual self-shielded ^{68}Ge/^{68}Ga generator system (Isotope
Technologies Garching)

The generator shown in Figure 2.8 gives a radiochemical yield of 85% using an ion exchange column (AG 50W-X4 (-400 mesh, H$^+$-form and AG 1-X8, 200-400 mesh, Cl$^-$ form, Bio-Rad Laboratories, USA). Compared to the other generators on the market, the percentage of ^{68}Ge breakthrough was found to be $\leq 10^{-5}$% of the total ^{68}Ga activity (Sen et al., 2012).

In a comparative study, a generator with SnO_2 (Aardaneh and Van der Walt, 2006) as a sorbent for a ^{68}Ga daughter radionuclide was produced at iThemba LABS, Republic of South Africa, and commercialized by IDB Holland B.V. (see Figure 2.9).

Figure 2.9: iThemba LABS SnO_2 based $^{68}Ge/^{68}Ga$ generator (Somerset West, South Africa)

The generator is eluted with 0.6 M HCl (suprapur) and has a ^{68}Ga elution efficiency of >80% in 5 mL of eluate and the ^{68}Ge breakthrough from the column in the eluate is < 0.002% at calibration time. A weakness with this generator, however, is that it uses a stronger acidic solution (0.6 M HCl) for the elution; an undesirable factor for processing of coordination chemistry for labelling of PET radiopharmaceuticals.

2.6   Current State/Outlook of the $^{68}Ge/^{68}Ga$ Generators

Today, $^{68}Ge/^{68}Ga$ radionuclide generators are commercially available and should satisfy four key parameters: 1) high ^{68}Ga elution yield, 2) low concentration of ^{68}Ge breakthrough, 3) no metallic ion impurities and 4) high chemical and radiation stability. As noted by Röesch and Knapp (2003), the separation technique should provide effective elution yield and highest radiochemical purity (i.e. lowest breakthrough of long-lived parent radionuclide). In an attempt to go beyond production of ^{68}Ge and separation of ^{68}Ga radionuclide, studies have focused on anything from elution efficiency, factors affecting elution yield, purity of the generator eluate radionuclidic purity, radiochemical purity and chemical purity.

While some research had focused only on the radiolabelling efficacy evaluation, other work has sought to show how inorganic matrices such as TiO_2, SnO_2, AlO_3, ZrO_2, $Al(OH)_3$ and

Fe(OH)$_3$ still assist developments of the ^{68}Ga generator. Some studies, however, have taken a different approach by looking at organic matrices in order to find answers to some of the challenges associated with routine clinical use. In a typical study of this type, Nakayama et al., (2003) developed an organic polymer containing N-methylglucamine groups as adsorbent for ^{68}Ge. The main limitation of their approach was the radiation degradation sensitivity of the organic matrix over the expected lifetime of the ^{68}Ga generator.

In a landmark study, Kozlova 's pioneering work (Kozlova et al., 1970) suggested that TiO$_2$ metal oxide displayed a range of features, such as 95% ^{68}Ge retention, 0.001-0.05 M HCl eluent and less than 5x10^{-3}% ^{68}Ge breakthrough. In addition, the metal impurities such as Ti, Fe and Si were found to be less than 2 ppm. While there are clearly some problems with Kozlova's work - his analysis did not provide specific details about the research he conducted, for example, 0.001-0.05 M HCl eluent and there were no details of how TiO$_2$ modification took place - the emphasis on production of the ^{68}Ga generator, capable of providing a ^{68}Ga eluate suitable for biomedical application has understandably remained at the centre of the present study.

2.7   Quality Control Techniques of the ^{68}Ge/^{68}Ga Generators

2.7.1   γ-ray Spectrometry

Part of the aim of this study was to collect data produced by emission intensities of the ^{68}Ga and the corresponding electron binding energies by using gamma ray spectrometry. Gamma ray spectral analysis is a powerful tool for identification and measuring radionuclides in a given sample. Analysis consists of determining the energy of each peak in a gamma ray spectrum and the net count rate associated with each characteristic peak of the radionuclides. In return, a radionuclide is identified by comparing the observed characteristic gamma ray peak and other peaks as well as their intensities to published tabulations of radionuclides, listed by gamma ray energies and half life, with additional information on gamma ray fractions. The radionuclide identified by gamma ray energy then is quantified by converting the net count rate measured under the characteristic peak to a disintegration rate by applying its gamma ray counting efficiency, gamma ray decay fraction and radioactive decay between the time of origin (or collection) and of counting. Reliability of radionuclide identification is

improved when several gamma rays attributed to the same radionuclide yield consistent results, whereas inconsistent results suggest errorness attribution.

A considerable amount of literature has been published on ^{68}Ge and ^{68}Ga decay schemes. These studies (Carter et al., 1968, Smith and Williams, 1971, Lange et al., 1973 and Waters et al., 1983) had the following in common:

- ^{68}Ge decays via electron capture to ^{68}Ga (T$_{\frac{1}{2}}$ = 270.95 d).
- The ^{68}Ga formed subsequently decays (T$_{\frac{1}{2}}$ = 67.63 min) to stable ^{68}Zn.
- ^{68}Ga is a positron emitter with 89% positron branching accompanied by low intensity photon emission (1077.4 keV, 3.23%).

A simplified scheme for the decays of ^{68}Ge and its ^{68}Ga daughter is shown in Figure 2.10.
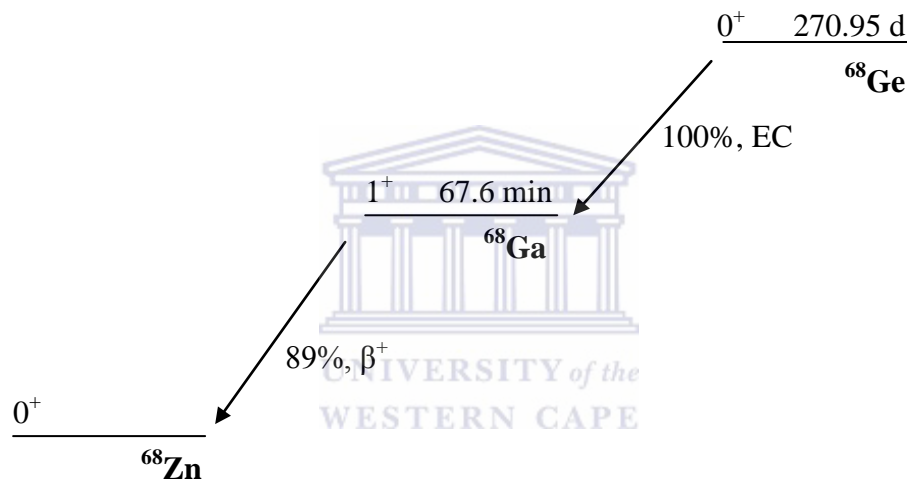
Figure 2.10: Simplified decay scheme of ^{68}Ga. Data taken from Zimmerman et al. (2008)

Earlier work (Carter et al., 1968, Smith and Williams, 1971, Lange et al., 1973 and Waters et al., 1983) also demonstrated that the high branching positron emission (89%) with maximum and mean positron energies of 1.9 and 0.79 MeV, respectively, provides intense 511 keV annihilation photon emission. Some studies (Marsden, 2003; Burger and Townsend, 2003) as a result, have taken a different approach by looking into the localization and tracking of radiopharmaceuticals by Single Photon Emission Computed Tomography (SPECT) as well as by Positron Emission Tomography (PET). In a typical study of this type Saha (2004) confirmed that the annihilation character with two 511 keV photons moving in opposite directions allows for coincidence detection and Positron Emission Tomography (PET).

Positrons can be emitted by a radioactive decay of neutron-deficit nuclei. A proton in the nucleus is converted to a neutron, a positron and a neutrino. In interaction with matter a positron loses its energy due to excitation, ionisation or Bremsstrahlung. Finally it collides with an electron and annihilates to produce (in most cases) two photons of 511 keV, which are emitted in opposite directions (180°). BGO (Bismuth Germanate, $Bi_4Ge_3O_{12}$) detectors are used in most of the PET systems due to higher stopping power because of the higher energy of photons detected. This offers the potential for determination of the radionuclide distribution with high local resolution.

2.7.2   Inductively Couple Plasma Optical Emission Spectroscopy

Inductively coupled plasma optical emission spectrometry (ICP-OES) is an analytical technique used for the detection of trace metals. There are numerous reports on utilization of this technique for analysis of $^{68}Ge/^{68}Ga$ generators (Chakravarty et al., 2011). It is a type of emission spectroscopy that uses the inductively coupled plasma to produce excited atoms and ions that emit electromagnetic radiation at wavelengths characteristic of a particular element. The intensity of this emission is indicative of the concentration of the element within the sample.
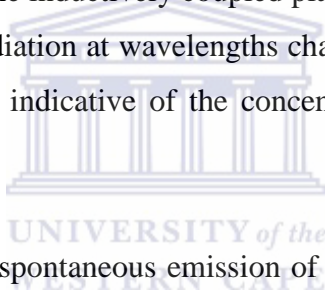
The technique is based upon the spontaneous emission of photons from atoms and ions that have been excited in a Radio Frequency (RF) discharge. Liquid and gas samples may be injected directly into the instrument, while solid samples require extraction or acid digestion so that the analytes will be present in a solution. The sample solution is converted to an aerosol and directed into the central channel of the plasma. At its core the inductively coupled plasma (ICP) sustains a temperature of approximately 10 000 K, so the aerosol is quickly vaporized. Analyte elements are liberated as free atoms in the gaseous state. Further collisional excitation within the plasma imparts additional energy to the atoms, promoting them to excited states. Sufficient energy is often available to convert the atoms to ions and subsequently promote the ions to excited states. Both the atomic and ionic excited state species may then relax to the ground state via the emission of a photon. These photons have characteristic energies that are determined by the quantized energy level structure for the atoms or ions. Thus the wavelength of the photons can be used to identify the elements from

which they originated. The total number of photons is directly proportional to the concentration of the originating element in the sample.

2.7.3 Powder X-ray Diffraction

X-Ray Diffraction (XRD) is a very important technique that has long been used to address numerous issues related to the crystal structures of solids, including lattice constants and geometry, identification of unknown mineral phases, orientation of single crystals, preferred orientation of polycrystals, defects, stresses etc. In XRD, a collimated beam of X-rays with a wavelength typically ranging from 0.7 to 2 Å, is incident on a specimen and is diffracted by the crystalline phases in the specimen according to Bragg's Law (West, 2005):

$$n\lambda = 2d \sin\theta$$

(2.3)

where, n is the order of diffraction, d is the spacing between atomic planes in the crystalline phase and λ is the X-ray wavelength. The intensity of the diffracted X-rays is measured as a function of diffraction angle 2θ and the specimen's orientation. The diffraction pattern is used to measure the specimen's crystalline phases and measure its structural properties. The most commonly used X-ray diffraction technique is the powder diffraction (West, 2005). Powder XRD can be used to determine the average crystallite size of a nanocrystalline material (West, 2005). If the average crystallite size in a powder is below a certain limit (~2000 Å diameter), additional broadening of diffracted X-ray beams occurs. From measurement of this extra broadening an average crystallite size can be obtained. However, a normal diffraction line might also have a finite width due to several reasons: the radiation is not absolutely monochromatic, the Kα line has finite breadth due to Heisenberg Uncertainty Principle and the focusing geometry of the instrument may not be perfect for a variety of reasons. In order to correct for the peak broadening which is caused by the diffractometer due to the aforementioned reasons, the peak broadening of a sample is always measured in comparison with that of a standard material. The crystallite size, D, might be estimated from the peak width using the Scherrer's formula:

$$D = \frac{0.9\lambda}{B\cos\theta}$$

(2.4)

where, λ is the X-ray wavelength and θ is the Bragg angle. B is the line broadening, indicating the extra peak width of the sample in comparison to the standard, derived using the Warren formula, $B^2 = B_M^2 - B_S^2$, where M and S refer to specimen and the standard. B_M and B_S are measured in radians at half the peak height (full width at half maxima, FWHM). The sample and standard must have peaks close to each other. With good experimental techniques, crystallite sizes up to 200 nm can be measured by using the Scherrer formula. In the range of 5-50 nm, the broadening is easy to determine. At larger particle sizes, the difference between the sample and standard is small and at small particle sizes, the peak is difficult to distinguish from the background. For smaller particles, low angle peaks are used for size determination as they are less broad compared to the large angle peaks.

2.7.4 X-ray Fluorescence

The analysis of major and trace elements in geological materials by x-ray fluorescence is made possible by the behaviour of atoms when they interact with radiation. Cesareo et al., (2000) explains that when materials are excited with high-energy, short wavelength radiation (e.g., X-rays), they can become ionized. If the energy of the radiation is sufficient to dislodge a tightly-held inner electron, the atom becomes unstable and an outer electron replaces the missing inner electron. When this happens, energy is released due to the decreased binding energy of the inner electron orbital compared with an outer one. The emitted radiation is of lower energy than the primary incident X-rays and is termed fluorescent radiation. Because the energy of the emitted photon is characteristic of a transition between specific electron orbitals in a particular element, the resulting fluorescent X-rays can be used to detect the abundances of elements that are present in the sample. The energy of the emitted X-ray identifies the element and the number of X-rays of a given energy is a measure of the concentration of that element in the sample matrix (Hechel and Ryon, 2001).

2.7.5 High Resolution Scanning Electron Microscopy

The basic principle is that a beam of electrons is generated by a suitable source, typically a tungsten filament or a field emission gun (Reimer, 1998; Goldstein, 2003). A normal scanning electron microscope operates at a high vacuum. The electron beam is accelerated through a high voltage (e.g.: 20 kV) and pass through a system of apertures and

electromagnetic lenses to produce a thin beam of electrons, then the beam scans the surface of the specimen by means of scan coils (Reimer, 1998; Eagerton, 2005).

Electrons are emitted from the specimen by the action of the scanning beam and collected by a suitably-positioned detector (Clarke, 2002). The scanning electron microscope (SEM) uses a focused beam of high-energy electrons to generate a variety of signals at the surface of solid specimens. The signals that derive from electron-sample interactions reveal information about the sample including external morphology (texture), chemical composition, and crystalline structure and orientation of materials making up the sample. In most applications, data are collected over a selected area of the surface of the sample, and a 2-dimensional image is generated that displays spatial variations in these properties (Clarke, 2002). Areas ranging from approximately 1 cm to 5 microns in width can be imaged in a scanning mode using conventional SEM techniques (magnification ranging from 20X to approximately 30,000X, spatial resolution of 50 to 100 nm).

2.7.6   Transmission Electron Microscopy

The combination of atomic-resolution Z-contrast microscopy, electron energy loss spectroscopy and first-principles theory has proved to be the means for structure property correlations at interfaces and nanostructures (Pennycook et al., 2003). In a TEM, the electrons are accelerated at high voltage (100-1000 kV) to a velocity approaching the speed of light (0.6-0.9 c); they must therefore be considered as relativistic particles. The associated wavelength is five orders of magnitude smaller than the light wavelength (0.04-0.008 Å). The magnetic lens aberrations limit the convergence angle of the electron beam to 0.5° (instead of 70° for the glass lens used in optics), and reduce the TEM resolution to the Å order. This resolution enables material imaging and structure determination at the atomic level.

2.7.7   Nitrogen (N_2) Gas Adsorption Technique

One of the significant current discussions in pore size analysis is the N_2 gas adsorption principle. Barnes & Gentle (2005) write that adsorption can be defined as the "tendency of one component of the system to have a higher concentration at the interface than it has in either of the adjacent bulk phases". In the case of solid-fluid system, there is an increase in the density of the fluid happens near the solid–fluid interface. Depending upon whether the

force of interaction between the fluid molecules and the surface layer is chemical or physical; adsorption can take place using two mechanisms: physisorption or chemisorption.

Physisorption experiments are done with different gases and at different pressure-temperature conditions. However, lower temperatures and higher pressures will make adsorption more prominent and easier. In low pressure adsorption experiments the temperature–pressure regime is below the critical point of the fluid used. These experiments yield valuable information about the textural properties of porous material, such as surface area and porestructure. Since the gas is below its critical point, capillary condensation becomes important in these experiments which give us the information of pore–sizes. N_2 (at 77 K) is the most commonly used gas for surface area and mesopore characterization, however, alternative gases can also be used, such as krypton (at 77 K), argon (at 87 K), carbon dioxide (at 273 K).

2.8 Overview of the Research Topic

With the general growth of PET work in biomedical applications, it is hardly surprising that the interest in the ^{68}Ga generators has attracted considerable attention in recent years. Research has shown that the chemical properties of ^{68}Ga and ^{68}Ge are different enough to permit an efficient separation of the two radionuclides. Accordingly, problems such as eluate volume, acidity and content of chemical impurity can be controlled (Breeman et al. 2007). Today, the most common commercially available ^{68}Ge/^{68}Ga radionuclide generators are based on TiO_2 and SnO_2 metal oxides (Razbash et al., 2005). The chief focus of the current approach has been to show how systematic chemical, radiochemical and radiopharmaceutical characteristics of SnO_2 and TiO_2 reflect the dominant position of TiO_2 in the radiopharmacy field.

Researchers such as Horiguchi et al., (1983), Kopecky et al., (1973), Kozlova et al., (1970) and Loc'h et al., (1980) have come to believe that obstacles such as eluate volume, chemical form of ^{68}Ga, contamination of ^{68}Ga with other cations, and contamination with ^{68}Ge still need to be solved. There is a general agreement that the ^{68}Ge/^{68}Ga radionuclide generator systems known today are not necessarily optimally designed for direct application in a medical context. For example, these researchers believe that there are some noticeable

differences in the practical handling and work-flow of the generators. Differences in the acidity of the eluate have to be considered in relation to potential post-processing of the eluate. The eluate from the commercial generator still contains measurable activities of long-lived ^{68}Ge. The rather large volume and the relatively high concentration of hydrochloric acid in many cases prevent the direct use for labeling reactions. Labeling yields and specific activities might not reach maximum values due to the presence of metallic impurities.

Much of current research on this topic has been focused on comparisons between, for example, experimental versus routine buildup of the final generator, consideration of the activity scale with regard to radiation stability (radiolysis) and radiation safety of the long shelf life ^{68}Ge/^{68}Ga generator system, regulatory requirements and commercial logistics. While Kozlova and colleagues' (1970) work lacks some critical information, the emphasis on smooth manufacturing transition has nevertheless been valuable in fostering research into TiO$_2$ metal oxide in the context of ^{68}Ge/^{68}Ga generator developments in order to meet the requirements of ^{68}Ga generator preparation.

Although the distinctions by Horiguchi et al., (1983), Kopecky et al., (1973), Kozlova et al., (1970) and Loc'h et al., (1980) were clearly useful ones, it also seemed evident that their approaches were by no means exclusive. Clearly, there is scope for a great deal of more research that is based on empirical data of the existing SnO$_2$ generator. It is also important that one operates with a complex understanding of ^{68}Ge and ^{68}Ga radionuclides. Finally, one must also look specifically at the contexts of TiO$_2$ metal oxide, rather than assuming broad metal oxide differences.

In 2006, Aardaneh and Van der Walt produced a ^{68}Ge/^{68}Ga generator by performing a number of experiments using SnO$_2$ metal oxide and explored various possible modifications. Developments in the field of ^{68}Ga generators have heightened the need for further studies to establish the role TiO$_2$ may play as a sorbent for ^{68}Ge adsorption and ^{68}Ga desorption.

In the present work, a lot of effort was devoted to the characteristics of the TiO$_2$ metal oxides given that phase and particle size are said to be the important parameters that influence the physical properties of the material. Several characterization techniques were used for the investigation of the TiO$_2$ metal oxides. In recent years TiO$_2$ has been well known as a sorbent

with ^{68}Ge adsorption and ^{68}Ga desorption qualities. In most of the cases, the size of the TiO$_2$ particle is an important factor affecting the performance of the material. Therefore, it comes as no surprise that much of the present work has been focused upon identifying the correct particle size responsible for optimal ^{68}Ge intake through techniques such as XRD, XRF, SEM, HRTEM and BET.

There have been no controlled studies that were conducted in South Africa for the production of ^{68}Ge/^{68}Ga generator using TiO$_2$ sorbent as means of separation of ^{68}Ga from ^{68}Ge. Both qualitative and quantitative research designs will be adopted to provide descriptive, interpretive and empirical data which will serve as the foundation on which the production of a TiO$_2$ based ^{68}Ge/^{68}Ga generator will be based on.

Following this literature review is an experimental chapter (Chapter 3) describing the approach used for the preparation of the TiO$_2$ based ^{68}Ge/^{68}Ga generator.

UNIVERSITY of the
WESTERN CAPE

Chapter Three

EXPERIMENTAL

3.1 Chemicals and Reagents

Analytical grade reagents were used throughout this work and suprapur Hydrochloric Acid (HCl) (30%) that was used during the elution of the generator was obtained from Merck, South Africa. The various types of TiO_2 powders that were used are shown Table 3.1. Deionised water from a Millipore Milli-Q Reagent Grade Water System, with a conductivity of greater than 10 megaohm cm^{-1} was used. There are several routes for the production of ^{68}Ge which apply nuclear reactions both in nuclear reactor and cyclotron. ^{68}Ge was produced by a proton irradiation of ^{69}Ga which produced ^{68}Ge in a (p, 2n) reaction whereby a proton was absorbed by the ^{69}Ga nucleus and two neutrons were subsequently lost forming ^{68}Ge. The target material was dissolved in HCl to give a solution containing ^{68}Ge which was absorbed on an alumina column which has been pre-treated with ethylenediaminetetraacetic acid (EDTA). The ^{68}Ge decays with a 280 day half-life to the positron emitter ^{68}Ga. This ^{68}Ga daughter may then be eluted from the system providing the basis of a ^{68}Ga generator.

Table 3.1:   Various types of TiO_2 used for the construction of $^{68}Ge/^{68}Ga$ generators

Code	Product Type	Product Code	Particle Size	Purity (%)	Supplier
TiO_2A_0	STMI Oxtain	N/A	10-500 µm	99.9	STMI, France
TiO_2A_1	Anatase	248576	325 mesh	99.0	Sigma Aldrich
TiO_2A_2	Rutile	44375	3-6 mm, sintered	99.9	Alfa Aesar
TiO_2A_3	Aeroxide® P-25	4612012698	$50\pm5\ m^2/g$	99.5	Evonik Industries
TiO_2A_4	Aerolyst®	48.7870.1000	3-6 mm, granules	99.9	Evonik Industries

It was necessary to understand the structure, physical and chemical properties of the titanium oxide (TiO_2) materials before and after modification. TiO_2 heat-treatment was performed in ambient atmosphere in an electric furnace (S33, Carbolite Furnace, Hope Valley, England) at a heating rate of 10 °C/min from room temperature. After maintaining the temperature at 850 °C for 3 hours, the temperature of the furnace was allowed to cool down without temperature control.

Table 3.2: List of the products and codes used for preparing heat-treated TiO_2 sample

Code	Products	Sample Amount (g)	Particle Size (μm)	Heat treatment
TiO_2A_0u150	STMI oxtain	10	90-150	No
TiO_2A_0h150	STMI oxtain	10	90-150	Yes
TiO_2A_0u212	STMI oxtain	10	90-212	No
TiO_2A_0h212	STMI oxtain	10	90-212	Yes
$TiO_2A_0u>212$	STMI oxtain	10	>200	No
$TiO_2A_0h>212$	STMI oxtain	10	>200	Yes
TiO_2A_3u	Aeroxide® P-25	10	As received	No
TiO_2A_3h	Aeroxide® P-25	10	As received	Yes
TiO_2A_4h212	Aerolyst®	10	90-212	No

.

3.2 Experimental Procedure for Preparing Adsorbents

When working with any metal oxide, it is good chromatographic practice to remove the finer particles from the metal oxide, such that filters do not get blocked when using them, thereby, increasing the pressure through the column. The following decantation process was followed before packing any column for experimental use:

- The TiO_2 metal oxide was poured into a suitable vessel for separation. Enough water was poured over the metal oxide and by means of shaking the material was suspended throughout the liquid.

- The supernatant was decanted off the metal oxide, the fine particle not having settled and remaining suspended in the supernatant solution.

- Fresh de-ionized water was added to the metal oxide and shaken. It was wise not to use a magnetic stirrer, as this would generate more fine particles.

- The metal oxide was, once again, allowed to settle, following which the supernatant was, again, decanted.

- The above process was repeated several times until the supernatant was a clear solution before the required column was packed with wet particles.

```
┌─────────────────────┐
│     Grinding        │──────────────────▶ ┌──────────────────────────┐
└─────────────────────┘                    │  With mortar and pestle  │
          │                                 └──────────────────────────┘
          ▼
┌─────────────────────┐
│     Washing         │──────────────────▶ ┌──────────────────────────┐
└─────────────────────┘                    │   With milli-Q water     │
          │                                 └──────────────────────────┘
          ▼
┌─────────────────────┐
│   Conditioning      │──────────────────▶ ┌──────────────────────────┐
└─────────────────────┘                    │   With 50 ml, 0.1 M HCl  │
          │                                 └──────────────────────────┘
          ▼
┌─────────────────────┐
│   Ge Loading        │──────────────────▶ ┌──────────────────────────────┐
└─────────────────────┘                    │ With Ge in 0.1 M HCl solution│
          │                                 └──────────────────────────────┘
          ▼
┌─────────────────────┐
│   Ga Elution        │──────────────────▶ ┌──────────────────────────────┐
└─────────────────────┘                    │ With 5 ml solution of 0.1 M HCl│
          │                                 └──────────────────────────────┘
          ▼
┌─────────────────────┐
│   Ga Radionuclide   │
└─────────────────────┘
```
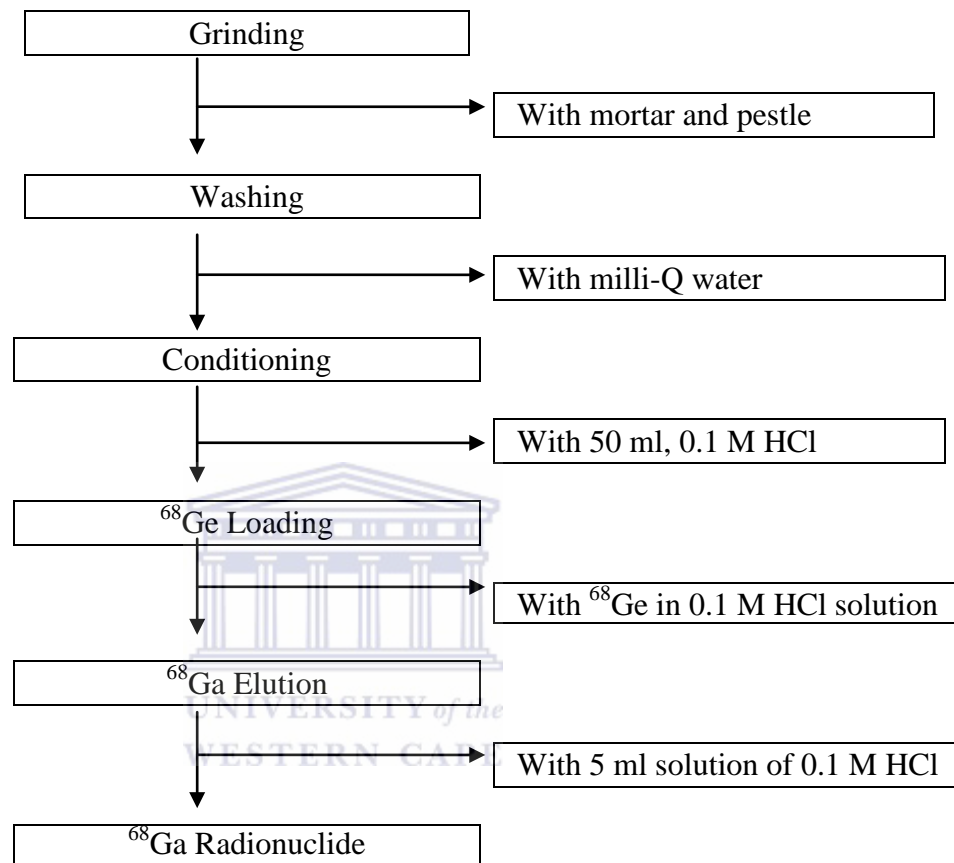
Figure 3.1: Process flow chart for the preparation of the TiO_2 based $^{68}Ge/^{68}Ga$ generator

3.2.1 Preparation of TiO_2 Columns

The prepared column (column: 3 mm i.d. x 30 mm length, 3 grams of TiO_2 sorbent) was connected at the inlet and outlet with polyethylene tubing (50 cm in length) and placed in a lead shield housing ensuring the inlet and outlet tubing was exposed to the outside for easy connection to a peristaltic pump. Using the peristaltic pump at a speed of 1 ml/min, the TiO_2 packed column was first conditioned with 50 ml 0.1 M HCl and thereafter the ^{68}Ge solution (as explained under section 3.1, in 0.1 M HCl matrix, 1-15 mCi) was loaded onto the TiO_2 column to immobilize the ^{68}Ge parent nuclide on the sorbent. The column was washed with

30 ml 0.1 M HCl. All the solutions that had passed through the column were collected separately and retained for later measurements (generally 24 h later).

^{68}Ge retention was achieved by pumping approximately 1 mCi of the ^{68}Ge radionuclide in an acidic media through the column containing TiO_2 metal oxide for the ^{68}Ge to adsorb onto the metal oxide by cation exchange mechanism. The following day, measurements of the ^{68}Ge eluate waste, column and the wash volume were taken to deduce the amount of ^{68}Ge activity in each. It was desired that the column should have all the ^{68}Ge activity as any amount that has managed to pass through the column will indicate a flaw in the method which was investigated. ^{68}Ge yield was determined by using the following equation:

$$\frac{Amount\ of\ ^{68}Ge\ activity\ in\ the\ column}{Total\ amount\ of\ ^{68}Ge\ activity\ loaded}\ x\ 100\%$$

3.1

Experiment 1-9

A TiO_2 column system using STMI $TiO_2.xH_2O$ (TiO_2A_0) metal oxide was set up in order that the ^{68}Ge could be loaded by means of adsorption, such that the Ge activity does not wash off the column. A 10 g sample of the metal oxide was finely ground and sieved to 90-150 µm particle size and a 3 g sample was loaded onto the plastic column after thorough rinsing without heat treating. A ^{68}Ge solution containing 5.221 mCi in 0.1 M HCl was loaded onto the column, which had first been equilibrated by the passage of 50 ml 0.1 M HCl. The column was thereafter allowed to stand for 24 hours before elution of ^{68}Ga could take place and thereby determine ^{68}Ga recovery.

The experiment was repeated several times, with various TiO_2A_0 samples of different particle size and the ^{68}Ge activity was investigated during each repetition. Below is a summary of the particle size and ^{68}Ge activity tried out for experiment 1 -9

Table 3.3: ^{68}Ge loading conditions using STMI (TiO$_2$A$_0$) metal oxide

Experiment	Type of TiO$_2$ and Code	Particle Size* (µm)	TiO$_2$ grams used	^{68}Ge loaded (mCi)	Acid Used	Comment
1	STMI, TiO$_2$A$_0$u150	90-150	3 g	5.221	0.005 M HCl	No heat applied
2	STMI, TiO$_2$A$_0$u212	90-212	3 g	5.115	0.005 M HCl	No heat applied
3	STMI, TiO$_2$A$_0$u>200	>200	3 g	2.352	0.005 M HCl	No heat applied
4	STMI, TiO$_2$A$_0$u>200	>200	3 g	3.625	0.1 M HCl	No heat applied
5	STMI, TiO$_2$A$_0$u150	90-150	3 g	3.022	0.1 M HCl	No heat applied
6	STMI, TiO$_2$A$_0$h150	90-150	3 g	3.118	0.1 M HCl	Heated (850 °C, 3hrs)
7	STMI, TiO$_2$A$_0$h212	90-212	3 g	4.251	0.1 M HCl	Heated (850 °C, 3hrs)
8	STMI, TiO$_2$A$_0$h212	90-212	3 g	4.227	0.1 M HCl	Heated (850 °C, 3hrs)
9	STMI, TiO$_2$A$_0$h>200	>200	3 g	3.210	0.1 M HCl	Heated (850 °C, 3hrs)

*sieved particle size fraction

Experiments 10-13

In a parallel investigation, approximately 20 g of the rutile (TiO$_2$A$_1$) were sieved to 90 – 212 and >212 µm particle sizes in separate batches. No heating was applied during the experimental process due to yellowing of the product which suggested phase change when initial experiments were performed. A total of four columns were prepared and treated with 0.005 and 0.1 M HCl each for ^{68}Ge loading step. As with the previous experiments, ^{68}Ge in activities of approximately 1 mCi were loaded onto the different column for analysis of ^{68}Ge adsorption and ^{68}Ga desorption. The conditions applied for various samples used in experiment 10-13 are set out in Table 3.4.

Table 3.4: ^{68}Ge loading conditions using rutile (TiO$_2$A$_1$) metal oxide

Experiment	Type of TiO$_2$; Code	Particle Size* (µm)	TiO$_2$ grams used	^{68}Ge (mCi)	HCl (M)	Comment
11	rutile, TiO$_2$A$_1$	90-212	3 g	1.002	0.005	No heat applied
12	rutile, TiO$_2$A$_1$	90-212	3 g	1.254	0.005	Heated (850 °C, 3hrs)
13	rutile, TiO$_2$A$_1$	>212	3 g	1.145	0.1	No heat applied
14	rutile, TiO$_2$A$_1$	>212	3 g	1.335	0.1	Heated (850 °C, 3hrs)

*sieved particle size fraction

Experiments 14-17

Once again, approximately 10 g of the anatase (TiO$_2$A$_2$) was sieved to 90 – 212 and >212 µm particle sizes in separate batches. As before, a sample from each batch was heated to 400 °C. A total of four columns were prepared and treated with 0.005 and 0.1 M HCl each for ^{68}Ge loading step. Once more, ^{68}Ge in activities of approximately 1 mCi were loaded onto the different column for analysis of ^{68}Ge adsorption and ^{68}Ga desorption. The conditions applied for experiment 14-17 are set out in Table 3.5.

Table 3.5: ^{68}Ge loading conditions using anatase (TiO$_2$A$_2$) metal oxide

Experiment	Type of TiO$_2$	Particle Size* (µm)	TiO$_2$ (g)	^{68}Ge (mCi)	HCl (M)	Comment
14	anatase, TiO$_2$A$_2$u212	90-212	3 g	1.021	0.005	No heat applied
15	anatase, TiO$_2$A$_2$h212	90-212	3 g	1.115	0.005	Heated (850 °C, 3hrs)
16	anatase, TiO$_2$A$_2$u>212	>200	3 g	1.251	0.1	No heat applied
17	anatase, TiO$_2$A$_2$h>212	>200	3 g	1.362	0.1	Heated (850 °C, 3hrs)

*sieved particle size fraction

Experiments 18-21

As with the previous two experimental sets, 3 g of the Aeroxide® (TiO$_2$A$_3$) metal oxide were weighed out in four sample batches. No sieving was performed for this analysis due to finely ground particles that the products possessed in its original packaging. Two batches were heated at 850 °C for a period of 3 hours as before. Thereafter, each mass was treated in the following manner: 0.9980 mCi (Experiment 18); 1.042 mCi (Experiment 19); 1.140 mCi (Experiment 20) and 1.244 mCi (Experiment 21) of ^{68}Ge activities were loaded onto columns prepared as previously and equilibrated with 50 ml 0.005 M HCl, for the first two columns, and 0.1 M HCl for the other two columns. 24 hours later ^{68}Ga was eluted using the same solutions (0.005 and 0.1 M HCl) used for loading. The conditions applied for experiments 18-21 are set out in Table 3.6.

Table 3.6: ^{68}Ge loading conditions using Aeroxide® (TiO$_2$A$_3$) metal oxide

Experiment	Type of TiO$_2$	TiO$_2$ (g)	^{68}Ge (mCi)	HCl (M)	Comment
18	Aeroxide®, TiO$_2$A$_3$u	3	0.998	0.005	No heat applied
19	Aeroxide®, TiO$_2$A$_3$h	3	1.042	0.005	Heated (850 °C, 3hrs)
20	Aeroxide®, TiO$_2$A$_3$u	3	1.140	0.1	No heat applied
21	Aeroxide®, TiO$_2$A$_3$h	3	1.244	0.1	Heated (850 °C, 3hrs)

Experiments 22-25

As with the previous experimental sets, 3 g of Aerolyst® (TiO$_2$A$_4$) metal oxide were weighed out in four sample batches. Particles were sieved manually to 90 – 212 and 212 -300 µm size. Once again, two batches were heated at 850 °C for a period of 3 hours as before. Thereafter, each mass was treated in the following manner: 1.118 mCi (Experiment 23); 1.555 mCi (Experiment 24); 1.612 mCi (Experiment 25) and 1.624 mCi (Experiment 26) of ^{68}Ge activities were loaded onto columns prepared as previously and equilibrated with 50 ml 0.005 and 0.1 M HCl each. 24 hours later ^{68}Ga was eluted using the same solutions (0.005 and 0.1 M HCl) used for loading as before. The conditions applied for experiment 22-25 are set out in Table 3.7.

Table 3.7: ^{68}Ge loading conditions using Aerolyst® (TiO_2A_4) metal oxide

Experiment	Type of TiO_2	Particle Size* (µm)	TiO_2 (g)	^{68}Ge (mCi)	HCl (M)	Comment
22	Aerolyst®, TiO_2A_4u	90-212	3	1.118	0.005	No heat applied
23	Aerolyst®, TiO_2A_4h	90-212	3	1.555	0.005	Heated (850 °C, 3hrs)
24	Aerolyst®, TiO_2A_4u	>212	3	1.612	0.1	No heat applied
25	Aerolyst®, TiO_2A_4h	>212	3	1.624	0.1	Heated (850 °C, 3hrs)

*sieved particle size fraction

Experiments 26-27

Once optimum conditions (column: 3 mm i.d. x 30 mm length, 3 grams of TiO_2 sorbent) were established and the method was refined (Aeroxide®: 0.1 M HCl, at 850 °C for 3 hours; Aerolyst®: 0.1 M HCl, 90 -212 µm, no heat), a 5 ml solution of 0.1 M HCl was pushed through the Aeroxide® and Aerolyst® TiO_2 columns using a 10 ml syringe. The ^{68}Ga eluate was collected in a labeled vial and allowed to decay after activity measurements for 24 hours. For each eluate the ^{68}Ga efficiency, ^{68}Ge breakthrough and metal impurities were determined. To study the elution yield and purity of the daughter radionuclide, the $^{68}Ge/^{68}Ga$ generator was eluted each morning, five days a week and for a period of over 12 months. The conditions applied for experiment 26-27 are set out in Table 3.8.

Table 3.8: ^{68}Ge loading conditions using Aeroxide®, (TiO$_2$A$_3$h) and Aerolyst®, (TiO$_2$A$_4$u) metal oxides

Experiment	Type of TiO$_2$	Particle Size*	TiO$_2$ (g)	^{68}Ge loaded (mCi)	HCl (M)	Comment
26	Aeroxide®, TiO$_2$A$_3$h	as is	3	15.225	0.1	Heated (850 °C, 3hrs)
27	Aerolyst®, TiO$_2$A$_4$u	90-212	3	15.448	0.1	No heat applied

*sieved particle size fraction

Experiment 28

The ^{68}Ga elution profile was also determined by collecting 1 ml fractions for a 10 ml elution of the optimal column (Aeroxide®: 0.1 M HCl, at 850 °C for 3 hours; Aerolyst®: 0.1 M HCl, 90 -212 µm, no heat) with 0.1 M HCl matrix. Immediately after collection, each 1 ml fraction was tested for ^{68}Ga activity content by using an ionization chamber. The ^{68}Ga eluate was placed in the centre of a 23.5 cm diameter hemisphere (hollow dome), whose inner surface was covered with phosphate BP-1 glass track detectors, for a period of a minute such that the glass track detectors could be exposed to the radioactive decay emissions from the eluate. The time and the ^{68}Ga activity reading were recorded for calculation purposes and thereafter vial containing the eluate was carefully placed in the lead container and kept for further analysis such as radionuclide identification and metal content determination. After testing each fraction for ^{68}Ga activity, ^{68}Ga elution profile of the Aerolyst® TiO$_2$ metal oxide (column: 3 mm i.d. x 30 mm length; sorbent: 3 g Aerolyst® TiO$_2$; ^{68}Ge loaded onto the column: 15 mCi; eluent: 0.1 M HCl) was determined.

3.3 Radionuclide Identification

3.3.1 ^{68}Ga Yield

Identification and yield determination of the radionuclide ^{68}Ga were carried out with a Capintec ionization chamber (model CRC-15R) and the quantification of the radionuclide ^{68}Ge was carried out using high resolution gamma ray spectrometry with an High Purity

Germanium detector. The instrumental parameters of the High Purity Germanium detector are given in Table 3.9.

Table 3.9:   Instrumental Parameters of the High Purity Germanium Detector

Mode	HVPS	Mode	Stability	Mode	Filter
Voltage	3500.6 V	Fine Gain	1.4004x	Rise time	5.6 secs
		S. Fine Gain	0.999998x	Flat top	0.8
		PUR Guard	1.10x	BLR mode	Auto
		Coarse Gain	x10		

A 5 ml ^{68}Ga solution was eluted daily for five days a week and for a period of over 12 months. The times of elution together with the activity of the ^{68}Ga radionuclide were recorded. ^{68}Ga efficiency was defined using the following equation:

$$\frac{^{68}Ga\ (mCi\ at\ time\ of\ elution)\ x\ 100\%}{^{68}Ge\ Activity\ on\ the\ column\ at\ time\ of\ elution}$$

$$=\ {}^{68}Ga\ (\%)$$

3.3.2 ^{68}Ge Breakthrough

In each case the ^{68}Ga elution sample was allowed to stand for 24 hours in order for the ^{68}Ga to decay entirely. Prior to gamma analysis, a quick verification was done using the Capintec Dose Calibrator. Spectra analyses were collected in the order of: (i) a background i.e the room measurements for interference purposes (ii) ^{68}Ge calibration standard, a solution of known Ge solution activity and time of elution (iii) ^{68}Ga elution sample, the sample that needed measuring. ^{68}Ge breakthrough was defined using the 511 keV peak counts and the following equation:

$$\frac{[Counts\ of\ sample - Counts\ of\ Background]\ x\ [Activity\ of\ Calibration\ Sample\ (mCi)]}{[Counts\ of\ Calibration\ Sample - Counts\ of\ Background]}$$

$$=\ \frac{^{68}Ge\ Acitvity\ (mCi)}{24\ hours\ after\ elution}$$

$$= \frac{[^{68}Ge\ Acitvity\ (mCi)\ 24\ hours\ after\ elution] \times 100\%}{[^{68}Ga\ Activity\ (mCi)\ at\ the\ time\ of\ elution]}$$

$$= {}^{68}Ge\ Breakthrough\ (\%)$$

3.4 Characterization of the TiO$_2$ metal oxides

TiO$_2$ was characterized using different techniques in order to investigate its structure and properties. The TiO$_2$ samples that were able to display ^{68}Ge adsorption were characterized using X-ray Powder Diffraction (XRD), X-Ray Fluorescence (XRF), Scanning Electron Microscopy, High Resolution Transmission Emission Microscopy Inductively Coupled Plasma-Optical Emission Spectroscopy (ICP-OES).

3.4.1 X-ray Diffraction (XRD) Analysis

Physical grinding method was adopted in this experiment for the size reduction of the TiO$_2$ powders. A 3 g amount of TiO$_2$ (TiO$_2$A$_1$, TiO$_2$A$_2$, TiO$_2$A$_3$ and TiO$_2$A$_4$ powdered samples) was put in a mortar and pestled uniformly and crushed well for 20 minutes with utmost precaution to avoid any contamination. At the end, the finely ground powder was separated using manual sieving mechanisms to get the desired particle size (90-212, 212-300, 0-90 µm). The powdered material was stored in plastic containers and at normal room temperature until use. About 0.5 g sample of the TiO$_2$ metal oxide sorbents samples were deposited onto a Plexiglas sample holder and the XRD patterns were recorded at angles between 20° and 80°, with a scan rate of 1.5 °/min. The recording parameters were:

Sample holder	Plexiglas (diameter 50 mm)
Mass of sample	0.5 g
Diameter of sample	35 mm
Recording	20 - 80°, 2θ
Step	0.04°, 2θ
Dwell time for one step	2 s
λ (Cu Kα)	1.54Å
Fixed slit opening	0.6°
Sample rotation	yes

The crystallite domain diameters (D) were obtained from the XRD peaks according to the Debye- Scherrer's formula

$$D= k\lambda/ (\beta \cos (2\theta)) \qquad (3.1)$$

where D is the average crystallite size (nm), λ is the wavelength of the incident X-ray beam (1.54 A° for the Cu Kα), θ the Bragg's angle of diffraction, β the full width at half maximum intensity of the peak observed at 2θ = 25.30 (converted to radians) and k, the constant, usually taken as 0.94.

3.4.2 X-ray Fluorescent (XRF) Analysis

The quantitative analysis of the chemical composition of the Aeroxide® P-25 and Aerolyst® TiO_2 powder samples was carried out using PANalytical PW2400 WD XRF (Wavelength Dispersive X-Ray Fluorescence spectrometer). The XRF spectrometer was equipped with a 3kW end-window X-ray tube. Diffraction crystals such as Lif220, Lif200, Ge, PE and PX were used to diffract the x-ray of the different wavelength in different directions. The instrument included an electronically cooled lithium-drifted silicon (Si[Li]) solid-state X-ray detector, a 10-position sample filter wheel, and pulse-processing electronics that communicate spectral data to a PC. This in turn displayed and processed spectral information and outputs sample concentration data. Determination of loss on ignition (LOI) of each sample was performed using approximately 1 g of TiO_2 powdered sample weighed in

ceramic beakers. Thereafter, the samples were heated at 900 °C for 30 minutes, weighed again, then heated for another 60 minutes at the same temperature and weighed for a third time.

XRF Instrument Calibration

Standards were used for calibration and consisted of metal oxides. The 7 standards used for calibration are listed in Table 3.1.

Table 3.10: XRF Calibration Standards

Standard	Analyte	Atomic Structure
1	Vanadium Oxide	V_2O_5
2	Titanium Oxide	TiO_2
3	Potassium Oxide	K_2O
4	Phosphorus Pentoxide	P_2O_5
5	Aluminium Oxide	Al_2O_3
6	Magnesium Oxide	MgO
7	Sodium Oxide	Na_2O

Precision of the XRF data were examined through analysis of duplicate measures. Samples were screened in triplicate to assess precision of screening methods. Triplicate measurements were taken in succession, without moving the sample between screenings.

3.4.3   Scanning Electron Microscope (SEM) Analysis

The surface state and the structure of the Aeroxide® and Aerolyst® TiO_2 metal oxides were studied using Hitachi X-650 Scanning Electron Microscopy (SEM) equipped with a CDU-lead detector at 25 kV. As before, samples of 10 g amounts (Aeroxide®: one sample in its as-received condition, the other sample heated at 850 °C, 3 h; Aerolyst®: 90-212 µm, unheated;) were examined to determine properties such as the crystallite size and morphology. Scanning electron microscopy was performed by putting a small amount of the TiO_2 samples on aluminium stubs coated with a thin carbon film to make the surface conductive and also to enhance the sample images. The coating process was done by EMITECH K950X carbon coater.

3.4.4 Transmission Electron Microscopy (TEM) Analysis

The samples were prepared from the Aeroxide® and Aerolyst® TiO$_2$ metal oxides for the Transmission Electron Microscope (TEM). A small amount of the powders was put in ethanol and the suspension was left for 15 minutes in an ultrasonic bath to avoid forming agglomerations of particles. Two drops of the suspension were placed on a 3 mm diameter carbon-coated copper grid (S147 - 4 Holey carbon film 400 mesh Cu grids) and the alcohol evaporated completely in air. The images were captured using a Field Emission gun, lens 1 was used with spot size 3, at 200 kV using HTEM-EDS Tecnai G2 F20 XT winMAT.

3.4.5 Brunauer-Emmett-Teller (BET) Analysis

The BET surface areas and pore size distributions of the TiO$_2$A$_3$ and TiO$_2$A$_4$ sources were determined by nitrogen adsorption at -196 °C using Quantachrome Autosorb 1 sorption analyzer (Quantachrome Instruments, USA). The samples were degassed at 90 °C for 4 hours prior to nitrogen measurements. The specific surface area of the TiO$_2$ powders was estimated from the amount of nitrogen adsorbed in relationship with its pressure, at the boiling temperature of liquid nitrogen under normal atmospheric pressure. The BET specific surface areas of the samples were subsequently calculated from the corresponding nitrogen isotherms. The experimental details were:

Test Method	TriStar II 3020 Version 2.00
Adsorbed Gases	Nitrogen
Analysis Bath Temperature	-195.800 °C
Temperature Correction	No
Warm Free Space	14.9400 cm³ Measured
Equilibration Interval	10 s
Sample Density	1.000 g/cm³
Sample Mass	0.5662 g
Cold Free Space	46.4707 cm³
Low Pressure Dose	None
Automatic Degas	No

3.4.6   Inductively Coupled Plasma-Optical Emission Spectroscopy (ICP-OES) Analysis

In the eluate, potential metal impurities that might be released from the TiO_2 and analytical grade reagents used were identified by subjecting the ^{68}Ga eluate sample to an ICP-OES analysis for elements such as Zn, Ti, Al, Fe, Cu, Ge, Ga and Sn. As mentioned before, the eluate was allowed to decay for at least 24 h. Reference standard solutions (Appendix A) of Zn, Ti, Al, Fe, Cu, Ge, Ga and Sn were used to prepare standard stock solutions of 1, 5 and 10 ppm of each metal in 0.1 M suprapur HCl to generate the calibration curves. The sample eluates were analysed directly without any dilutions necessary. The calibration curves are shown in Appendix 2. The ICP-OES measurements were performed using a Jobin Yvon Ultima 2 ICP-OES instrument (Model JY-238, Emission Horiba Group, France) equipped with WinLab32™ for ICP Version 5.0 software. The operating parameters of the ICP-OES are shown in Table 3.11.

Table 3.11:   ICP-OES Instrument Conditions

ICP-OES	JY Ultima
Plasma forward power	1100 W
Plasma Height	Bullet shape halfway between coil top and torch top
Coolant gas flow rate	Instrument default
Auxillary gas glow rate	Low
Nebulizer	Glass Expansion Sea Spray
Nebulizer pressure	26 psi
Spray chamber	Glass Expansion Tracey Cyclonic
Pump rate	100 rpm
Tubing	Black-clear-black
Sample uptake rate	1.2 mL/min
Sample uptake time	30 s
Acquisition	30 s wave length range
Wash solution	De-ionized water
Wash time	15 s

Chapter Four

RESULTS AND DISCUSSION

4.1 Introduction

As reviewed in Chapter 2, it was shown that various types of physicochemical separation methods such as distillation, ion exchange chromatography and liquid/liquid extraction have been used to separate the ^{68}Ga radionuclide from the ^{68}Ge radionuclide. It was shown by De Blois et al., (2011); Breeman et al., (2005); Meyer et al., (2004) and Velikyan et al., (2004), that several types of ^{68}Ge/^{68}Ga generator systems with different inorganic absorption materials for the absorption of ^{68}Ge and the desorption of ^{68}Ga existed.

Commercially available TiO$_2$ matrices have been proposed since the 1970's as very promising ion exchangers for ^{68}Ge and ^{68}Ga radionuclides for medical use (Kopecky et al., 1973; Mirzadeh and Lambrecht, 1995). It was also shown by Kozlova et al., (1970) that ion exchange chromatography using TiO$_2$ in low hydrochloric acid mixtures also gave very promising results for the separation of ^{68}Ge from ^{68}Ga. The adsorption capacity for Ge^{+4} is approximately 120 mg Ge per gram sorbent in 0.1 M HCl solutions. Furthermore, the distribution coefficient (K$_d$) is greater than 10 000 ml/g for carrier-free ^{68}Ge^{+4} ions and 2 ml/g for ^{68}Ga^{+3}, when evaluated in 0.1 M HCl solution. Lastly, the decision to perform ^{68}Ga elutions with 0.1 M HCl seemed to be an advantage for further labelling studies with the ^{68}Ge radionuclide.

In the present study the investigations were limited to evaluating only the TiO$_2$ matrix as an absorption material. Experimental evidence also revealed that heating TiO$_2$ metal oxide to a temperature exceeding 400 °C, caused an irreversible change which was supported by observing yellowing of the TiO$_2$. Brady (1971) writes that rutile is a high temperature stable

phase and anatase, on the other hand, is a lower temperature phase. Therefore, a decision was taken to heat anatase up to 400 °C whilst rutile was heated to temperatures of up to 850 °C, as set out in Table 4.6. After the milling and sieving of the appropriate TiO_2 samples from the various suppliers, the structural characterization of the TiO_2 metal oxide materials was carried out using various analytical techniques such as X-ray Diffraction (XRD), X-ray Fluorescence (XRF), and Scanning Electron Microscopy (SEM). TiO_2 was analyzed by X-ray diffraction (XRD) for phase identification and crystallite size estimation. The XRD patterns obtained for the TiO_2 metal oxide materials using the method given in section 3.4.1 are shown in Figure 4.1 to Figure 4.6.
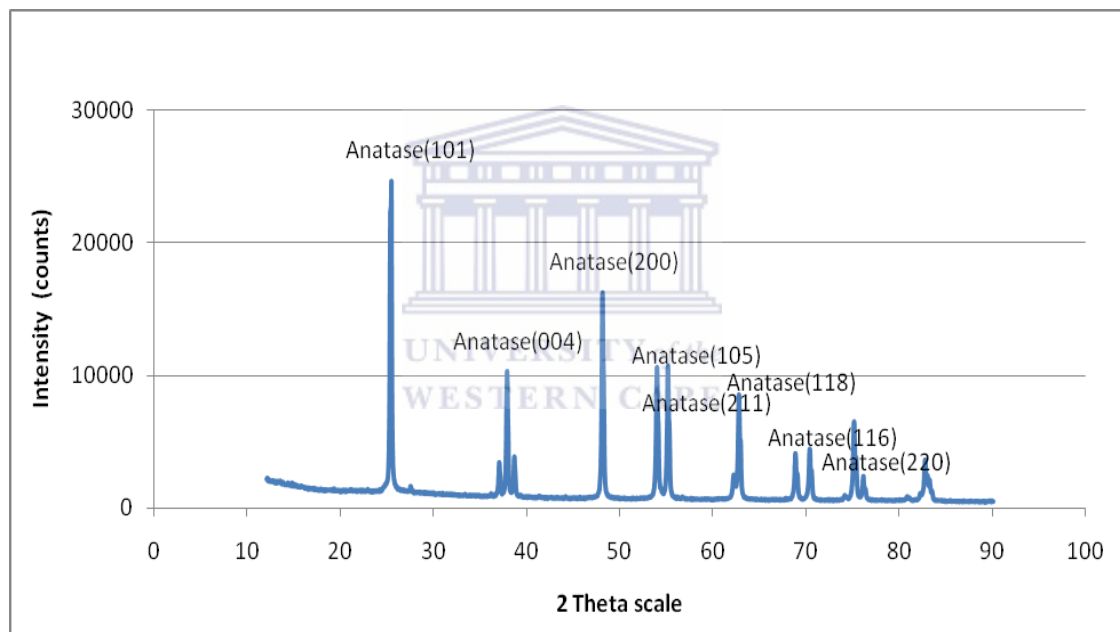
4.2 XRD – Mineral phase Analysis

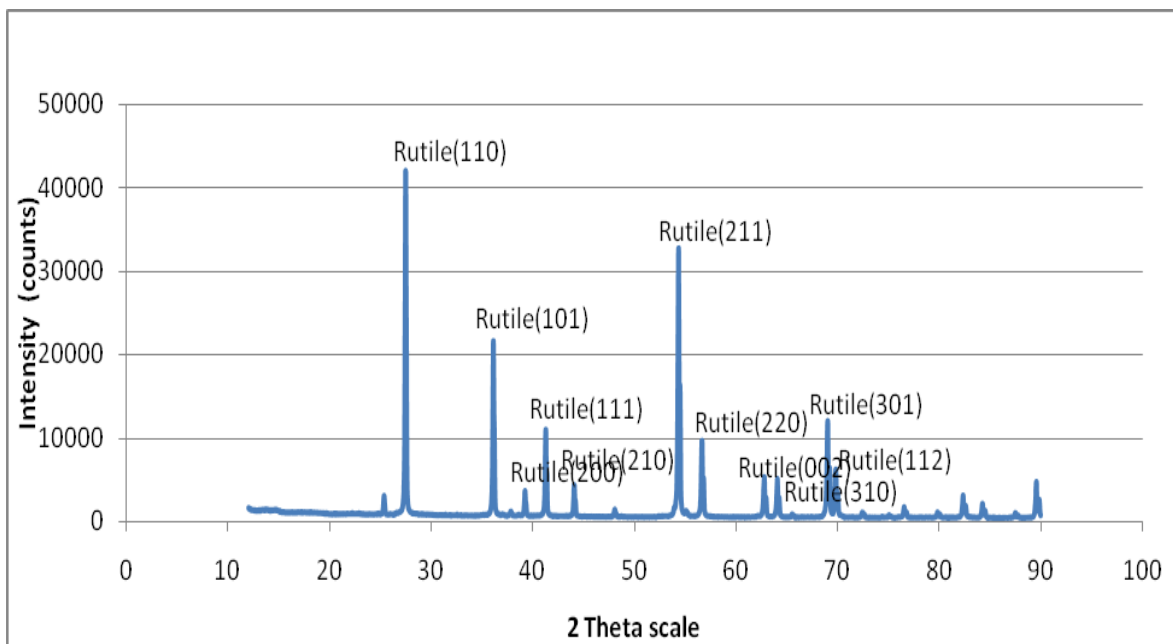Figure 4.1: X-ray diffraction of the TiO_2A_1 from Sigma-Aldrich

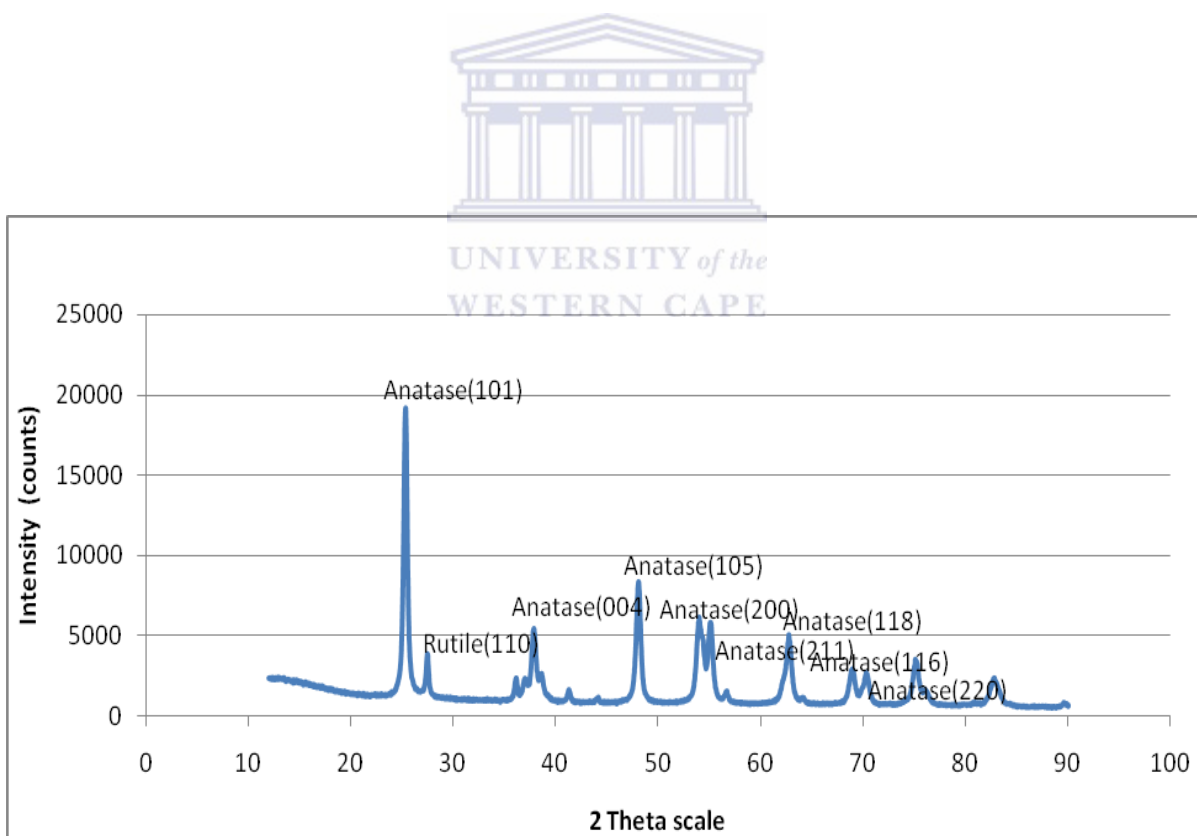Figure 4.2: X-ray diffraction of the TiO_2A_2 from Sigma-Aldrich

Figure 4.3: X-ray diffraction of the TiO_2A_3 from Evonik Industries; unheated
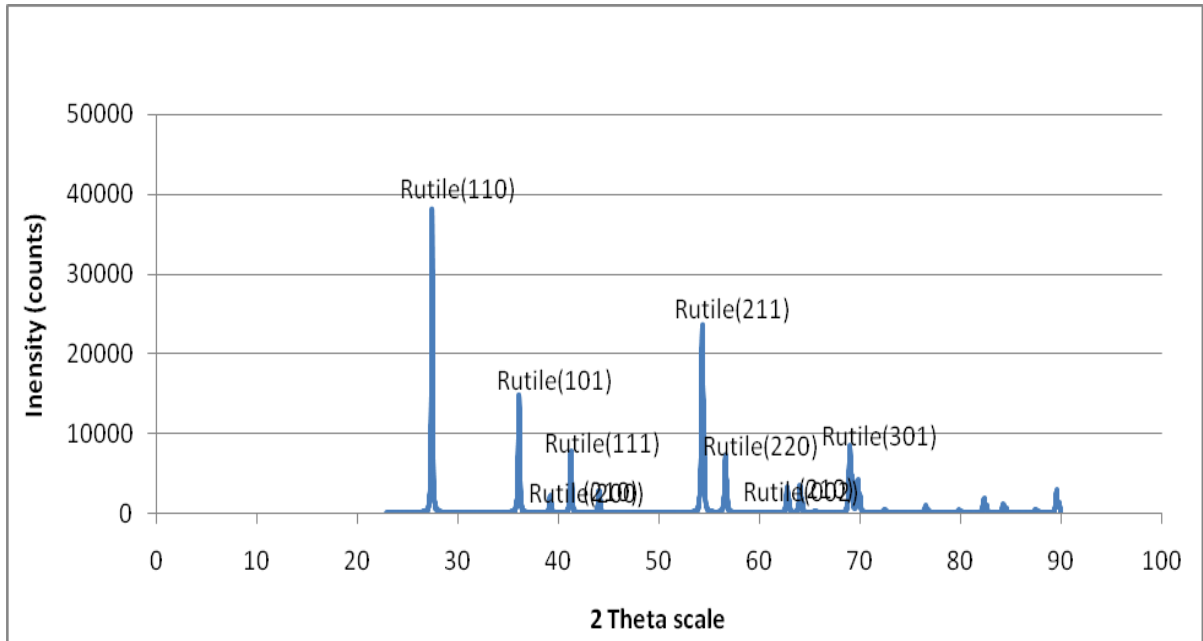
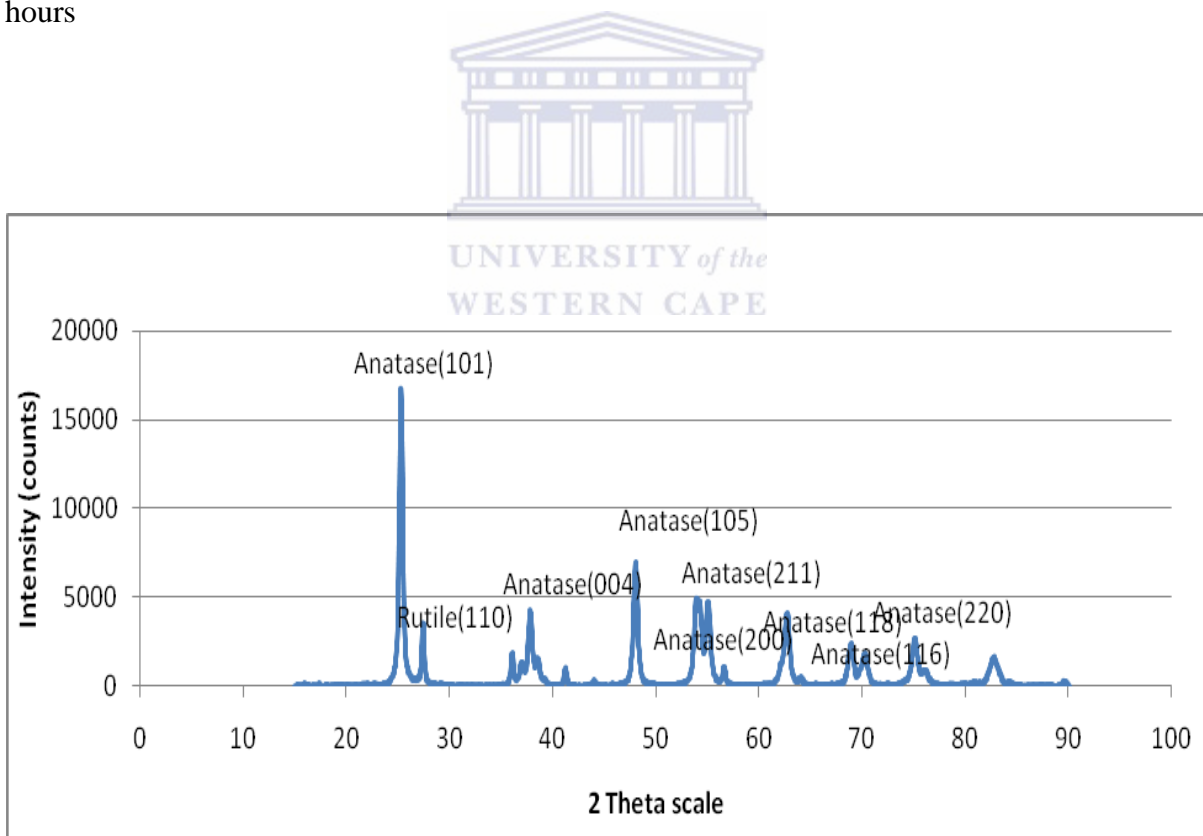Figure 4.4: X-ray diffraction of the TiO_2A_3 from Evonik Industries; heated at 850°C for 3 hours

Figure 4.5: X-ray diffraction of the 90-212 µm TiO_2A_4 from Evonik Industries; unheated
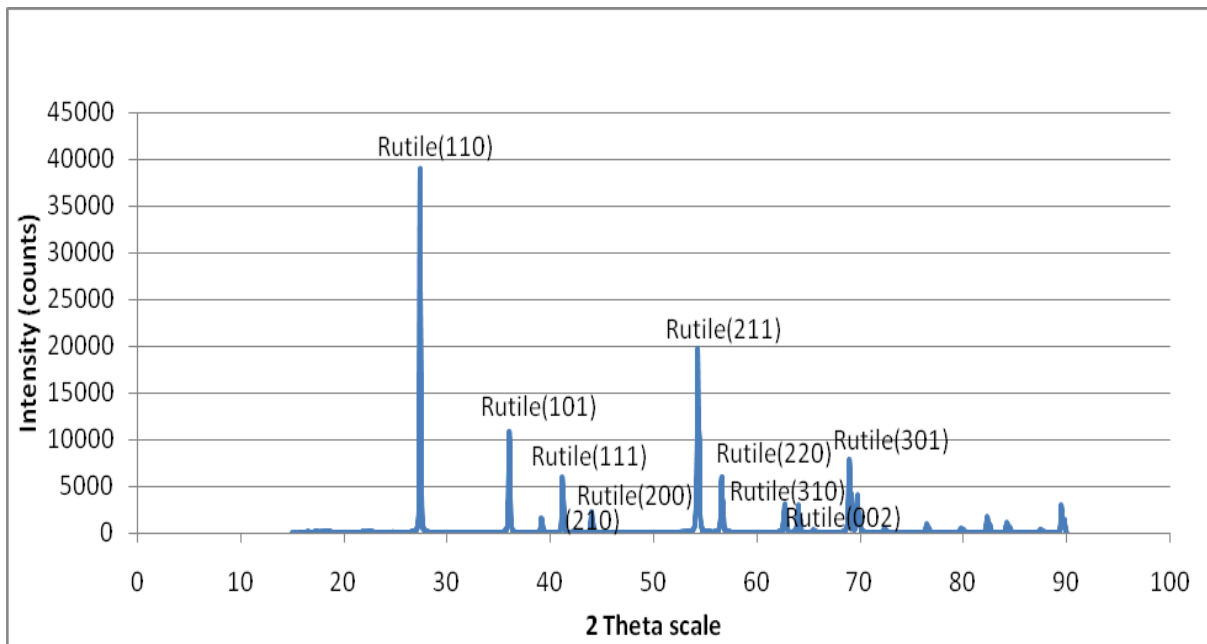
Figure 4.6: X-ray diffraction of the 90-212 µm TiO_2A_4 from Evonik Industries; heated at 850 °C for 3 hours

Figure 4.1 shows the X-ray diffraction patterns of the TiO_2A_1 (anatase) without temperature to prevent phase transformation from anatase to rutile. Analysis of the X-ray diffraction patterns of the TiO_2A_1 revealed the presence of one phase: anatase. Quantification was possible because the intensity of the diffraction pattern of a phase depends on its concentration. The intensity data showed that the material contained 100% of anatase and no rutile material was present. No peak broadening was observed due to large crystallite size effect when compared to diffraction patterns of the various commercial TiO_2 sources. By using Scherrer's formula (equation 2.4), the crystallite size of the TiO_2A_1 powder was found to be 12.16 nm.

Figure 4.2 shows the X-ray diffraction patterns of the TiO_2A_2 (rutile) without temperature to prevent phase transformation from anatase to rutile. As before, analysis of the X-ray diffraction patterns of the TiO_2A_2 revealed the presence of one phase: rutile. The intensity data showed that the material contained 100% of rutile and no anatase material was present. Again, no peak broadening was observed due to large crystallite size effect when compared to diffraction patterns of the various commercial TiO_2 sources. By using Scherrer's formula (equation 2.4), the crystallite size of the TiO_2A_2 powder was found to be 11.10 nm.

Figure 4.3 shows the X-ray diffraction patterns of the TiO_2A_3 (anatase) without temperature to prevent phase transformation from anatase to rutile. Analysis of the X-ray diffraction patterns of the TiO_2A_3 revealed the presence of two phases: anatase and rutile in different weight percentages. Once again, quantification was possible because the intensity of the diffraction pattern of a phase depended on its concentration. The intensity data showed that the material contained 95% of anatase and about 5% rutile material was present. Peak broadening was observed due to small crystallite size effect when compared to diffraction patterns of the various commercial TiO_2 sources. By using Scherrer's formula (equation 2.4), the crystallite size of the TiO_2A_3 powder was found to be 12.15 nm.

Figure 4.4 shows the X-ray diffraction patterns of the TiO_2A_3 (anatase) heat treated in the Carbolite furnace at 850 °C for 3 hours. This diffraction pattern changed to 100% rutile phase structured TiO_2 peaks at 850 °C. The TiO_2A_3 powder which has a 95% rutile phase structure and 5% anatase phase structure with an average particle size of 12.15 nm had undergone phase transformation from the anatase phase structure to the rutile phase structure during heating. Again, no peak broadening was observed due to large crystallite size effect when compared to diffraction patterns of the various commercial TiO_2 sources. By using Scherrer's formula (equation 2.4), the crystallite size of the heat treated TiO_2A_3 powder was found to be 24.43 nm.

Figure 4.5 shows the X-ray diffraction patterns of the TiO_2A_4 (anatase) without temperature to prevent phase transformation from anatase to rutile. Analysis of the X-ray diffraction patterns of the TiO_2A_4 revealed the presence of two phases: anatase and rutile in different weight percentages. Once again, quantification was possible because the intensity of the diffraction pattern of a phase depended on its concentration. The intensity data showed that the material contained 95% of anatase and about 5% rutile material was present. Peak broadening was observed due to small crystallite size effect when compared to diffraction patterns of the various commercial TiO_2 sources. By using Scherrer's formula (equation 2.4), the crystallite size of the TiO_2A_3 powder was found to be 11.05 nm.

Figure 4.6 shows the X-ray diffraction patterns of the TiO_2A_4 (anatase) heat treated in the Carbolite furnace at 850 °C for 3 hours. This diffraction pattern changed to 100% rutile

phase structured TiO$_2$ peaks at 850 °C. The TiO$_2$A$_4$ powder which has a 95% rutile phase structure and 5% anatase phase structure with an average particle size of 21.37 nm had undergone phase transformation from the anatase phase structure to the rutile phase structure during heating. Again, no peak broadening was observed due to large crystallite size effect when compared to diffraction patterns of the various commercial TiO$_2$ sources. By using Scherrer's formula (equation 2.4), the crystallite size of the heat treated TiO$_2$A$_3$ powder was found to be 21.37 nm.

Common to all the figures, the peaks located at 2θ = 27.5, 36.1, 54.4 corresponded to the (110), (101), (211) planes of the rutile phase (JCPDS 21-1276) and the peaks located at 2θ = 25.4, 37.8, 48.0, 54.5 corresponded to the (101), (004), (200), (105 and 211) planes of the anatase phase (JCPDS 21-1272), respectively. Furthermore, the intense diffraction lines like (110) and (101) indicated high crytallinity. Generally, anatase will transform into rutile at ~600°C (Depero et al., 1993). An investigation of intensities showed that when no heat was applied to the TiO$_2$ samples (Figure 4.1, 4.3 and 4.5), the diffraction peaks were broad indicating small crystallite size and the broadening decreased with temperature (Figure 4.2, 4.4 and 4.6). Also, when heat was applied, intensities were observed in the region of 40 000 counts, implying strong crystallization from the samples. In turn, when heat was not applied, intensities were observed in the region of 20 000 counts, implying lower crystallinity.

The position (2θ) and the full width at half height (FWHM were used to identify the particle size of the TiO$_2$ metal oxide examined (Table 4.1). When particle size became smaller, the peaks became broad (Figure 4.3 and Figure 4.5) and the width larger. The broadening occurs due to micro strains of the crystal structure arising from defects like dislocation and twinning (Zhang et al., 2011). The anatase (101) and rutile (110) peaks were used to determine the grain size by Scherrer's formula. The results of the grain size analysis are shown in Table 4.1.

Table 4.1:   XRD Data of the TiO$_2$ Materials

TiO$_2$ Type	2θ	θ	Cos θ	Sin θ	FWHM (º)	FWHM (radians)	Size (nm)
TiO$_2$A$_1$	25.4	12.7	0.9755	0.2198	0.70	0.0122	12.16
TiO$_2$A$_2$	27.7	13.9	0.9707	0.2402	0.77	0.0134	11.10
TiO$_2$A$_3$u	25.1	12.6	0.9759	0.2174	0.70	0.0122	12.15
TiO$_2$A$_3$h	27.7	13.9	0.9707	0.2402	0.35	0.0134	24.43
TiO$_2$A$_4$u	25.4	12.7	0.9755	0.2198	0.77	0.0134	11.05
TiO$_2$A$_4$h	27.6	13.8	0.9711	0.2385	0.20	0.0126	21.37

It was concluded that the phase structure and the particle size could play an important role in the [68]Ge loading of the titanium dioxide based [68]Ge/^{68}Ga generator system. From the XRD data, it was evident that the crystallite size increased with temperature and that the diffraction peaks became more intense and their FWHM gradually became narrower suggesting an increase in particles size and increase in the amount of the relevant phase.

4.3 XRF- Elemental Analysis

For XRF analysis, a decision was taken to only investigate the chemical composition of the TiO$_2$A$_3$ Aeroxide and TiO$_2$A$_4$ Aerolyst metal oxide from Evonik due to the promising results obtained when the two materials were investigated for [68]Ge loading and ^{68}Ga desorption, as set out in section 3.4.2. The weight percent of the metal oxides using the XRF technique is given in Table 4.2.

Table 4.2:   Chemical composition of TiO$_2$A$_3$ and TiO$_2$A$_4$ metal oxides by XRF (weight %) (n=3)

Sample	V$_2$O$_5$	TiO$_2$	K$_2$O	P$_2$O$_5$	Al$_2$O$_3$	MgO	Na$_2$O	LOI	Total
*CRM 61	0.45	93.38	0.06	0.05	1.18	0.17	0.10	0.31	98.17
TiO$_2$A$_3$u	0.27	95.09	0.06	0.01	0.00	0.10	0.65	3.05	99.44
TiO$_2$A$_3$u	0.28	95.34	0.06	0.01	0.00	0.10	0.67	3.05	99.53
TiO$_2$A$_3$u	0.27	95.28	0.06	0.01	0.00	0.10	0.66	3.05	99.45
TiO$_2$A$_3$h	0.27	98.91	0.00	0.01	0.00	0.05	0.00	0.21	99.63
TiO$_2$A$_3$h	0.27	99.20	0.00	0.01	0.00	0.06	0.00	0.21	99.75
TiO$_2$A$_3$h	0.28	99.18	0.00	0.01	0.00	0.07	0.00	0.21	99.76
TiO$_2$A$_4$u	0.28	97.38	0.00	0.01	0.00	0.07	0.03	1.27	99.04
TiO$_2$A$_4$u	0.28	97.41	0.00	0.01	0.00	0.07	0.05	1.27	99.09
TiO$_2$A$_4$u	0.27	97.56	0.00	0.00	0.00	0.07	0.03	1.27	99.21

*Certified Reference Material (External source: Scientific Services measurement facility)

Table 4.3: Statistical Analysis of the TiO_2A_3 and TiO_2A_4 XRF experimental data

Sample	A (%)	B (%)	C (%)	Average (%)	Standard Deviation (%)	Relative Standard Deviation (%)
TiO_2A_3u	99.44	99.53	99.45	99.4733	0.0493	0.050
TiO_2A_3h	99.63	99.75	99.76	99.7133	0.0723	0.070
TiO_2A_4u	99.04	99.09	99.21	99.1133	0.0874	0.090

The chemical composition of the TiO_2A_3 and TiO_2A_4 samples revealed the presence of the following elements: V_2O_2, TiO_2, CaO, K_2O, P_2O_5, AlO_3, MgO, and NaO. This procedure was performed in triplicate to ensure its reliability. Analysis results had good relative precision (repeatability) (see Table 4.3). Before TiO_2 sources were analyzed, the samples were dried to permit accurate weighing. As said before (Experimental section 3.4.2), the loss on ignition (LOI) was determined by first weighing approximately 1 g sample of TiO_2 followed by heating at 900 °C for 30 minutes, weighed again, then heated for another 60 minutes at the same temperature and weighed for a third time.

While it was desirable for the impurities of the TiO_2 sources to be less than 1%, extended drying was not carried out to avoid possible over-drying problems. These might result in hardness and probably phase change. The XRF results (Table 4.2) indicated that TiO_2A_3h was the purest of the three TiO_2 sources, as the impurities were less than 1%. The same cannot be said for the TiO_2A_3u and TiO_2A_4u sources as they had impurities that were more than 1%. The results in Table 4.2 revealed larger LOI values (3.27 for TiO_2A_3u and 1.27 for TiO_2A_4u), indicating high moisture content in the TiO_2 sources. It was noted that such large LOI values were the results of the more than 1% impurity levels obtained for the TiO_2A_3u and TiO_2A_4u sources. The moisture content can be solved by introducing other means of drying but again the loading of ^{68}Ge can be affected if complex means are adopted. A simple, short and less complicated drying mechanism was preferred, because no phase change could occur while the source is undergoing drying.

4.4 SEM- Surface Morphology Analysis

Next, Scanning Electron Microscopy (SEM) was carried out to analyse the effect of heat treatment on the surface morphology of the TiO_2A_3 and TiO_2A_4 samples. The experimental

procedure for the SEM technique is detailed in section 3.4.3. The generated SEM microgram images are shown in Figure 4.10.
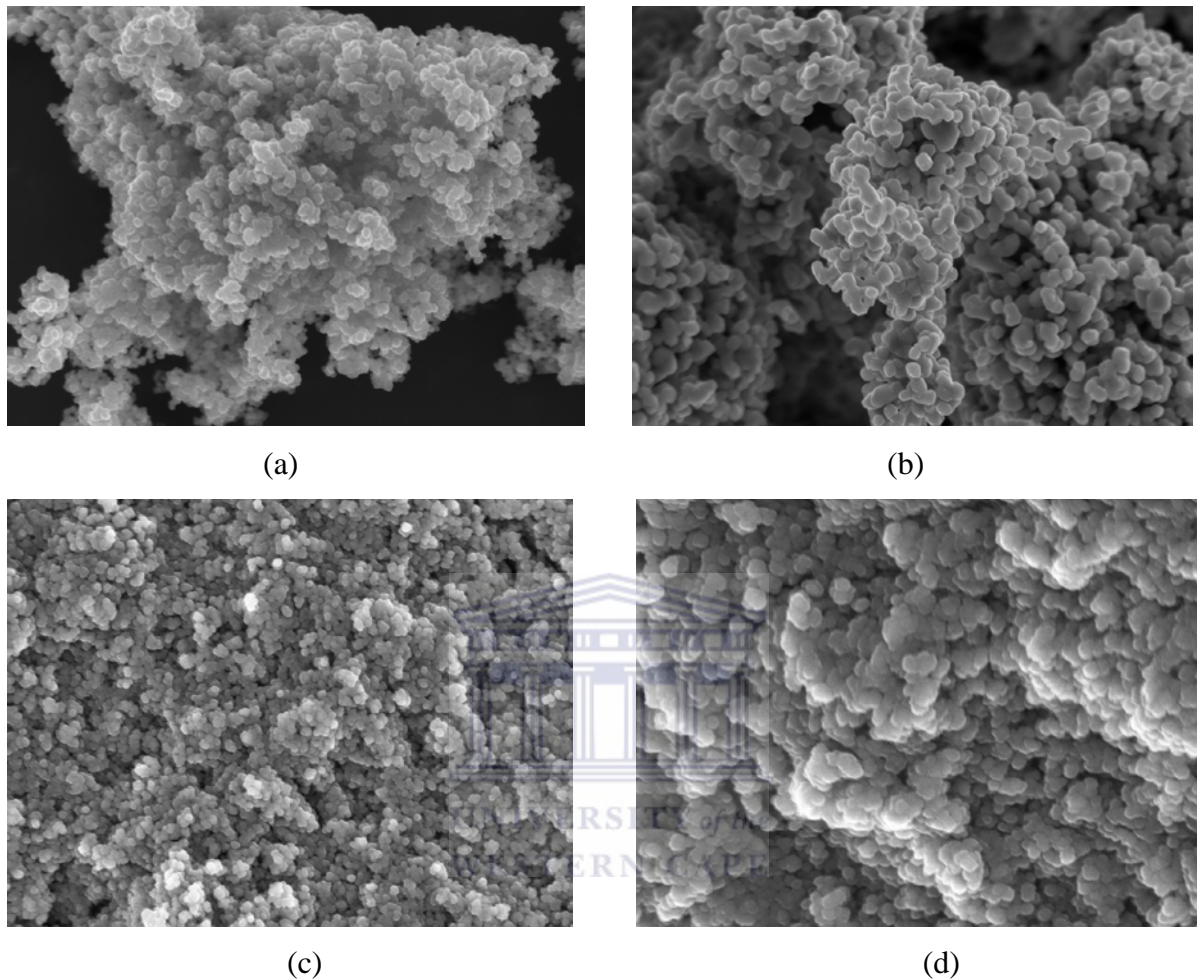

(a)

(b)

(c)

(d)

Figure 4.7: Scanning Electron Microscopy (SEM) micrographs of the carbon-coated TiO_2A_3 and TiO_2A_4 metal oxides; (a) TiO_2A_3 (unheated) (x200), (b) TiO_2A_3 (heated at 850 °C for 3 h)(x200), (c) TiO_2A_4 (90-212 µm, unheated)(x200), (d) TiO_2A_4 (90-212 µm, heated) (x100) (External source: University of the Western Cape measurement facility)

The observed micro-structural characteristics of the TiO_2A_3 and TiO_2A_4 samples revealed a fine grained structure suggestive of a crystalline matrix. In the first SEM image, Figure 4.7(a), the TiO_2A_3 untreated sample displayed an irregular shaped particulate morphology compared to the more spherical shaped particulate morphology exhibited by TiO_2A_3 in Figure 4.7(b). Moreover, the SEM image of 4.7(c) corresponding to the TiO_2A_4 unheated, demonstrates that the particle size of the material is smaller than that of the TiO_2A_3, but both displayed crystallite particles on the surface which was in agreement with XRD detection.

Also, there is some particle agglomeration observed in all images. Statistical analysis of different SEM images showed that the average diameter of the agglomerated particles was in the range of 10 -30 nm.

4.5 TEM- Particle Analysis

In order to see the individual TiO_2 particles of the TiO_2A_3 and TiO_2A_4 samples, analysis of the TiO_2 powdered samples was done using the transmission electron microscopy (TEM) technique. The experimental procedure for TEM technique is detailed in section 3.4.4. Images of the TiO_2A_3 and TiO_2A_4 samples can be seen in Figure 4.8.

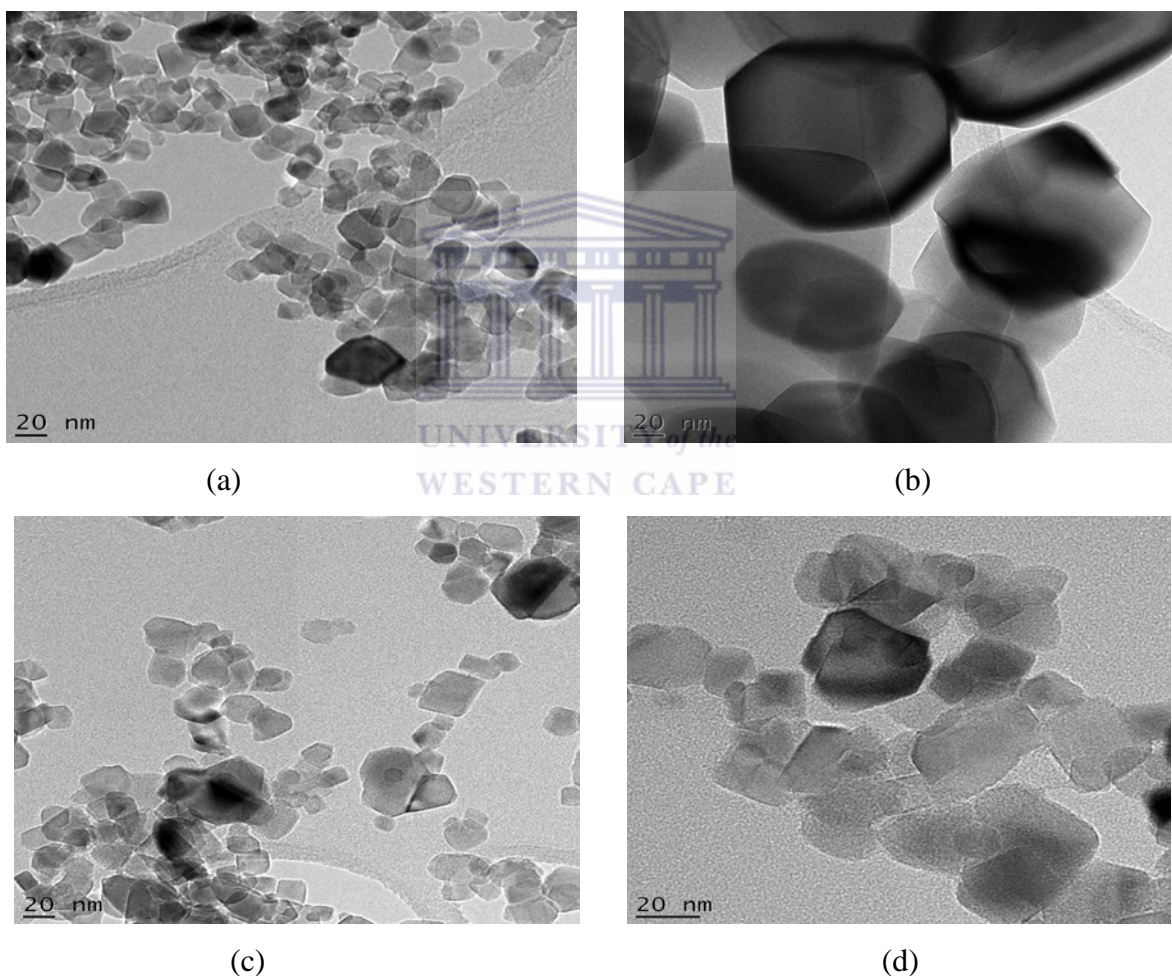

Figure 4.8: Transmission Electron Microscopy (TEM) micrographs of the carbon-coated TiO_2A_3 and TiO_2A_4 metal oxides; (a) TiO_2A_3 (unheated) (x200), (b) TiO_2A_3 (heated at 850 °C for 3 h)(x200), (c) TiO_2A_4 (90-212 µm, heated)(x200), (d) TiO_2A_4 (90-212 µm, heated) (x100) (External source: University of the Western Cape measurement facility)

Initial TEM examination of the samples using TEM showed that the particles were in hexagonal structure, which was not visible from the images observed using SEM. The images shown in Figures 4.8(a) and 4.8(b) revealed that the TiO_2A_3 samples were not only uniform but also well dispersed compared to that of sample TiO_2A_4 in Figures 4.8(c) and 4.8(d). It can be seen that there is an obvious growth in the particle size between Figures 4.8(a) and 4.8(b), due to heat-treatment of the sample. Consequently, the difference in the particle size can be attributed to the heat treatment and phase transformation. This phenomenon is in agreement with results reported by other investigators (Depero et. al., 1993; Goldstein, 2003; Egerton, 2005). Figures 4.8(c) and 4.8(d) presents the TiO_2A_4 without heat. Based on the TEM micrographs, the size of individual particles was measured using image-analyzing methods and found to be ~ 19 nm. In any event the driving force for morphological shape change to the rutile structure will be the overall reduction in surface energy. Theoretically, the presence of an amorphous film on the surface will clearly affect the surface energy, aid the movement of ionic species and hence speed the changes in morphology of the structure.

4.6 BET- Surface Area Analysis

In order to explore the specific surface area of the TiO_2A_3 and TiO_2A_4 sources, BET analyses were determined by physical adsorption of a nitrogen gas on the surfaces of the solids (see Experiment 3.4.5). As a high [68]Ge uptake correlates with a high specific surface area of the TiO_2 source, the varying [68]Ge uptake were explained when the expression of the surface area was studied. Thereafter, from the volumetric adsorption measurements of each sample, respective isotherms were drawn to visualize key factors such as surface areas, pore sizes and pore volumes which may be responsible for providing useful information in developing a test model that loads [68]Ge successfully onto the TiO_2 sources. Table 4.4 shows the pore characteristics of the heated and unheated TiO_2 sources obtained by the nitrogen sorption measurements.

Table 4.4: Summary of BET Surface Areas of the TiO_2A_3 and TiO_2A_4 sources

Sorbent	Surface Area (m^2/g)	Mean Pore Size (nm)	Mean Pore Volume (cm^3/g)
TiO_2A_3u	31.2147	7.28553	0.101590
TiO_2A_3h	7.2003	13.01821	0.013115
TiO_2A_4u	45.5329	9.81666	0.111745
TiO_2A_4h	0.2574	12.96791	0.000834

From the data, the immediate observation was that the unheated TiO_2A_3 sample (TiO_2A_3u) showed a higher surface area (31.2147 m^2/g) and pore volume (0.101590 cm^3/g) when compared to the heated sample (7.2003 m^2/g and 0.013115 cm^3/g, respectively). This trend was additionally supported by the TiO_2A_4 sample. The averages of the pore sizes and the averages of pore volumes are also presented in Table 4.4. However, the data show no clear distinction between the heated and unheated samples. Therefore, a much more detailed investigation will be to look at parameters such as the pore size distributions and the micro pore volumes. The two parameters will be discussed in this section.

Ideally the surface area should be increased so that it can allow adsorption of as much [68]Ge radionuclide as possible without complicated chemical manipulation. In order to load the [68]Ge effectively for ^{68}Ga generator investigation, the larger surface area is most desirable. The nitrogen adsorption-desorption isotherms of the TiO_2A_3 and TiO_2A_4 sources are summarized in Figures 4.9 and 4.10.
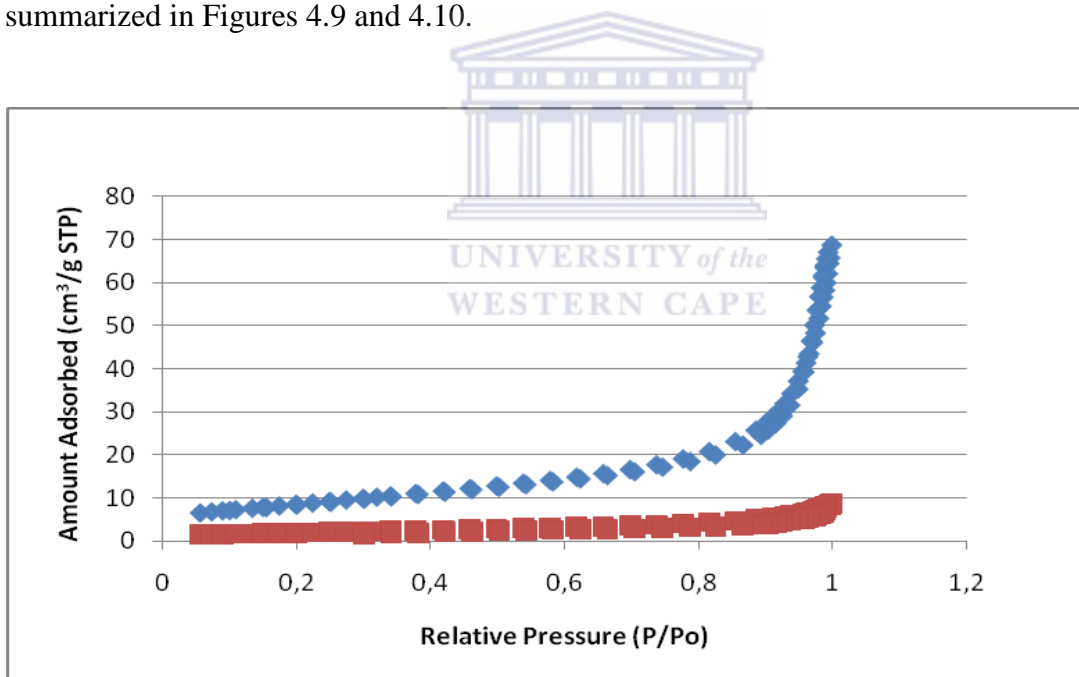
(a) ◆ TiO_2A_3 (unheated); (b) ■ TiO_2A_3 (heated)

Figure 4.9: Comparison of N_2 sorption isotherms at -196 °C of (a) TiO_2A_3 (unheated) and (b) TiO_2A_3 (heated at 850 °C) from Evonik Industries by BET analysis (External source: University of Cape Town measurement facility)
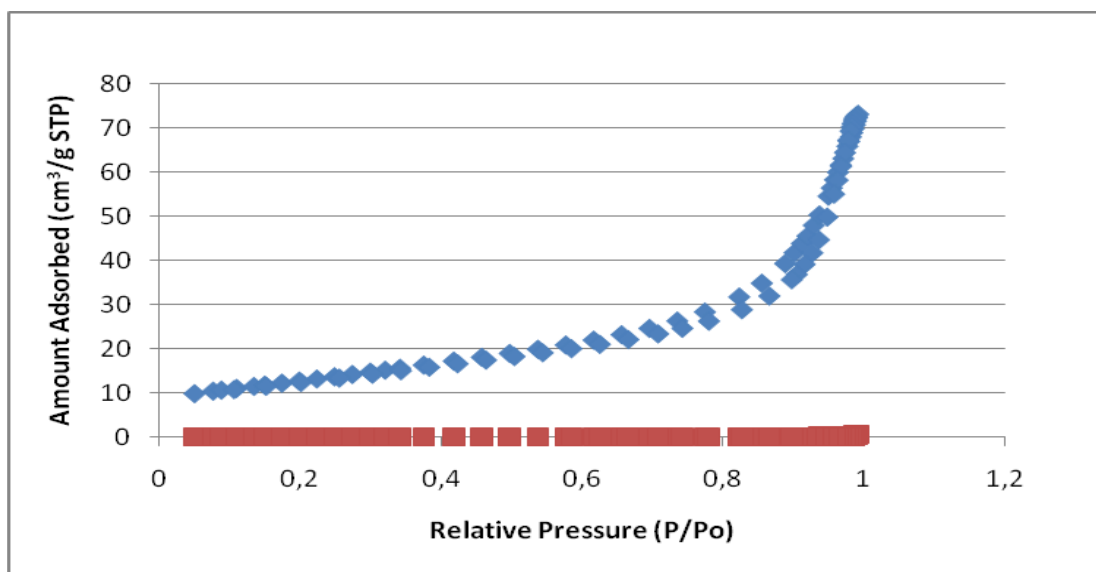
(a) ◆ TiO_2A_4 (unheated); (b) ■ TiO_2A_4 (heated)

Figure 4.10: Comparison of N_2 sorption isotherms at -196 °C of (a) 90-212 µm TiO_2A_4 (unheated) and (b) 90-212 µm TiO_2A_4 (heated at 850 °C) from Evonik Industries by BET analysis (External source: University of Cape Town measurement facility)

During the N_2 adsorption process of the heated and unheated TiO_2A_3 samples, the plots exhibited completely reversible isotherms, where the adsorption and desorption of the N_2 with slight hysteresis was observed. Detailed comparisons between the heated and unheated TiO_2A_3 samples showed a higher N_2 adsorption by the unheated sample (Figure 4.9), indicating the porous nature of the sample. On the other hand, the low N_2 adsorption exhibited by the heated N_2 adsorption showed the non-porous nature of the sample. The shape of the isotherms indicated that TiO_2A_3 is dominantly macroporous. The hysteresis was extremely narrow on both TiO_2A_3 samples and this indicated the presence of fine macropores. Another marked observation was the low adsorbed volume at P/P_o <0.01, an indication that TiO_2A_3 had negligible or non–existent micropores.

Figure 4.10 shows the N_2 adsorption/desorption isotherms of the TiO_2A_4. During the process of N_2 adsorption on the unheated TiO_2A_4, as before, adsorption of N_2 occurred at relatively high pressure when compared to the heated samples. There is a noticeable similarity in the shapes that the two unheated samples exhibit, indicating a consistent relation for the two TiO_2 sources. Comparing the two curves of the heated sample TiO_2A with that of the unheated

sample, it can be seen that the adsorption capacity for the heated TiO_2A_4 sample was extremely low, practically nil, as measured in this work. From the previous surface area discussion, it can be seen that the heated samples did not perform at all; and the curves obtained were broadly consistent with the XRD, SEM and TEM results. Again, the hysteresis was narrow but visible for the unheated TiO_2A_4 samples, indicating a significant presence of fine macropores.

On the other hand, the gas phase in pores with different diameters will condense at different pressures and thus provide quantitative information about the relative volume of different pore–sizes in the TiO_2 samples. The pore–size distribution (PSD) is obtained by application of a BJH (Barret, Joyner, and Halenda) technique (Raj and Viswanathan, 2009). Results of pore–size distribution from the four TiO_2 samples are presented in Figure 4.11 for comparison.

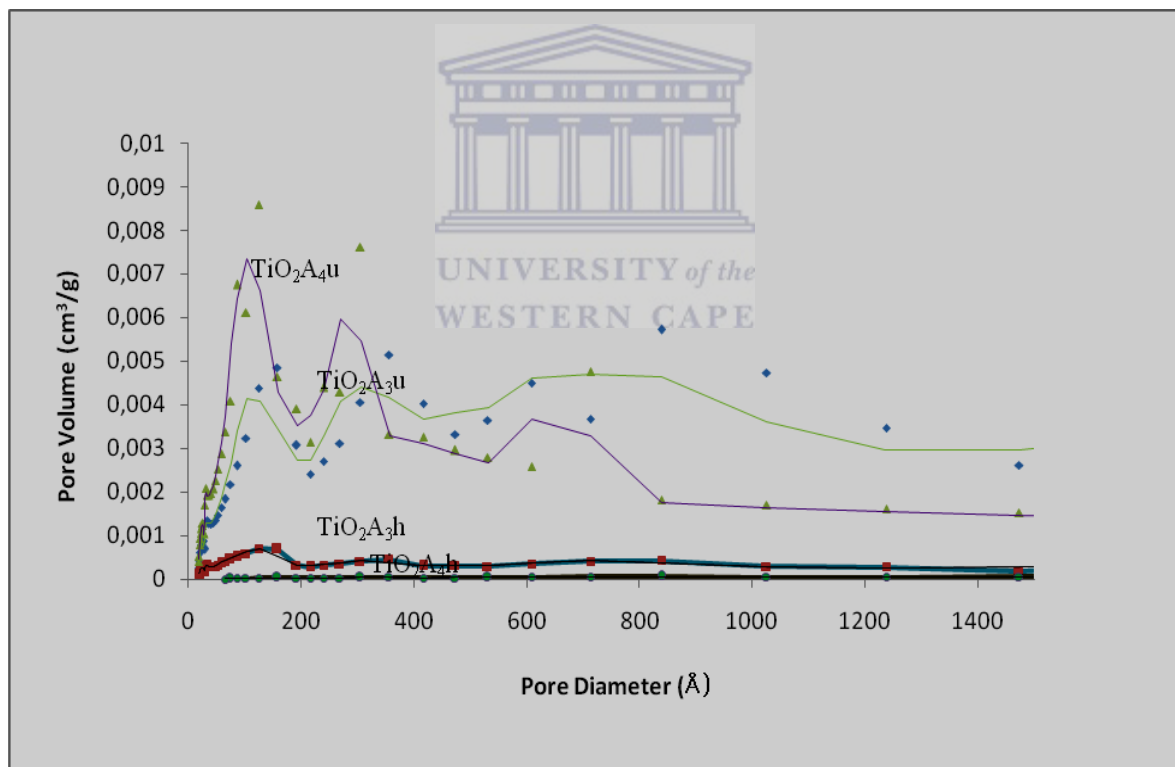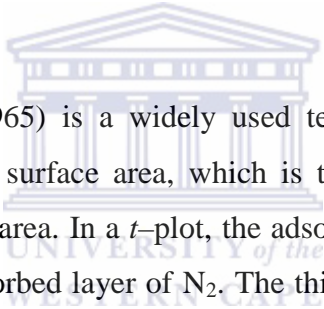Figure 4.11: Comparison of pore size distribution of (a) TiO_2A_3 (unheated); (b) TiO_2A_3 (heated at 850 °C for 3 h); (c) TiO_2A_4 (90-212 µm, heated); (d) TiO_2A_4 (90-212 µm, heated) (External source: University of Cape Town measurement facility)

A detailed comparison between pore size distributions from N_2 adsorptions for the unheated TiO_2 samples indicated broadly similar modal mesopore sizes and pore size ranges however the heated samples show very low mesopor180. The data from the unheated TiO_2 sources also showed higher pore volume and therefore higher profiles (Figure 4.11). On the contrary, the heated TiO_2 samples showed lower pore volumes and the peak for the TiO_2A_4h sample at higher pore–size is missing. Additionally, the pore diameters of all the samples were in the range of 0 - 20 nm calculated by the BJH adsorption of size distribution. In each case, the dominant pore modes remained the same but the differential pore volume for each pore-size differed significantly, particularly for the unheated samples. The PSD profiles from N_2 gas adsorptions (Figure 4.11) suggest that pore diameter distribution emphasizes the benefits of no heat treatment, even though, compositionally the samples contain the same chemical contents. The higher measured pore volume in the unheated samples by N_2 gas adsorption techniques indicates that these samples have a significant volume of small pores with <20 nm pore–size.

T–plot (Lippens & De Boer, 1965) is a widely used technique to estimate the specific micropore volume and the open surface area, which is the surface area from mesopores, macropores, and external surface area. In a t–plot, the adsorbed N_2 volume is plotted against statistical thickness (t) of the adsorbed layer of N_2. The thickness (t) depends on the relative pressure (P/Po). Webb & Orr (1997) write that if the V vs. t plot yields a straight line that passes through the origin, then the sample is considered to be free of micropores and t–plot of microporous material shows a straight line at medium t and a concave–down curve at low t. Results of t–plots from the four TiO_2 samples are presented in Figure 4.12 for comparison.
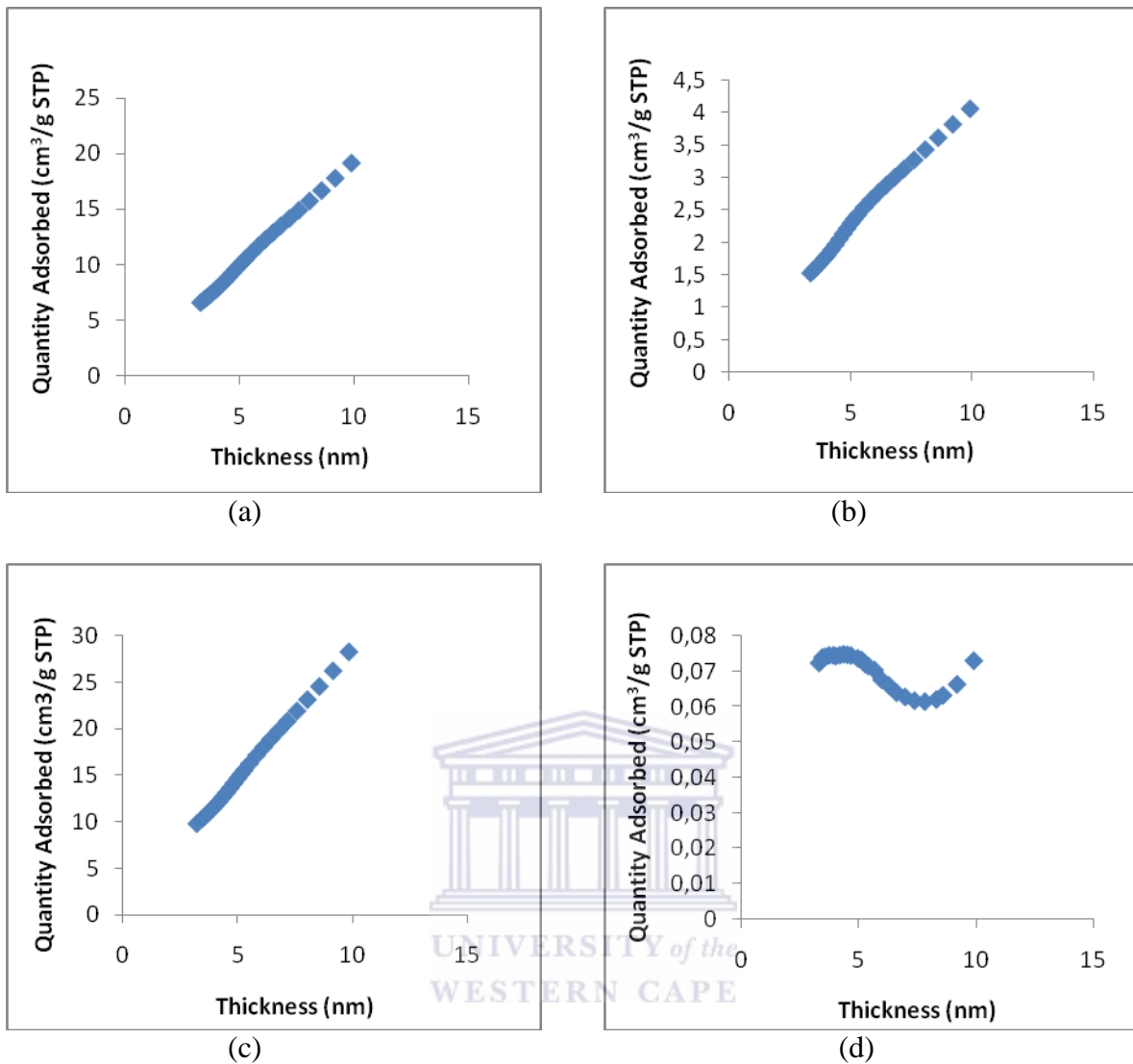
Figure 4.12: T-plot curves of (a) TiO_2A_3 (unheated); (b) TiO_2A_3 (heated at 850 °C for 3 h); (c) TiO_2A_4 (90-212 µm, heated); (d) TiO_2A_4 (90-212 µm, heated) (External source: University of Cape Town measurement facility)

Form the t-plot curves it was possible to estimate the volume of the micropores of all the TiO_2 sources. The first thing to note about the N_2 sorption isotherms is the significant differences in the volumes adsorbed by the samples during the adsorption process. The unheated TiO_2A_3 and TiO_2A_4 sources samples have a very high pore volume of 20 and 30 cm^3/g STP, respectively, compared to the heated samples. The heated TiO_2A_4 has an exceptionally low volume of micropores compared to the pore volumes measured in the heated TiO_2A_3 (Figure 4.12(d)). The extremely low porosity and adsorption of these samples are consistent with the pore size diameter results obtained (Figure 4.11). The N_2 sorption isotherms at -196 °C showed a similar trend where the heated samples revealed absence of

open micropore and mesopores (Figure 4.9 and 4.10) and extremely low surface area and pore volume. The dominance of 4–12 nm pores in these samples (Figure 4.12) correlate well with presence of pores of <200 Å diameters (Figure 4.11).

It is demonstrated in this study that detailed and qualitative descriptions of the TiO_2 porosity can provide detailed pore–structure quantification. The understanding of the N_2 gas adsorption technique to understand the pore–structures can aid in modelling a cation exchange capacity during sample preparation with significant production implications. The studies conclusively indicated that unheated TiO_2A_3 and TiO_2A_4 samples can be used for $^{68}Ge/^{68}Ga$ generator applications without any heat applied to the sorbents. By omitting heat treatment of the TiO_2 sample powders, the sample preparation became easier and quicker compared with that in earlier literatures. Adsorptive capacity of solids absorbents generally is proportional to the specific surface area. Overall, this work provided a much-needed framework for a good study design before data collection began. TiO_2A_4, as shown in the results of experimental section 3.4.1, has lower particle size than TiO_2A_3, which makes the former an ideal raw material for the production of $^{68}Ge/^{68}Ga$ generators, without additional heating steps.

4.7 ^{68}Ge Loading Conditions using the various commercial TiO_2 sources

The five commercially available TiO_2 metal oxide materials, TiO_2A_0 (Experiment 1-9), TiO_2A_1 (Experiment 10-13), TiO_2A_2 (Experiment 14-17), TiO_2A_3 (Experiment 18-21) and TiO_2A_4 (Experiment 22-25) that were evaluated for their absorption of ^{68}Ge and desorption of ^{68}Ga are shown in Tables 4.5 (TiO_2A_0) to Table 4.9 (TiO_2A_4). The experimental procedures for the five various sources of the TiO_2 metal oxide are detailed in section 3.2., where *n* is the number of observations in the original sample.

Table 4.5: ^{68}Ge retention using STMI TiO$_2$.xH$_2$O (TiO$_2$A$_0$) metal oxide in 0.005 M and 0.1 M HCl (n=3)

Exp.	Type of metal oxide	Particle size (µm)	Temp. (°C)	^{68}Ge loaded (mCi)	HCl (M)	^{68}Ge Retained (%)	^{68}Ga Eluted (%)
1	TiO$_2$A$_0$u150	90-150	No heat	5.221	0.005	70	46
2	TiO$_2$A$_0$u212	90-212	No heat	5.115	0.005	80	40
3	TiO$_2$A$_0$u>212	>212	No heat	3.352	0.005	100	34
4	TiO$_2$A$_0$u150	90-150	No heat	3.022	0.1	41	28
5	TiO$_2$A$_0$h150	90-150	850	3.118	0.1	21	4
6	TiO$_2$A$_0$u212	90-212	No heat	4.251	0.1	71	26
7	TiO$_2$A$_0$h212	90-212	850	4.227	0.1	60	50
8	TiO$_2$A$_0$u>212	>212	No heat	3.188	0.1	80	5
9	TiO$_2$A$_0$h>212	>212	850	3.210	0.1	65	25

In experiment 1, when a particle size fraction of 90-150 µm (TiO$_2$A$_0$u150) was used to load ^{68}Ge in a 0.005 M HCl media, 70% of the ^{68}Ge radionuclide managed to adsorb on the TiO$_2$, suggesting a 30% loss. When the same metal oxide (90-150 µm, TiO$_2$A$_0$u150) was investigated under the same conditions, with acid media changed to 0.1 M HCl (Experiment 5), the yield decreased to 41%. This indicated a loss of 59% of the ^{68}Ge, which could be attributed to the high acid content of the eluate. Overall the 90-150 µm (TiO$_2$A$_0$u150) size was rejected due to low ^{68}Ge retention.

In experiment 2, when a particle size fraction of 90-212 µm (TiO$_2$A$_0$u212) was used to load ^{68}Ge in a 0.005 M HCl media, the yield increased to 80%. Again, 20% of the ^{68}Ge was lost and this suggested further analysis of the metal oxide. For the same metal oxide, when using 0.1 M HCl media (experiment 6), the yield was decreased to 71%, a decline when the acid concentration was increased. Therefore, the 90-212 µm (TiO$_2$A$_0$u212) was discarded.

In experiment 3, when a particle size fraction of >212 µm (TiO$_2$A$_0$u>212) was used to load ^{68}Ge in a 0.005 M HCl media, the yield was 100%, suggesting a zero loss. For the first time, a 100% loading of ^{68}Ge was achieved when a >212 µm particle size fraction was used when loading ^{68}Ge in a 0.005 M HCl media. Again, when the same metal oxide (>212 µm (TiO$_2$A$_0$u>212) was used in experiment 8, this time changing the ^{68}Ge media to 0.1 M HCl, the yield was reduced to 80%. The two experiments (3 and 8) suggested that the optimum eluent was 0.005 M HCl rather than 0.1 M HCl when >212 µm size (TiO$_2$A$_0$u>212) was used as a sorbent.

In experiment 4, when a particle size fraction of 90-150 µm (TiO$_2$A$_0$u150) was used to load ^{68}Ge and compared to experiment 6, when 90-212 µm (TiO$_2$A$_0$u212) was used to load ^{68}Ge, with both experiments using 0.1 M HCl media, the yield increased from a retention of 41% for the 90-150 µm (TiO$_2$A$_0$u150) to a retention of 71% for the 90-212 µm (TiO$_2$A$_0$u212). The comparison suggested that a bigger particle size was more appropriate for good retention, in this case 90-212 µm (TiO$_2$A$_0$u212). In experiment 8 and 9, in which case both experiments used >200 µm (TiO$_2$A$_0$u>212) to load ^{68}Ge, except that in one case (experiment 9, >212 µm (TiO$_2$A$_0$h>212) the metal oxide was heated to 850 C for 3 hours, the ^{68}Ge yield was found to be 80% for the unheated >212 µm (TiO$_2$A$_0$u>212) and 65% for the heated >212 µm (TiO$_2$A$_0$h>212). Again, the comparison in this case suggested that heat treatment did not improve the loading of the ^{68}Ge radionuclide. In experiment 6 and 7, when 90-212 µm (TiO$_2$A$_0$212) particle size was used to load ^{68}Ge in 0.1 M HCl for both experiments, (with heat-treatment as the only factor added to experiment 7), the retention of the ^{68}Ge was found to be 71% or 60% for the unheated or heated TiO$_2$A$_0$h212, respectively. As before, the experiments (6 and 7) suggested that heat-treatment when using the STMI product did not contribute positively to the retention of the ^{68}Ge radionuclide.

In summary, in the first 3 experimental runs, when using the TiO$_2$A$_0$ (STMI oxtain) in the 0.005 M HCl eluent, 100% retention of ^{68}Ge could be ideally achieved on a sample with a particle size >212. Also, it was shown, when starting with a 0.005 M HCl eluent as shown in experimental runs 1-4 that, as the particle size increased with no heat, the retention of ^{68}Ge increased from 70% (90-150 µm), to 80% (90-212 µm) and 100% (>212 µm). It was furthermore shown that as the particle size of the TiO$_2$A$_0$ increased with heating at 850 °C that retention of ^{68}Ge was only 21% (90-150 µm), 60% (90-212 µm) and 65% (>212 µm). When the TiO$_2$A$_0$ was not heated, improved retention of the ^{68}Ge with increasing particle size (90-150 µm, a retention of 41%), and 90-212 µm with a retention of 71% and >212 µm with a retention of 80% was evident, but this was still not adequate for the generator requirements. The optimal experimental conditions were obtained in run 3 when using the TiO$_2$A$_0$ with a particle size of >212 µm, with no heating and in 0.005 M HCl matrix, where retention of 100% ^{68}Ge was achieved. In the end, the initial experiments (Experiment 1-9) involving TiO$_2$A$_0$ proved to be unsuccessful, as STMI stopped producing its TiO$_2$ on a commercial basis and therefore no further investigations were pursued with this TiO$_2$ compound. Another

disadvantage of the product was that while the 100% loading (Experiment 3) was impressive, no ^{68}Ga was found in the eluate when elution with 10 ml of the 0.005 M HCl was performed.

Subsequent experiments were performed using TiO$_2$A$_1$ (Sigma-Aldrich) and TiO$_2$A$_2$ (Alpha-Aesar). Table 4.6 and Table 4.7 present the HCl concentration and the temperature dependence of the TiO$_2$A$_1$ and TiO$_2$A$_2$, respectively for ^{68}Ge retention. The samples were sieved into two size fractions (90-212 or 212-300 µm). Again, *n* is the number of observations in the original sample.

Table 4.6: ^{68}Ge retention of the TiO$_2$A$_1$ with 0.005 M and 0.1 M HCl (n=3)

Exp.	Type of metal oxide	Particle size (µm)	Temp. (°C)	^{68}Ge loaded (mCi	HCl (M)	^{68}Ge Retained (%)
10	TiO$_2$A$_1$u212	90-212	No heat	1.002	0.005	0
11	TiO$_2$A$_1$h212	90-212	850	1.254	0.005	0
12	TiO$_2$A$_1$u300	212-300	No heat	1.145	0.1	0
13	TiO$_2$A$_1$h300	212-300	850	1.335	0.1	0

Table 4.7: ^{68}Ge retention of the TiO$_2$A$_2$ with 0.005 M and 0.1 M HCl (n=3)

Exp.	Type of metal oxide	Particle size (µm)	Temp. (°C)	^{68}Ge loaded (mCi	HCl (M)	^{68}Ge Retained (%)
14	TiO$_2$A$_2$u212	90-212	No heat	1.021	0.005	0
15	TiO$_2$A$_2$h212	90-212	400	1.115	0.005	0
16	TiO$_2$A$_2$u300	212-300	No heat	1.251	0.1	0
17	TiO$_2$A$_2$h300	212-300	400	1.362	0.1	0

In experiment 10-13 (Table 4.6), when a particle size fraction of 90-212 or 212-300 µm of the TiO$_2$A$_1$ from Sigma-Adrich were used to load the ^{68}Ge in either 0.005 or 0.1 M HCl media, the yield obtained revealed that no ^{68}Ge was retained by the TiO$_2$A$_1$, irrespective of the temperature or the particle size used. Therefore, the use of TiO$_2$A$_1$ as a sorbent was rejected due to zero percent loading of the ^{68}Ge. Similarly, in experiment 14-17 (Table 4.7), when 90-212 and 212-300 µm of the TiO$_2$A$_2$ were used to load the ^{68}Ge in either 0.005 or 0.1

M HCl media, once again, the yield obtained revealed that no ^{68}Ge was retained by the TiO$_2$A$_2$, irrespective of the temperature or the particle size used. As before, the use of TiO$_2$A$_2$ as a sorbent was rejected due to zero percent loading of the ^{68}Ge. No ^{68}Ga elution was performed for both sources (TiO$_2$A$_1$ and TiO$_2$A$_2$) due to zero amount of ^{68}Ge loaded onto the column.

Thereafter, different kinds of TiO$_2$ were investigated in order to find conditions where the metal oxide material could load ^{68}Ge effectively, and, thereafter, release the ^{68}Ga. It was thus decided to purchase the TiO$_2$A$_3$ and TiO$_2$A$_4$ powders from Evonik Industries. Table 4.8 and 4.9 represent the results of the Evonik samples TiO$_2$A$_3$ and TiO$_2$A$_4$, where approximately 1 mCi of the ^{68}Ge was used for loading.

Table 4.8: ^{68}Ge retention of the TiO$_2$A$_3$ with 0.005 M HCl and 0.1 M HCl (n=3)

| Exp.	Type of metal oxide	Particle size (µm)	Temp. (°C)	^{68}Ge loaded (mCi)	HCl (M)	^{68}Ge Retained (%)	^{68}Ga Eluted (%)
18	TiO$_2$A$_3$u	No Sieving	No Heat	0.998	0.005	100	20
19	TiO$_2$A$_3$h	No Sieving	850	1.042	0.005	40	62
20	TiO$_2$A$_3$h	No Sieving	850	1.140	0.1	50	40
21	TiO$_2$A$_3$u	No Sieving	No heat	1.244	0.1	100	45

Table 4.9: ^{68}Ge retention of the TiO$_2$A$_4$ with 0.005 M HCl and 0.1 M HCl (n=3)

Exp.	Type of metal oxide	Particle size (µm)	Temp. (°C	^{68}Ge loaded (mCi	HCl (M)	^{68}Ge Retained (%)	^{68}Ga Eluted (%)
22	TiO$_2$A$_4$u300	212-300	No heat	1.118	0.005	60	39
23	TiO$_2$A$_4$h212	90-212	850	1.555	0.005	30	24
24	TiO$_2$A$_4$u212	90-212	No heat	1.612	0.1	100	54
25	TiO$_2$A$_4$h300	212-300	850	1.624	0.1	35	35

When using these TiO$_2$ sources (Table 4.8 and Table 4.9), the use of 0.005 M HCl as eluent of ^{68}Ga was immediately rejected albeit impressive loading results (Experiment 18, 21 and 22), as there was massive breakthrough of ^{68}Ge, thereby, disqualifying the use of this method. The use of TiO$_2$A$_4$ with heat treatment (850 ^{o}C, 3 hours) showed retention of the ^{68}Ge of 50% with the 0.1 M HCl eluate (Experiment 20) and 40% in the 0.005 M HCl eluate (Experimental 19). However when heat pretreatment was not used on the TiO$_2$A$_4$ (Experiment 18 and 21), 100% retention of ^{68}Ge was obtained with both the 0.1 M HCl and 0.005 M HCl eluent. This could be attributed to the morphology and particle size of the TiO$_2$A$_3$, two important factors to control for an effective application of the TiO$_2$ powders as ^{68}Ge/^{68}Ga generator sorbents.
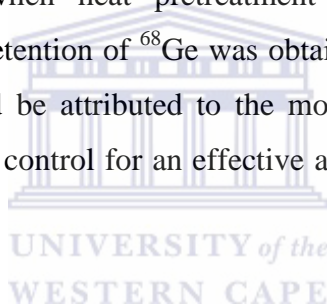
Because heat treatment of the sample increased particle size (see Table 4.1) and simultaneously reduced the surface area, the untreated TiO$_2$A$_3$ and TiO$_2$A$_4$ sample (Experiment 18, 21 and 24) showed higher adsorption of ^{68}Ge of 100%. While, on the other hand, the untreated sample showed adsorption of ^{68}Ge of 60% (Experiment 22). Additionally, a particle size of 90-212 µm meant a reduced particle size when compared to a particle size of 212-300 µm (Experiment 22-25); this in turn, implied an increased surface area. The improved ^{68}Ge retention observed for experiment 24 could be attributed to the more theoretical plates that could be available with the smaller particle size (90-212 µm) TiO$_2$A$_4$ compared to the larger particle size (212-300 µm). Because of this reason, the particle size fraction of 212-300 µm obtained much lower ^{68}Ge adsorption when compared to 90-212 µm. Experiment 23 and 25 showed low ^{68}Ge adsorption due to bigger particle size which played a more significant role than the heat treatment. From the results, it was deduced that the anatase form of TiO$_2$ and a smaller particle size are essential for effective ^{68}Ge adsorption.

4.8 ^{68}Ga Elution and ^{68}Ge Breakthrough Analysis

Of the five TiO$_2$ metal oxides investigated, the TiO$_2$A$_0$ (>212 µm, unheated, 0.005 M HCl), TiO$_2$A$_3$ (heated, 0.1 M and 0.005 M HCl) and TiO$_2$A$_4$ (90-212 µm, unheated, 0.1 M HCl), showed 100% retention of ^{68}Ge. Both the Sigma Aldrich TiO$_2$ (TiO$_2$A$_1$ and TiO$_2$A$_2$) showed no retention of ^{68}Ge at the particle size or treatment evaluated. During the course of the investigations, STMI stopped producing its TiO$_2$ on a commercial basis and therefore no further investigations were pursued with this TiO$_2$ source. The TiO$_2$A$_3$ (850°C, 0.1 M or 0.005 M HCl) and TiO$_2$A$_4$ (90-212 µm, unheated, 0.1 M HCl), was therefore pursued for further investigations as set out in Table 4.10. Table 4.10 represents the results of the TiO$_2$A$_3$ and TiO$_2$A$_4$ after each metal oxide was loaded with approximately 15 mCi ^{68}Ge in 0.1 M HCl. Again, n is the number of observations in the original sample.

Table 4.10: ^{68}Ge **retention and** ^{68}Ga **desorption of the TiO$_2$A$_3$ and TiO$_2$A$_4$ with 0.1 M HCl (n=3)**

Exp.	Type of metal oxide	Particle size (µm)	Temp. (°C)	^{68}Ge loaded (mCi)	HCl (M)	^{68}Ge Retained (%)	^{68}Ga Elution (%)
26	TiO$_2$A$_3$u	No Sieving	No heat	15.225	0.1	100	45
27	TiO$_2$A$_4$h212	90-212	No heat	15.448	0.1	100	54

A 15 mCi TiO$_2$A$_3$ based ^{68}Ge/^{68}Ga generator and TiO$_2$A$_4$ based ^{68}Ge/^{68}Ga generator system, prepared as described in Chapter 3, section 3.2 (Experiment 26 and 27), were evaluated over a 12 month period and results are shown in Figures 4.13 to Figure 4.16.
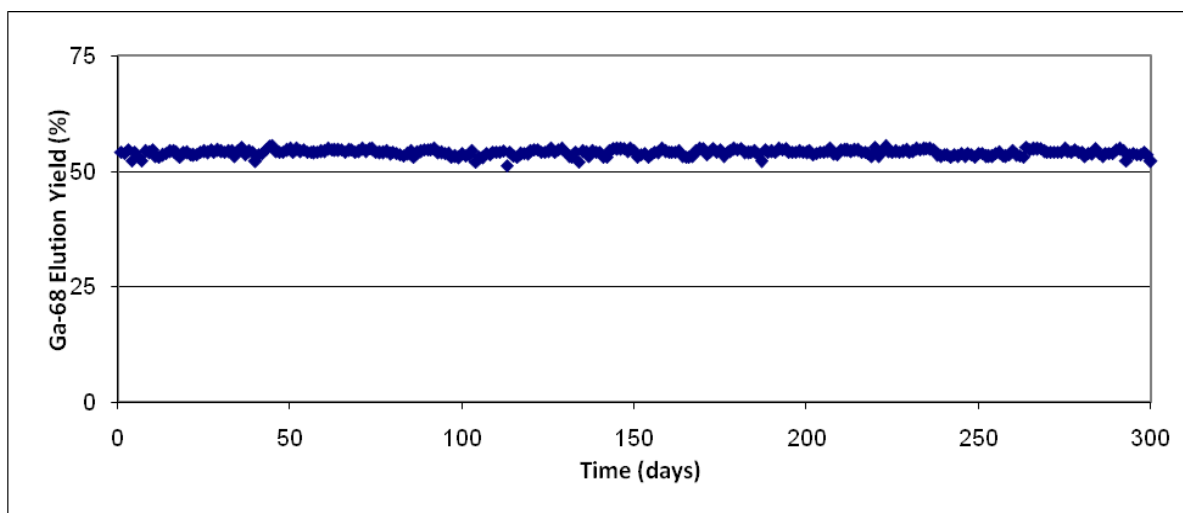
Figure 4.13: Elution Efficiency of ^{68}Ga of TiO$_2$A$_4$ in 0.1 M HCl (column: 3 mm i.d. x 30 mm length; sorbent: 3 g TiO$_2$A$_4$; ^{68}Ge loaded onto the column: 15 mCi; eluent: 0.1 M HCl)

Figure 4.14: Elution Efficiency of ^{68}Ga TiO$_2$A$_3$ in 0.1 M HCl (column: 3 mm i.d. x 30 mm length; sorbent: 3 g TiO$_2$A$_3$; ^{68}Ge loaded onto the column: 15 mCi; eluent: 0.1 M HCl)

Figure 4.13 shows the ^{68}Ga elution curve of the TiO$_2$A$_4$ based ^{68}Ge/^{68}Ga generator showing a consistent yield of 54% at over 300 elutions and Figure 4.14 shows the ^{68}Ga elution curve of TiO$_2$A$_3$, which yielded 40% ^{68}Ga over 300 elutions. For both these TiO$_2$ samples evaluated, the ^{68}Ga elution curves appeared relatively stable throughout the 300 elutions, displaying good stability and no physical degradation over the more than 12 month period.

The immediate difference between the two TiO_2 metal oxides (TiO_2A_3 and TiO_2A_4) could be seen in the intensity of the peaks when XRD as well as the images generated by SEM and TEM technique were analyzed, which revealed the crystallite size and crystallinity, respectively. The peaks of the TiO_2A_3 metal oxide were higher, indicating a larger crystallite size, with higher overall crystallinity, while the peaks of the TiO_2A_4 metal oxide were were smaller, sharper and more defined, representing larger, more uniform crystallite in terms of size and distribution. Therefore, the higher ^{68}Ga elution of TiO_2A_4 metal oxide compared to the TiO_2A_3 may be associated with three key parameters: smaller particle size, no heat treatment and high anatase content. The use of a heat treatment to preheat the TiO_2A_3 had a negative effect on the surface area. Breakthrough of ^{68}Ge was determined 24 hours after elution (see Experiment 3.3.2), using 50 cm distance at which the ^{68}Ge detector was calibrated. After a period of 12 months, the ^{68}Ga generator was still performing well, with no visible sign of breakthrough of ^{68}Ge or metal oxide discolouration. As shown in Figure 4.15 and Figure 4.16, the ^{68}Ge breakthrough for the TiO_2A_4 metal oxide for over 300 elutions was averaging at about 0.05% compared to less than 0.05% for the TiO_2A_3 metal oxide**.** This implied that, even though the ^{68}Ga efficiency for the TiO_2A_4 was above 50% mark, more work needed to be done in order to improve the ^{68}Ge breakthrough.
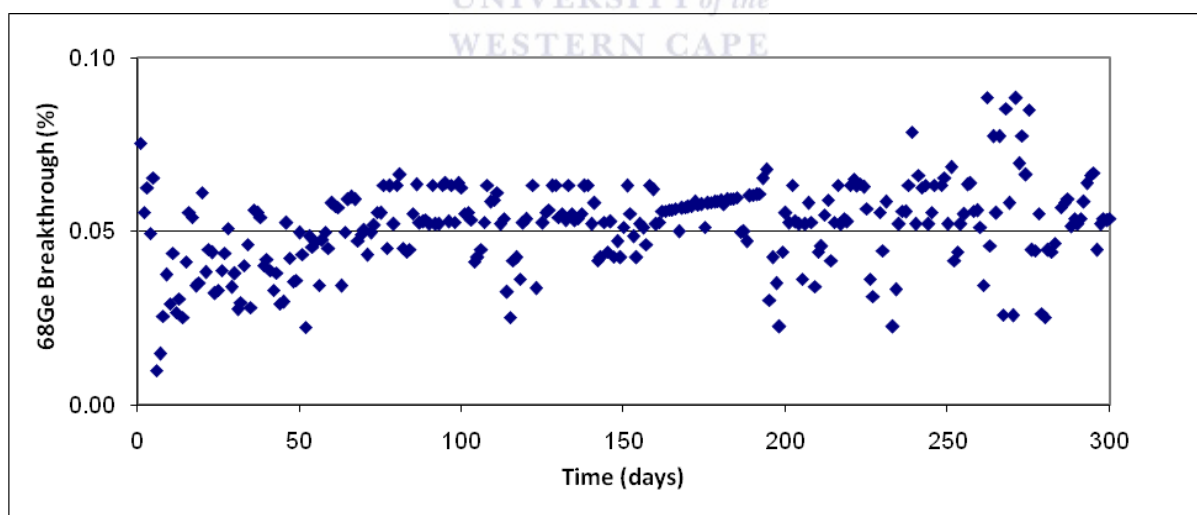
Figure 4.15: ^{68}Ge breakthrough of TiO_2A_4 in 0.1 M HCl (column: 3 mm i.d. x 30 mm length; sorbent: 3 g TiO_2A_4; ^{68}Ge loaded onto the column: 15 mCi; eluent: 0.1 M HCl)
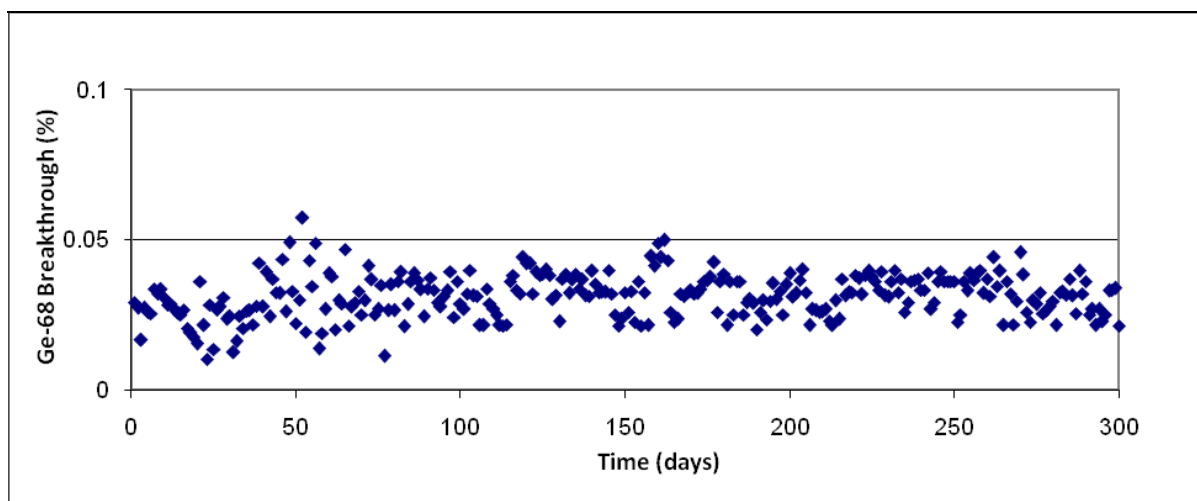
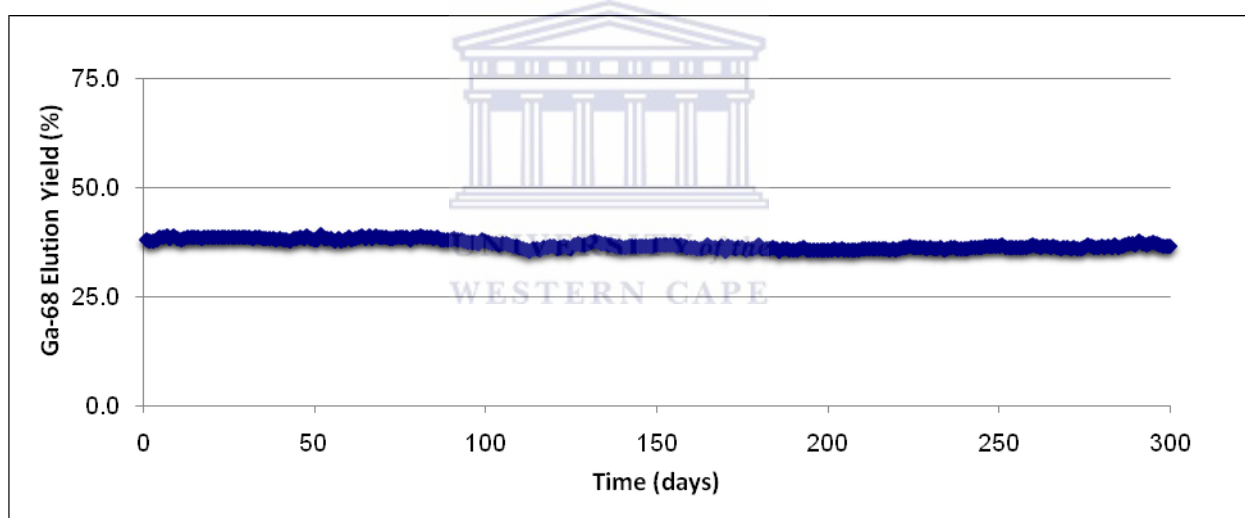Figure 4.16: ^{68}Ge breakthrough of TiO$_2$A$_3$ in 0.1 M HCl (column: 3 mm i.d. x 30 mm length; sorbent: 3 g TiO$_2$A$_3$; ^{68}Ge loaded onto the column: 15 mCi; eluent: 0.1 M HCl)

Because of the superior ^{68}Ga elution of above 50%, further investigations were limited to the TiO$_2$A$_4$ based ^{68}Ge/^{68}Ga generator. On the other hand, the ^{68}Ge breakthrough of the TiO$_2$A$_4$ metal oxide implied that more work was required for the improvement of this limitation.

Figure 4.17 shows the elution profile of the ^{68}Ga of the TiO$_2$A$_4$ based ^{68}Ge/^{68}Ga generator where it was shown that generally >95% of the ^{68}Ga was eluted in the first 6-7 ml and >80% of the ^{68}Ga could be found in a single 6 ml fraction.

Figure 4.17: ^{68}Ga Elution Profile of the TiO$_2$A$_3$ metal oxide (column: 3 mm i.d. x 30 mm length; sorbent: 3 g TiO$_2$A$_4$; ^{68}Ge loaded onto the column: 15 mCi; eluent: 0.1 M HCl)

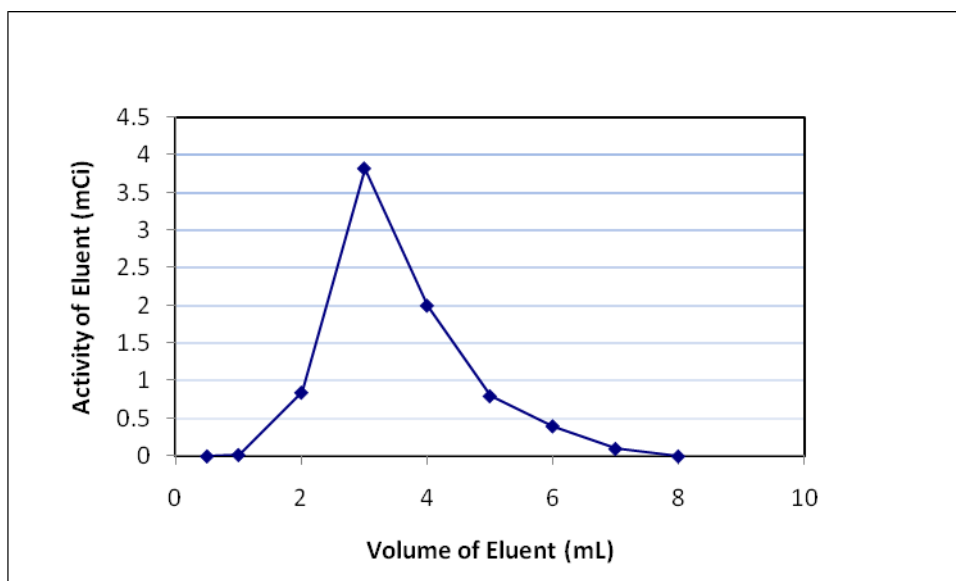The elution profile step, as explained in Section 3.2 (Experiment 28), was performed to recover the maximum amount of ^{68}Ga in the minimal volume of 0.1 M HCl from the ^{68}Ge generator eluate. The elution profile of the ^{68}Ga from the TiO$_2$A$_4$ metal oxide shows the highest elution in the first 4 ml 0.1 M HCl fraction, i.e. >80% in fraction # 1-5 and >10% in fraction # 5-6. Altogether, about 95% of ^{68}Ga were being successively eluted in only 6 ml of HCl. This implied that a smaller elution volume was required in order to elute the sorbed ^{68}Ga. This is a ^{68}Ge/^{68}Ga generator requirement as it leads to a short chemical separation process and can be an important factor in the final product as the yield is dependent on the half-life of a specific radionuclide. It would also minimize the quantities of waste solutions being generated (which are normally radioactive, should the separation involve radioactivity), which are monitored and, normally, have to be stored for a period of time before being released to waste storage dams on site.

4.9 ^{68}Ga Eluate Metal Analysis

Table 4.11 represents the results of analysis for the determination of the elemental composition of the eluate using the TiO$_2$A$_4$ source. The analytical curves for the Zn, Fe, Sn, Ti, Cu, Al, Ga and Ge were done according to the procedure described in the experimental part (3.4.6). The curves are shown in Appendix B. The analysis was for Zn, Fe, Sn, Ti, Cu,

Al, Ga and Ge determinations in the several ^{68}Ga eluate samples over a period of 12 months. The results are described in Table 4.10. As before, *n* is the number of observations in the original sample.

Table 4.11: Random metal analysis of ^{68}Ga eluate of the TiO$_2$A$_4$ (ppm) (n=3)

Run No.	Zn	Fe	Sn	Ti	Cu	Al	Ga	Ge
1	<1	<1	<1	<1	<1	<1	<1	<1
2	<1	<1	<1	<1	<1	<1	<1	<1
3	<1	<1	<1	<1	<1	<1	<1	<1
4	<1	<1	<1	<1	<1	<1	<1	<1
5	<1	<1	<1	<1	<1	<1	<1	<1
6	<2	<1	<1	<1	<1	<1	<1	<1
7	<1	<1	<1	<1	<1	<1	<1	<1
8	<1	<1	<1	<1	<1	<1	<1	<1
9	<1	<1	<1	<1	<1	<1	<1	<1
10	<1	<1	<1	<1	<1	<1	<1	<1
11	<1	<1	<1	<1	<1	<1	<1	<1
12	<1	<1	<1	<1	<1	<1	<1	<1

The results of Table 4.11 demonstrated that random metal analysis of the 300 daily elutions (eluate) of the TiO$_2$A$_4$ had shown that the metal ion impurities of Zn, Fe, Sn, Ti, Cu, Al, Ga and Ge, were found to be <1 ppm for each metal. This was an important requirement as any chemical impurities in the ^{68}Ga eluate would interfere in the complexation of ^{68}Ga with the various ligands and biomolecules. As was pointed out in the introduction to this study in chapter 1, section 1.3, high metallic impurities would adversely affect the ^{68}Ga labelling yields as well as the activity of the labelled product. The regular analysis of ^{68}Ga eluates for a range of metals, i.e. Zn, Fe, Sn, Ti, Cu, Al, Ga and Ge, was carried out and any sudden change in concentration of a particular metal would have indicated a defect before the TiO$_2$ based ^{68}Ge/^{68}Ga generator fails completely.

4.10 Chapter Summary

In this chapter, a ^{68}Ge/^{68}Ga radionuclide generator based on an inorganic cation exchange mechanism on a titanium oxide (TiO$_2$) is presented. A more detailed description of ^{68}Ge/^{68}Ga generators is given in Chapter 2. In a first approach, the determination of adsorption parameters by the various TiO$_2$ sources was investigated in batch studies. In a second approach, characterization studies (XRD, XRF, SEM and TEM) of the supplied TiO$_2$ samples

were performed to better understand parameters such as particle size, morphology as well as chemical composition. In a third approach, the effectiveness of any TiO_2 source relies on the ^{68}Ga radioactivity produced, ^{68}Ge breakthrough and metallic ion contamination of the ^{68}Ga eluate. Quality assessment and operational performance evaluation were carried out in order to determine the difference between the TiO_2 sources on the required properties of a $^{68}Ge/^{68}Ga$ generator. Unfortunately, during this time STMI stopped production of the oxtain TiO_2 used for initial experiments, before any valuable information could be gained from the STMI TiO_2 metal oxide. In the literature, several examples of metal oxides were presented, that could, instead, be used for the ^{68}Ge adsorption; however, due to time constraints it was opted to only pursue commercially available TiO_2 compounds. As a result, Sigma-Aldrich and Alfa-Aesar TiO_2 in anatase and rutile form as well as Aeroxide® and Aerolyst® sourced from Evonik TiO_2 powders were then investigated. Unfortunately, the experiments involving anatase and rutile form had to be abandoned due to a low ^{68}Ge adsorption displayed by both sorbents.

With complete understanding of the principle of ^{68}Ge loading of the two sorbents (Aeroxide® and Aerolyst® sources from Evonik), it was possible to carry out ^{68}Ga elution performance and ^{68}Ge breakthrough and its evaluation. Excellent results were obtained when both Aeroxide® and Aerolyst® sources from Evonik TiO_2 powders were investigated. When the Aerolyst® source was used, more than 50% of the ^{68}Ga radioactivity was eluted in 5 ml 0.1 M HCl solution over a period of 12 months. On the other hand, when the Aeroxide® was used, more than 40% of the ^{68}Ga radioactivity was eluted in 5 ml 0.1 M HCl solution over the same period of time. The long half-life of the ^{68}Ge provided long operating lifetime of the ^{68}Ga generator. The regular analysis of the ^{68}Ga eluate for a range of quality control parameters (^{68}Ga efficiency, ^{68}Ge breakthrough and metal contaminants) was carried out and any sudden change in these response parameters would have indicated a wear of the column before the TiO_2 source fails completely. Finally, analysis of the metal contaminants followed.

Based on the encouraging results from the preliminary experiments, a study was performed using Aeroxide® and Aerolyst® (Evonik Industries) TiO_2 powders (TiO_2A_3 and TiO_2A_4). In the case of the Aeroxide® (TiO_2A_3), the optimum parameters (100% load with 0.1 M HCl) for the ^{68}Ge loading were found to be: 3 g, unsieved, 850 °C for 3 h. Again, in the case of the

Aerolyst®, the optimum parameters were found to be: 3 g, 90-212 µm and no heat treatment. The elution yield of the TiO_2A_3 and TiO_2A_4 were found to be 45 and 54%, respectively. An elution value of less than 60% indicates poor yield. Such low value was the result of HCl concentration (0.1 M) which had to be unchanged due to labeling studies which uses this acid strength as means of elution medium. The ^{68}Ge breakthrough in the ^{68}Ga eluate from the TiO_2A_4 was low and consistent at 0.05% when compared to that of TiO_2A_3 which was also consistently less than 0.05%. The ^{68}Ge breakthrough of the TiO_2A_4 implied that more work had to be done in order to reduce the amount of ^{68}Ge co-eluted with ^{68}Ga. Morphological characterization was performed to understand characteristics of the samples. X-ray diffraction (XRD was used to calculate the crystallite size. Scanning Electron Microscopy (SEM) and Transmission Electron Microscopy (TEM) were performed to determine the grain size and particle size, respectively. In almost all the cases, when the particle size was decreased, significant amounts of ^{68}Ge could be loaded onto the TiO_2 metal oxides and this was attributed to the large surface area exhibited by the reduced particle size.

The adsorption of nitrogen method for determination of porous structure for the heated and unheated TiO_2A_3 and TiO_2A_4 samples was investigated. Analysis of the shapes of the N_2 isotherms, the amount of the N_2 adsorbed and the relative pressure values, provided useful information about the pore volumes, specific surface areas and pore sizes by means of the solid and gas interactions, which were used to qualitatively predict the types of pores present in the adsorbent. The influence of temperature upon porosity of the TiO_2 sources was studied by BET derived from the isotherms, pore volumes and surface area data of the nitrogen gas. Nitrogen adsorption isotherms of the TiO_2A_3 and TiO_2A_4 were of type I and II, respectively, as mesoporous class in the Brunauer classification. Characteristics of different pore size distribution of the TiO_2 sources under investigation were used to describe the adsorption process. The pore volumes calculated from t-plot were found to be approximately 0 to 4 cm^3g^{-1} for the heated samples and between 20 and 30 cm^3g^{-1} for the unheated samples. The shape of the isotherms changes extremely due to high temperature treatment, an indication of the effect of contracting surface area due to increased particle size during the thermal modification process, which is proved to have an adverse effect on adsorption properties.

The presence of metallic impurities in the ^{68}Ga eluate is highly relevant and can affect the utility of the product. Quantification of the amounts of metallic impurities was done by Inductively Coupled Plasma Optical Emission Spectrometry (ICP-OES) and no impurities were detected during HCl elution of the Aeroxide® and Aerolyst® sourced from Evonik TiO_2 powders.

In conclusion, the objective of the present study, namely to obtain a radiochemically pure ^{68}Ga from a TiO_2 based $^{68}Ge/^{68}Ga$ generator in a short a period, was achieved. A number of techniques, in conjunction with production of a $^{68}Ge/^{68}Ga$ generator, were used to determine the physico-chemical forms of the TiO_2 sources that allowed the separation of ^{68}Ga from the ^{68}Ge radionuclide. A number of TiO_2 sources are commercially available. The most important commercial TiO_2 source for this study is the Aerolyst® sourced from Evonik TiO_2 powders. This metal oxide has a stable crystallite structure, allowing long-term use of the ^{68}Ga generator; high corrosion resistance, that can otherwise affect the quality of the ^{68}Ga eluate negatively, TiO_2 with a purity of 98% was used, implying fewer impurities found in the TiO_2 source for contamination purposes. Under optimum conditions (eluate concentration, column dimensions, TiO_2 source, amount of TiO_2 used) the ^{68}Ga radionuclide was eluted from the ^{68}Ge generator; and radionuclidic purity aspects needed during radiochemical processing to provide ^{68}Ge eluate of high radionuclidic, radiochemical and chemical purity were achieved.

Chapter Five

CONCLUSION

^{68}Ge/^{68}Ga generators serve as a reliable source for the radionuclide ^{68}Ga (half-life = 68 mins) which when coupled to DOTA-peptides is used effectively as a nuclear medicine diagnostic tool for neuro-endocrine tumours. It is becoming increasingly difficult to ignore the attractive and ideal chemical properties of this PET radionuclide. As more PET-CT scanners are installed and commissioned in nuclear medicine departments across the world, the demand for an efficient and commercially available ^{68}Ge/^{68}Ga generator is increasing. In the past three decades a number of researchers have sought to find an ideal sorbent material for the ^{68}Ge/^{68}Ga generator which would provide favourable properties for ^{68}Ga efficiency, with minimum ^{68}Ge breakthrough and that would minimize metal impurities found in the eluate over the life span of the generator which is generally 9-12 months.

Little is known about the conditions necessary for the ^{68}Ge adsorption and it is not clear what factors supports ^{68}Ga desorption. There are several reasons that could affect the retention of ^{68}Ge on the column negatively, for instance, complex chemical, physicochemical, radiochemical processes in the column, mechanical defects and insufficient volume of the eluent. When it comes to TiO_2 sources, different microstructures could lead to different physical properties which, in turn, lead to different applications. This conclusion is supported by the results (Table 4.4 to Table 4.8) of the various TiO_2 sources that were analyzed where the knowledge of microstructure (grain size, crystalline structures, surface composition, etc) was indispensable for understanding the macroscopic behaviour of the TiO_2 sources. In addition, no research that surveyed the surface area, particle size and the morphology of the TiO_2 has been found. The key research question of this study was to determine whether TiO_2 could be used as a sorbent material for the production of a ^{68}Ge/^{68}Ga generator that could be

used in clinical application. Various types of commercially available TiO_2 were investigated to determine whether these sources of TiO_2 differed in their properties.

As shown in the literature survey, commercially available $^{68}Ge/^{68}Ga$ generators have generally used SnO_2 or TiO_2 as the generator column eluate. Kozlova et al., (1970) were the first researchers who produced a TiO_2 based $^{68}Ge/^{68}Ga$ where 3 g of the TiO_2 in 0.005 M HCl was used for the absorption of ^{68}Ge and 0.1 M HCl was used for the desorption of ^{68}Ga. Kozlova and colleague's work was used as a basis for this work. In this study five commercially available TiO_2 metal oxide materials, STMI TiO_2, Sigma-Aldrich rutile TiO_2, Sigma-Aldrich anatase TiO_2, Aeroxide® P-25 TiO_2 and Aerolyst® TiO_2 were evaluated for the absorption of ^{68}Ge and desorption of ^{68}Ga by varying TiO_2 particle size, heat treated or unheated and varying the HCl concentration (0.005 M - 0.1 M) for the loading of ^{68}Ge and stripping of ^{68}Ga.

Characteristics of the TiO_2 metal oxide such as morphology, particle size and composition were assessed and evaluated for their impact upon the ^{68}Ge loading obtained under acidic conditions. The higher loading of ^{68}Ge obtained corresponded well to small particle size as determined by XRD, SEM, TEM and BET techniques.

 The STMI TiO_2 (>200 µm, unheated, 0.005 M HCl), Aeroxide® P-25 TiO_2 (heat-treated at 850 °C , 0.1 M and 0.005 M HCl) and Aerolyst® TiO_2 (90-212 µm, unheated, 0.1 M HCl), showed the best absorption qualities of ^{68}Ge at 100%. This source of TiO_2 was used to bench-mark further experiments as the manufacturing of the TiO_2 product came to an abrupt end. Both the Sigma Aldrich TiO_2 (rutile and anatase) showed no absorption of ^{68}Ge at any particle size or heating profile. The Evonik Aeroxide® TiO_2 (heated, 0.1 M and 0.005 M HCl) and Aerolyst® TiO_2 (90-212 µm, unheated, 0.1 M HCl), were pursued for further investigations.

Between the two sorbents (Aeroxide® P-25 and Aerolyst®), the Aerolyst® makes the better sorbent for a ^{68}Ga generator, as the ^{68}Ga desorption was marginally better than when Aeroxide® TiO_2 was used. Additionally, the study also found that no heat was required when the Aerolyst® was used as a sorbent. This is particularly important in sorbents as less time

and energy is required for modification. Nevertheless, the use of either of the sorbents produced a ^{68}Ge/^{68}Ga generator that had vastly fewer impurities than the existing production method in use in iThemba LABS, making this a ^{68}Ge/^{68}Ga generator that can be regarded as ultrapure.

A 15 mCi Aerolyst® TiO$_2$ based ^{68}Ge/^{68}Ga generator and Aeroxide® TiO$_2$ based ^{68}Ge/^{68}Ga generator system was evaluated over 12 months and it was shown that the ^{68}Ga elution of the Aerolyst® TiO$_2$ based ^{68}Ge/^{68}Ga generator was 54% at over 300 elutions and the ^{68}Ga elution of Aeroxide® TiO$_2$ was only 40% at over 300 elutions. For both sources of TiO$_2$, the ^{68}Ga elutions appeared relatively stable throughout the 300 elutions, displaying good stability and low chemical degradation over the 12 month period. However, the ^{68}Ge breakthrough for the Aerolyst® TiO$_2$ metal oxide for the 300 elutions was averaging at about 0.05% compared to less than 0.05% for the Aeroxide® TiO$_2$ metal oxide. The Aerolyst® TiO$_2$ based ^{68}Ge/^{68}Ga generator was further investigated for metal impurities and it was shown that for a random metal analysis of the 300 daily elutions (eluate), the metal ion impurities of Zn, Fe, Sn, Ti, Cu, Al, Ga and Ge were found to be <1 ppm for each element.

The discovery of the relevancy of the Aerolyst® TiO$_2$ source was extremely valuable for the production of ^{68}Ge/^{68}Ga generators as it expedites the process by not requiring heat treatment, yet results in pure ^{68}Ga product. By using the SEM, TEM XRD and XRF techniques, the current study demonstrated that Aerolyst® TiO$_2$ metal oxide applied as a sorbent in the sorption of the ^{68}Ga radionuclide has the characteristics required to function in the ^{68}Ge/^{68}Ga generator capacity. It was possible to deduce the ^{68}Ga efficiency, ^{68}Ge breakthrough and metal analysis. This showed that a successful ^{68}Ge/^{68}Ga generator was achieved. Despite several other studies that have been conducted on ^{68}Ge/^{68}Ga generators, no other attempts have been made to provide information about the sorbent modifications. Through this study, it was shown that the Aerolyst® metal oxide can contribute considerably to the development of a TiO$_2$ based ^{68}Ge/^{68}Ga generator. This study, also described for the first time, a controlled investigation which compare and quantified the differences between the commercially available TiO$_2$ metal oxides. This study has three immediate benefits:

(a) By characterization of the various TiO$_2$ sources by XRD and XRF, techniques, the identification of phase and particle size as well as level of purities were confirmed.

(b) When SEM and TEM of the of Aeroxide® and Aerolyst® TiO_2 metal oxide were performed, information covering particle size, crystallinity and morphology was obtained.

(c) Consequently, insight into the finer details about the behaviour of the TiO_2 sources during [68]Ge loading, ^{68}Ga elution, breakthrough analysis and metal impurity analysis were deduced.

(d) Understanding of the factors affecting phase stability and phase transformation was important to design and controllably manipulate phase types and concentrations for more efficient use.

5.1 Recommendations and Future Work

To further develop understanding of a maximum ^{68}Ga efficiency accompanied by a non-existent [68]Ge breakthrough, future larger studies with statistical analyses of a TiO_2 based [68]Ge/^{68}Ga generator are of great interest. More research in this area is necessary before meaningful decision can be taken for the TiO_2 based [68]Ge/^{68}Ga generator. Secondly, despite its long clinical success, [68]Ge/^{68}Ga generators have a number of problems in use: leaking of columns which are attributed to degradation of the metal oxides and safety concerns. Several questions remain to be solved about the safety of the prolonged use of the [68]Ge/^{68}Ga generators. Therefore, it is recommended that a higher than 15 mCi generator be set up using the Aerolyst® TiO_2 metal oxide, eluted daily such that the ^{68}Ga eluted from the generator can be effectively, and directly, used for the labelling of peptides. Breakthrough studies, thereafter, should commence, and because this model is readily available, the values of the breakthrough of the Aerolyst® TiO_2 metal oxide will be closely assessed in an attempt to reduce them considerably. Results from such an exercise will be published in the near future. Further work on the Aerolyst® TiO_2 metal oxides should be focused on their treatment, as well as the assessment of their long-term stability.

Chapter Six

REFERENCES

Aardaneh, K. and Van Der Walt, T.N. (2006). Journal of Radioanalytical and Nuclear Chemistry, vol. 268, no. 1, pp. 25-32.

Antunes, P., Ginj, M., Zhang, H., Waser, B., Baum, R.P. and Reubi, J.C. (2007). Gallium-labelled DOTA-conjugated somatostatin analogues uperior to those labelled with other radiometals? European Journal of Nuclear Medicine and Molecular Imaging, vol. 34, pp. 982–93.

Bao, B. and Song, M. (1996). A new ^{68}Ge/^{68}Ga generator based on CeO_2, Journal of Radioanalytical Nuclear Chemistry, vol. 213 no. 1, pp. 233–238.

Barnes, G. and Gentle, I. (2005). Interfacial science: An Introduction, Oxford University Press Oxford, United Kingdom.

Baum, R.P. and Roësch, F. (2012) Theranostic, Ga-68 and other radionuclides: A Pathway to Personalized Diagnosis and Treatment. Radiotherapy and Molecular Imaging, Springer Heildeberg, New York, pp. 594 – 600.

Bauwens, M., Cheko, R. and Van Billoen, H. (2010). Optimal Buffer Choices for the Radiosynthesis of ^{68}Ga-DOTATOC for Clinical Application, Nuclear Medicine Communication, vol. 31, pp. 753-758.

Bjørnstad, T. (2004). "Industrial radionuclide generators — status and perspectives", paper presented at Conf. on Tracer and Tracing Methods, Ciechocinek, Poland.

Brady, G.S. (1971). Materials Handbook. New York: McGraw-Hill.

Breeman, W.A.P and Verbruggen, A.M. (2007). The ^{68}Ge/^{68}Ga generator has high potential, but when can we use ^{68}Ga-labelled tracers in clinical routine? European Journal of Nuclear Medicine of Molecular Imaging, vol. 34, pp. 978–981.

Breeman, W.A.P., de Jong, M., de Blois, E., Bernard, B.F., Konijnenberg, M. and Krenning, E.P. (2005). Radiolabelling DOTA-peptides with ^{68}Ga, European Journal of Nuclear Medicine, vol. 32, pp. 478– 485.

Breeman, W.A.P., Marion, J., Visser, T.J., Erion, J.L., Krenning, E.P. (2003). Optimising conditions for radiolabelling of DOTA-peptides with ^{90}Y, ^{111}In and ^{177}Lu at high specific activities, European Journal of Nuclear Medicine for Molecular Imaging, vol. 33, pp. 917 – 920.

Burger, C. and Townsend, D.W. (2003). Basic of PET Scanning. In: Schultess, G. Clinical PET, PET/CT and SPECT/CT. Lippincott, vol. 3, pp. 14 – 39.

Caletka, R. and Kotas, P. (2004). Separation of Germanium from some elements by adsorption of silica gel. Journal of Radioanalytial Chemistry, vol. 21, pp. 349-353.

Carter, H. K. Hamilton, J. H. Ramayya, A. V. and Pinajian J. J. (1968). Evidence of a O+ State in *Zn populated by "Ga". Physics Revision, vol. 174, pg. 1329.

Cesareo, R., Gigante, G.E., Castellano, A. and Iwanczyk, J.S. (2000). Portable Systems for Energy-dispersive X-ray Fluorescence, in: Encyclopedia of Analytical Chemistry, R. A. Meyers (Ed.), J. Wiley & Sons Ltd., Chichester, pp. 13327-13338.

Chakravarty, R., Shukla, R., Ram, R., Tyagi, A.K., Dash, A. and Venkatesh M. (2011). Development of a nano-zirconia based [68]Ge/^{68}Ga generator for biomedical applications, Nuclear of Medical Biology, vol. 38, no. 4, pp. 575-83.

Clarke, A. R. (2002). Microscopy Techniques for Materials Science. CRC Press (electronic resource)

De Blois, E, Sze-Chan, H., Naidoo, C, Prince, D., Krenning, E.P. and Breeman, W.A. (2011). Characteristics of SnO_2-based [68]Ge/[68]Gagenerator and aspects of radiolabelling DOTA-peptides. Applied Radiation Isotope, vol. 69, pp. 308–315.

Decristoforo, C., Knopp, R., von Guggenberg, E., Rupprich, M., Dreger, T., and Hess, A. (2007). A fully automated synthesis for the preparation of ^{68}Ga-labelled peptides. Nuclear Medicine Communication, vol. 28, pp. 870–875.

Decristoforo, C., Von Guggenberg, E., Haubner, R., Rupprich, M., Schwarz, S. and Virgolini, I. (2005). Radiolabelling of DOTA-derivatised peptides with ^{68}Ga via a direct approach: optimization and routine clinical application, 27th

International Symposium: Radioactive isotopes in clinical medicine and research, Nuclear Medicine, vol. 6, pg. 191.

Depero, L.E., Bonzi, P., Zocchi, M., Casale, M. and De Michele, G. (1993). "Study of the Anatase-Rutile Transformation in TiO_2 Powders Obtained by Laser-Induced Synthesis," Journal of Materials Research, vol. 8, no. 10, pp. 2709-2715.

Deutsch, E. (1993). Clinical PET: its time has come? Journal of Nuclear Medicine, vol. 34, pp. 1132–1133.

Egerton, R. F. (2005). Physical principles of electron microscopy: an introduction to TEM, SEM, and AEM. Springer, New York, pg. 202.

Erhardt, G.J. and Welsh, M.K. (1978). A new germanium ^{68}Ge/^{68}Ga generator. Journal of Nuclear Medicine, vol. 19, pp. 925-929.

Gleason, G.I. (1960). A positron cow. International Journal of Applied Radiation and Isotopes, vol. 8, pp. 90–94.

Goldstein, J. (2003). Scanning Electron Microscopy and X-ray Microanalysis. Kluwer Academic/Plenum Publishers, pg. 689.

Greene, W.T. and Tucker, W.D. (1961). An Improved gallium-68 cow, Internal Journal of Applied Radiation and Isotopes, vol. 12, pg. 62.

Hechel, J. and Ryon, R.W. (2001). Polarized Beam X-ray Fluorescence Analysis, Chapter 10 in: Handbook of X-ray Spectrometry, 2nd edition, (R.E.Van Grieken and A.A. Markowicz, Eds.), Marcel Dekker, New York.

Henze, M. Schuhmacher, J. Hipp, P. Kowalski, J. Becker, D.W. and Doll, J. (2001). PET imaging of somatostatin receptors using [^{68}Ga] DOTA-D-Phe1-Tyr3-octreotide: first results in patients with meningiomas, Journal of Nuclear Medicine, vol. 4, pp. 1053–1056.

Hofmann, M., Mäecke, H., Borner, R., Weckesser, E., Schoffski, P. and Oei, L. (2001). Bio-kinetics and imaging with the somatostatin receptor PET radio-ligand ^{68}Ga-DOTATOC, European Journal of Nuclear Medicine, vol. 28, pp. 1751–1757.

Horiguchi, H., Kumahora, H., Inoue, H. and Voshizawa, Y. (1983). "Excitation functions of Ge(p,xnyp) reactions and production of ^{68}Ge", International Journal of Applied Radiation and Isotopes, vol. 34, pg. 1531.

International Atomic Energy Agency, (2005). Report of Consultants Meeting on Radionuclide Generators for Industrial Radiotracer Technology, IAEA, Vienna, Austria.

International Atomic Energy Agency, (2013). Radiotracer Generators for Industrial Applications, IAEA Radiation Technology Series Publications, Vienna, Austria.

Keidar, Z., Israel, O and Krausz, Y. (2003). SPECT/CT in tumour imaging: technical aspects and clinical applications, Journal of Nuclear Medicine, vol. 33, pp. 205-208.

Kopecky, P. and Mudrova, B. (1974) ^{68}Ge/^{68}Ga generator for the production of ^{68}Ga in ionic form, International Journal of Applied Radiation and Isotopes, vol. 25, pp. 263-268.

Kopecky, P., Mudrova', B. and Svoboda, K. (1973). The study of conditions for the preparation and utilization of ^{68}Ge/^{68}Ga generator, International Journal of Applied Radiation and Isotopes, vol. 24, pp. 73–80.

Kozlova, M.D., Malinin, A.B., Kodina, G.E. and Sevastyanova, A.S. (1970). Radiopharmaceutical Department, Institute of Biophysics, Ministry of Public Health, Moscow, Russia, vol. 12, pg. 505.

Lange, J. Hamilton, J. H. Little, P. E. HalTox, D. L. Morton, D. C. Whitlock, L. C. and Pinajian, J. J. (1973). E2-Ml admixture of transitions in "Zn", Physics Revision, vol. 7, pg. 177.

Lippens, B.,and De Boer, J. (1965). Studies on pore systems in catalysts: V. the t method. Journal of Catalysis, vol. 4, pp. 319–323.

Loc'h, C., Maziere, B. and Comar, D.A. (1980). New generator for ionic gallium-68, Journal of Nuclear Medicine, vol. 21, pp. 171–173.

Mäecke, H.R., Hofmann, M. and Haberkorn, U. (2005). ^{68}Ga-labeled peptides in tumor imaging. Journal of Nuclear Medicine, vol. 46, no. 1, pp. 172S–178S.

Makinen, T.J. Lankinen, P. Poyhonen, T. (2005) Comparisons of ^{18}F-FDG and ^{68}Ga PET imaging in the assessment of experimental osteomyelitis due to Staphylococcus aureus, European Journal of Nuclear Molecular Imaging, vol. 32, pp. 1259-1268.

Mardsen, P.K. (2003). Detector technology challenges for nuclear medicine and PET, Nuclear Instruments and Methods of Physical Research; vol. 513, pp. 1 – 7.

Meyer, G-J, Macke, H., Schuhmacher, J., Knapp, W.H. and Hofmann, M. (2004). ^{68}Ga-labelled DOTA-derivatised peptide ligands, European Journal of Nuclear Medicine Molecular Imaging, vol. 31, pp. 1097–104.

Meyer, G-J., Gielow, P., Borner, A.R., Hofmann, M. and Knapp, W.H. (2005). Ga-67 and Ga-68 labelled DOTA-derivatised peptide-ligands, Journal of Nuclear Medicine, vol. 6, pg. A192.

Mirzadeh, S. (1978). Some Observations on the Chemical Behaviour of Carrier-Free ^{68}Ge, PhD Thesis, University of New Mexico.

Mirzadeh, S. and Lambrecht, R.M. (1995). Radiochemistry of Germanium, Journal of Radioanalytical and Nuclear Chemistry, vol. 202, no. 1-2, pp. 7-102.

Naidoo, C. Van Der Walt, T. and Raubenheimer, H.G. (2002). Cyclotron production of ^{68}Ge with Ga$_2$O target, International Journal of Radio-Analytical and Nuclear Chemistry, vol. 253, no. 2, pp. 221-225.

Naidoo, C., 1998. M.Sc. Thesis, University of Cape Town, South Africa.

Nakayama, M., Haratake, M., Ono, M., Koiso, T., Harada, K., Nakayama, H., Yahara, S., Ohmomo, Y. and Arno, Y. (2003). A new ^{68}Ge/^{68}Ga generator system using an organic polymer containing N-methylglucamine groups as adsorbent for ^{68}Ge, Applied Radiation Isotope, vol. 58, pg. 9.

Neirinckx, R.O. and Davis, M.A. (1980). Potential Column Chromatography for Ionic Ga-68: Organic Ion Exchangers as Chromatographic Supports, Journal of Nuclear Medicine, vol. 21, pg. 81.

Pennycook, S.J. Lupini, A.R. Borisevich, A. Varela, M. Peng, Y. Nellist, P.D. Duscher, G. Buczko, R. and Pantelides, S.T. (2003). Transmission Electron Microspy: Overview and Challenges in Characterization and Metrology for ULSI Technology, American Institute of Physics, New York, pg. 627.

Prasad, V. and Baum, R.P. (2010) Bio-distribution of ^{68}Ga labelled somatostatin analogue DOTA-NOC in patients with neuroendocrine tumours: characterization of uptake in normal organs and tumour lesions, Journal of Nuclear Medicine and Molecular Imaging, vol. 44, pp. 61-67.

Qaim, S.M. (2003). "Cyclotron production of medical radionuclides", Handbook of Nuclear Chemistry, Academic Publishers, Dordrecht, vol. 4, pp. 47–80.

Raj, K.J.A. and Viswanathan, B. (2009). Effect of surface area, pore volume and particle size of P25 titania on the phase transformation of anatase to rutile, Indian Journal of Chemistry, vol. 48A, pp. 1378-1382.

Razbash, A.A., Sevastianov, Y., Krasnov, N.N., Leonov, A.I. and Pavlikhin, V.E. (2005). Germanium-68 row of products, 5th International Conference on Isotopes, 5ICI, Brussels, Belgium, pp. 147-151.

Reimer, L. (1998). Scanning electron microscopy: physics of image formation and microanalysis, Springer, Heidelberg, pg. 527.

Reubi, J.C. Schar, J.C. Waser, B. Wenger, S. Heppeler, A. Schmitt,J.S.(2000). Affinity profiles for human somatostatin receptor subtypes SST1-SST5 of somatostatin radiotracers selected for scintigraphic and radiotherapeutic use, European Journal of Nuclear Medicine, vol. 27, pp. 273–282.

Röesch, F. and Knapp, F.F. (2003). Radionuclide generators, Handbook of Nuclear Chemistry. Dordrecht, The Netherlands: Kluwer Academic Publishers; vol. 4, pp. 811-812.

Röesch, F. and Riss, P.J. (2010). The renaissance of the ^{68}Ge/^{68}Ga radionuclide generator initiates new developments in ^{68}Ga radiopharmaceutical chemistry, Current Topics Medicinal Chemistry, vol. 10, no. 16, pp. 1633-1668.

Rösch, F. and Filosov, D.V. (2010). Production, Processing and Quality Evaluation of Ge-68 suitable for production of a ^{68}Ge/^{68}Ga generator, International Atomic Energy Agency.

Sadeghi, M., Kakavand, T., Rajabifar, S., Mokhtari, L. and Nezhad, A. R. (2009). "Cyclotron production of ^{68}Ga via proton induced reaction on ^{68}Zn target", Nukleonika vol. 54, pg. 25.

Saha, G.B. (2004). Basics of PET imaging/ Physics, Chemistry, and Regulations. Springer, New York.

Schumacher, J. and Maier-Borst, W. (1981). A new ^{68}Ge/^{68}Ga radionuclide generator system for production of ^{68}Ga in dilute HCl, Internal Journal of Applied Radiation and Isotopes, vol. 32, pg. 31.

Sen, K., Wolterbeek, H.T. and Breeman, W.A.P. (212). Speciation of no-carrier-added ^{68}Ga prior to its labeling for PET imaging, Journal of Radioanalytical and Nuclear Chemistry, vol. 29, pp. 683–687.

Smith, D. and Williams, A. (1971). A 4x/J-y coincidence method for mixed electron-capture/positron emitters: the absolute measurement of "Ga", Journal of Applied Radiation Isotopes, vol. 22, pg. 615.

Ujula, T., Salomaki, S. and Autio, A. (2009). ^{68}Ga chloride PET reveals human pancreatic adenocarcinoma xenografts in rats-comparison with FDG, Molecular Imaging Biology, vol. 12, pp. 259-268.

Van der Meulen, N. P. (2008). The Cyclotron Production of Selected Radionuclides using Medium Energy Protons, PhD Thesis, University of Stellenbosch, South Africa.

Van Der Walt, T.N. and Vermeulen, C. (2004). Thick targets for the production of some radionuclides and the chemical processing of these targets at iThemba LABS, Nuclear Instrument Methods for Physics Research, vol. 521, pp. 171–175.

Velikyan, I., Beyer, G.J. and Langstrom, B. (2004). Microwave-supported preparation of ^{68}Ga bio-conjugates with high specific radioactivity, Bio-conjugate Chemistry, vol. 15, pp. 554–560.

Waters, S.L. Horlock, P.L. Kensett, M.J. (1983). The application of hydrous tin(IV) oxide in radiochemical separations and, in particular, for the ^{68}Ge/^{68}Ga and ^{82}Sr/^{82}Rb generator system, International Journal of Applied Radiisotopes, vol. 34, pg. 1023.

Webb, P.A. and Orr, C. (1997). Analytical methods in fine particle technology, Micromeritics Norcross, GA, volume 229.

Wernick, N.M. and Aarsvold, J.N. (2004). Emission Tomography: The Fundamentals of PET and SPECT, Elsevier Academic Press, California, pp. 57-80

West, A.R. (2005). X-Ray Diffraction. In: Solid State Chemistry and its Applications. 1st Edition, John Wiley and Sons, Singapore, pp. 115-186.

Yano, Y. and Anger, H.O. (1964). A gallium-68 positron cow for medical use, Journal of Nuclear Medicine, vol. 5, pg. 484.

Zhang, D., Yang, X., Zhu, J., Zhang, Y. Zhang, P. and Li, G. (2011). Graphite- like carbon deposited anatase TiO_2 single crystals as efficient visible-light photocatalysts, Journal of Sol-Gel Science Technology, vol. 58, pp. 594–601.

Zhernosekov, K., Harfensteller, M., Moreno, J., Leib, O., Buck, O. and Tuerler, A. (2010). Development of a novel metal-free ^{68}Ge/^{68}Ga radionuclide generator system,

European Journal of Nuclear Medicine and Molecular Imaging, vol. 37, no. 2, pg. S251.

Zhernosekov, K.P., Filosofov, D.V. and Baum, R.P. (2007). Processing of generator – produced ^{68}Ga for medical application, Journal of Nuclear Medicine, vol. 48, no. 10, pp. 1741–1748.

Zimmerman, B.E., Cessna, J.T. and Fitzgerald, R. (2008). Standardization of ^{68}Ge/^{68}Ga Using Three Liquid Scintillation Counting Based Methods, Ionization Radiation Division, National Institute of Standards and Technology, Gaithersburg, vol. 113, pp. 265-280.

UNIVERSITY *of the*
WESTERN CAPE

Chapter Seven

APPENDICES

Appendix A: Reference Standard Solutions of the ICP-OES Analysis

Element	Concentration (ppm)	Catalogue Number	Supplier
Zinc (Zn)	1000	88118	Alfa-Aesar
Gallium (Ga)	1000	88066	Alfa-Aesar
Germanium (Ge)	1000	88067	Alfa-Aesar
Cupper (Cu)	1000	88061	Alfa-Aesar
Iron (Fe)	1000	88073	Alfa-Aesar
Titanium (Ti)	1000	35771	Alfa-Aesar
Aluminium (Al)	1000	33557	Alfa-Aesar
Tin (Sn)	1000	88112	Alfa-Aesar

Appendix B – ICP-OES Curves Analysis

**Table 7.2   The ICP intensities of standard concentrations**

Std's (ppm)	Intensities							
	Sn	**Ge**	**Zn**	**Fe**	**Cu**	**Ti**	**Al**	**Ga**
Blank	12.2	55.4	102.3	295.3	45.4	54.5	41.2	20.8
1	429.8	691.8	2874.2	1121.9	2452.1	3224.2	9655.7	3892.8
5	2252.2	3952.1	14970.	5584.5	13286	16254.	48233.4	20033.8
10	4536.5	8254.1	29075.9	12242.2	23847.4	33490.5	89666.9	40181.7
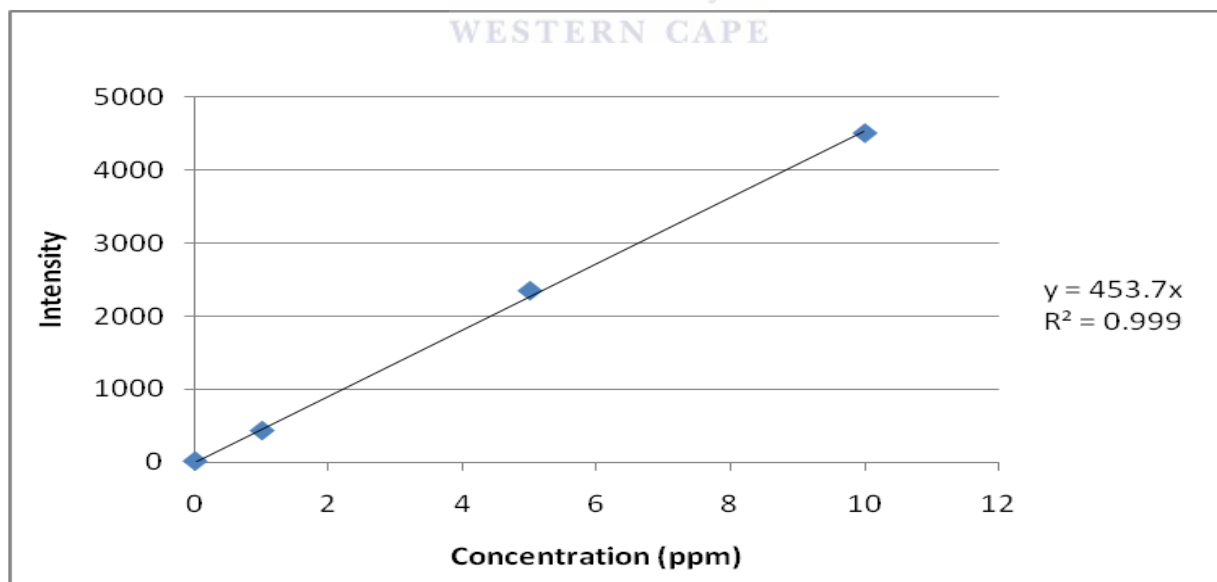
Figure 7.1 Calibration curve of Tin metal element
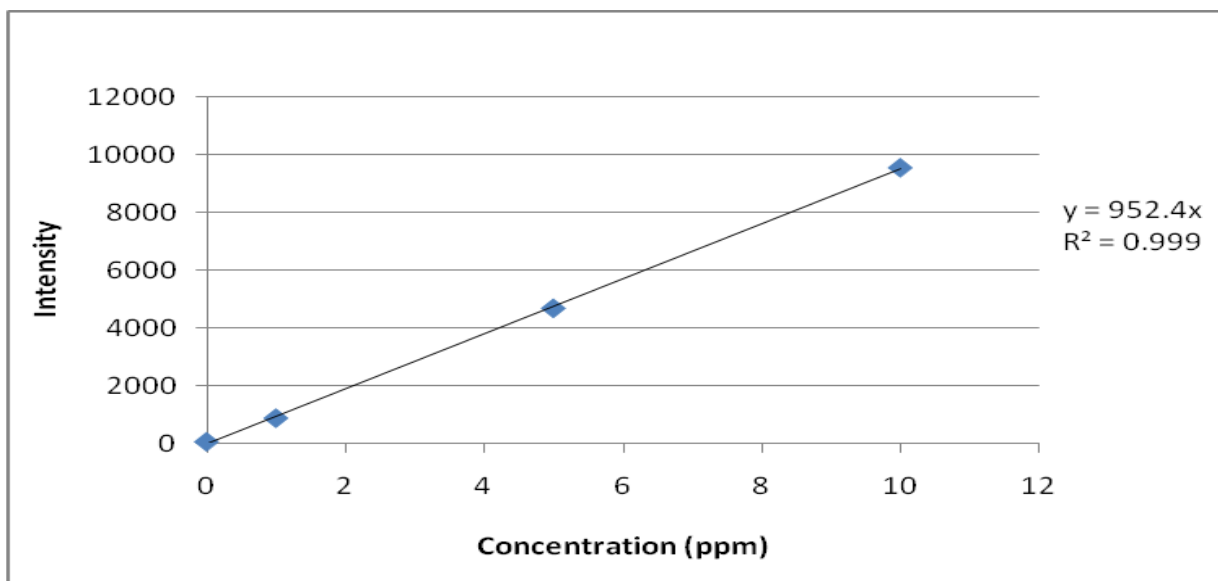
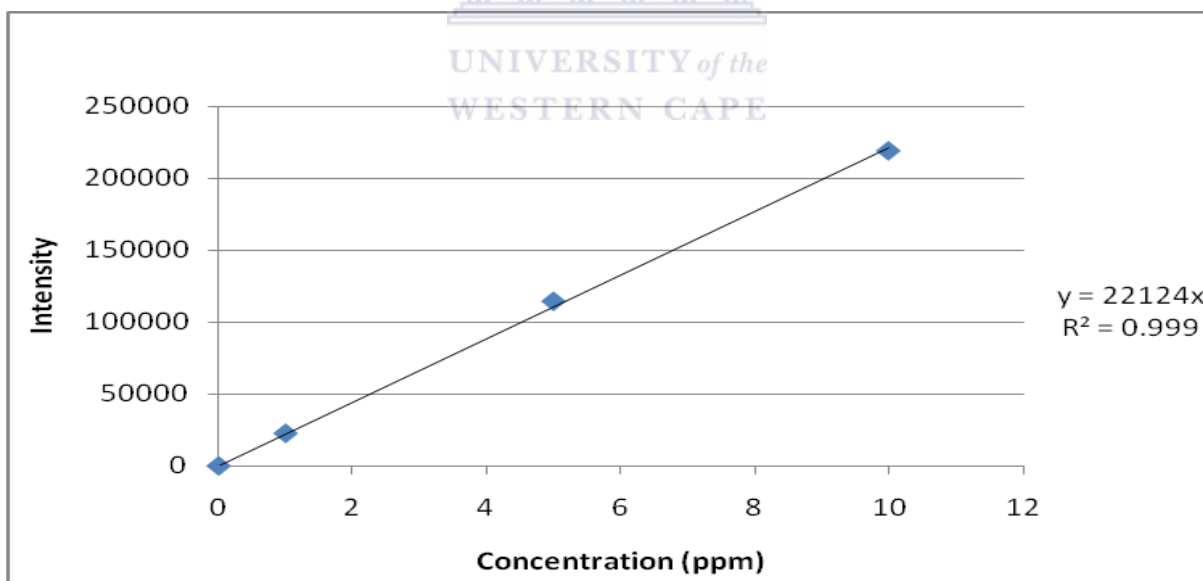**Figure 7.2: Calibration curve of Germanium metal element**
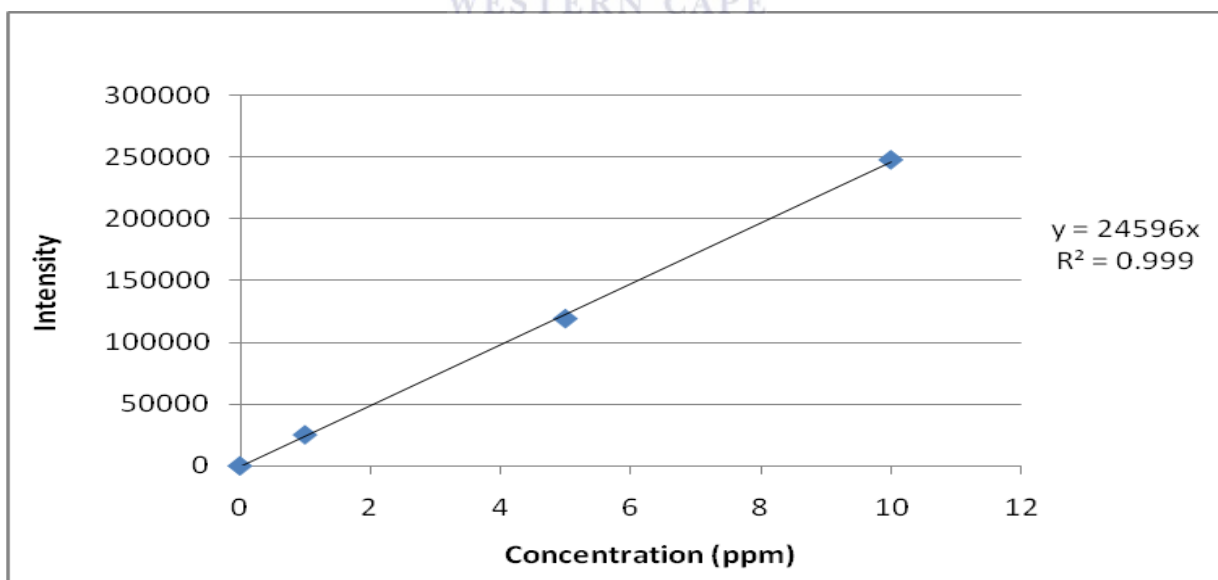
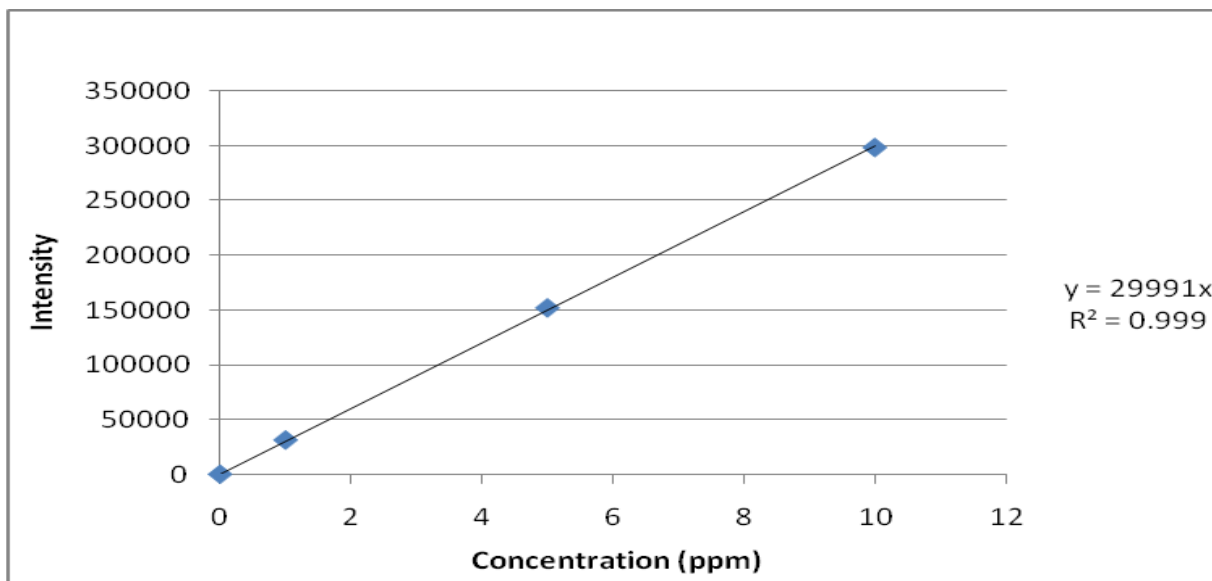**Figure 7.3: Calibration curve of Zinc metal element**
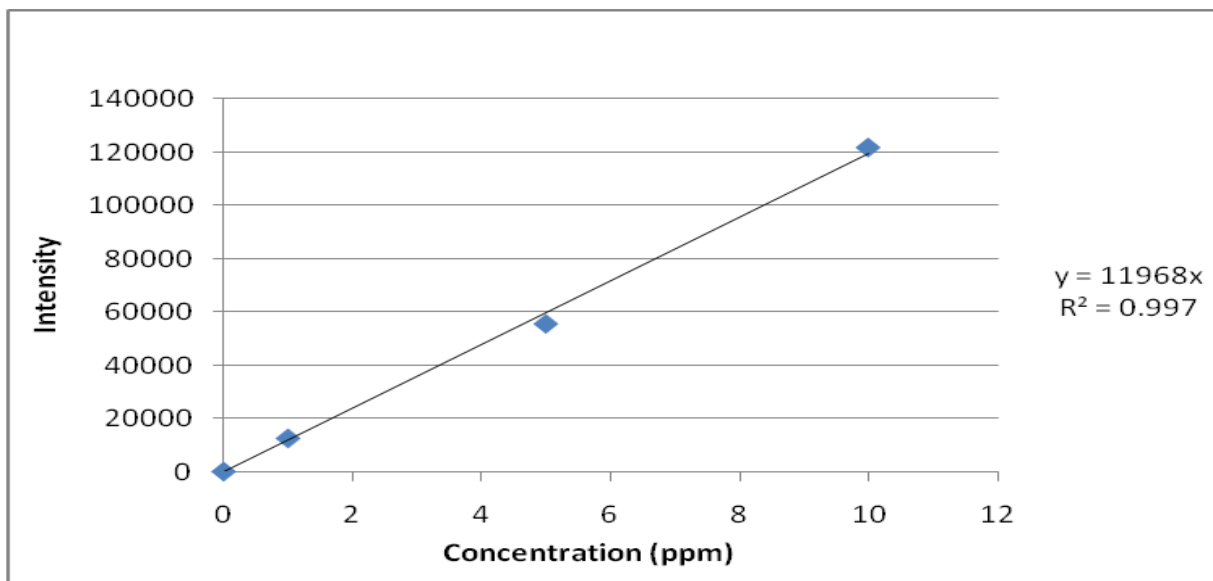
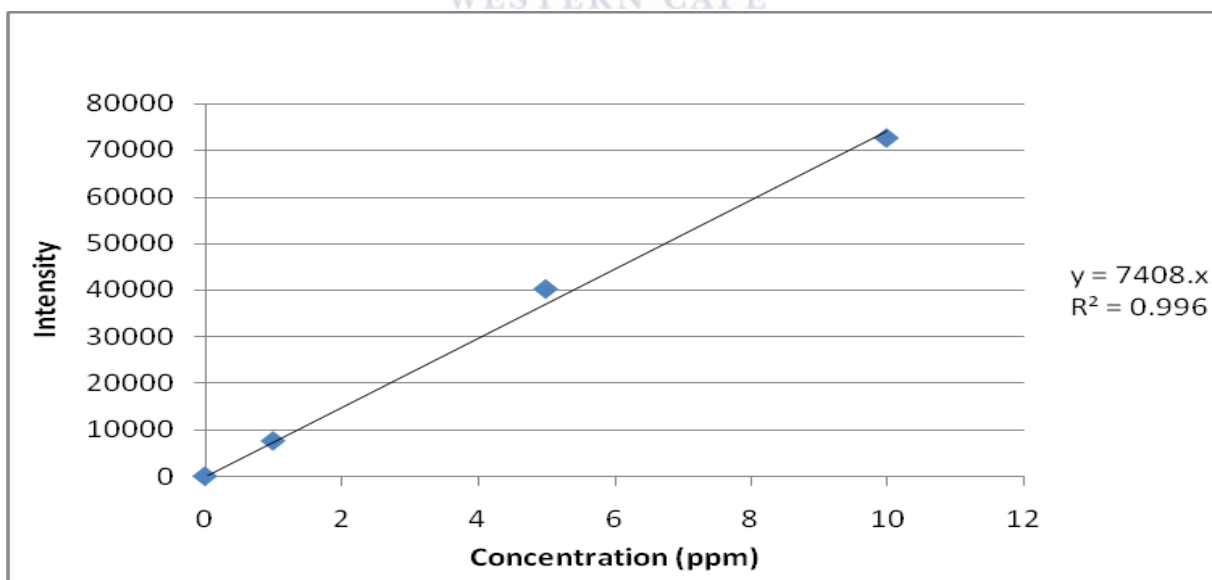**Figure 7.4: Calibration curve of Iron metal element**

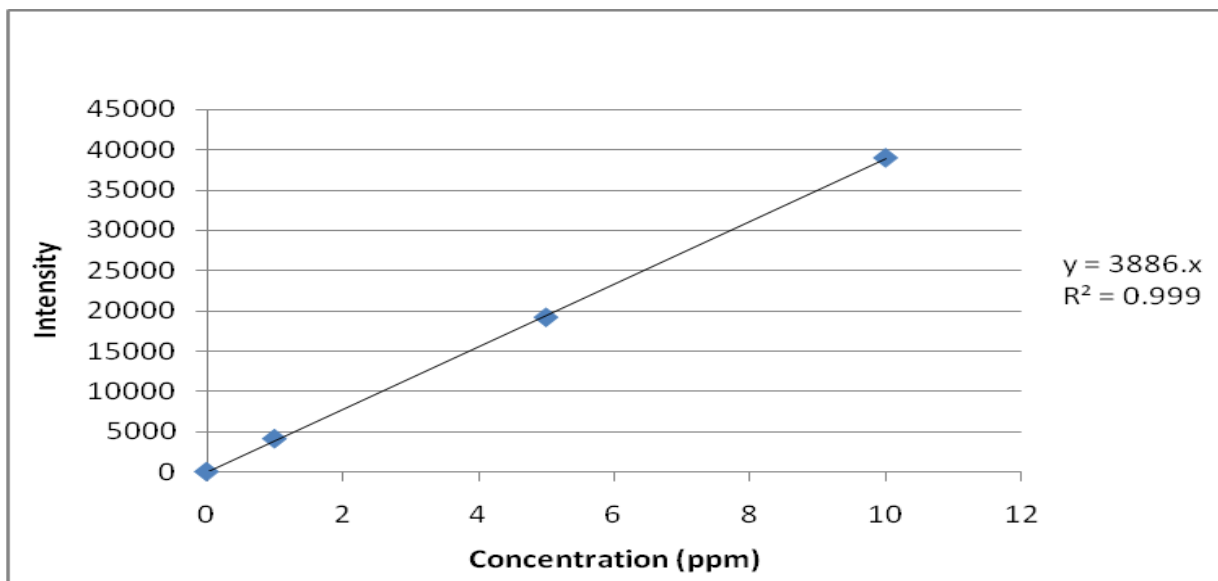**Figure 7.5: Calibration curve of Copper metal element**

Figure 7.6: Calibration curve of Titanium   metal element

Figure 7.7: Calibration curve of Aluminium   metal element

Figure 7.8: Calibration curve of Gallium metal element